The erosion and redistribution of sediment from the Haringvliet delta after construction of the Haringvliet dam

Masterhesis Earth surface and Water

Carolien Wegman

Utrecht University

Faculty of Geosciences

Supervision: Dr. M. Van der Vegt and Dr. A. P. Oost

Final version 23rd of December 2015

Student number: 3472108

Universiteit Utrecht

Abstract

The aim of the present study was to find out how the sediment of the Haringvliet delta was redistributed after construction of the Haringvliet dam. The Haringvliet deltas evolution is driven by river flow, tides and waves. After the closure of the Haringvliet tidal basin by the Haringvliet dam in 1970, both the river influence and the tidal influence in the area decreased. This caused the Haringvliet delta to decrease in size. The present research was conducted with GIS and hydrodynamic depth averaged computer modelling. Bathymetry data of 1970, 1984, 1998 and 2012 were used to analyse current directions and sediment transport for the period 1970 to 2012. The present research showed that after closure mainly tidal currents redistributed sediment from the Haringvliet delta front downdrift. The delta front experienced cross-shore sediment transport in landward direction by wave induced currents. Moreover, storms from the northwest had a large impact by transporting sediment inland. It could be concluded that the Haringvliet delta front migrated inland since 1970. Both calm weather and storm conditions redistributed sediment predominantly cross-shore in landward direction. The large impact of the human interventions in the Haringvliet can give insight into implications of human measures in similar tidal inlets.

Acknowledgements

First of all, I would like to thank Dr. Maarten van der Vegt for the supervision, discussions and direction. Furthermore, I am very grateful for the help, support and all the information provided by Ir. Arie de Gelder. I also want to thank Ir. Sonja Ouwerkerk for bringing me into contact with Arie regarding the subject of this thesis. I would like to thank Bas Bodewes, Jouke van der Velden and Lisanne Braat for helping me with the problems I encountered using Delft3D. Jasper Leuven, Evelien Brand and Stefan Pluis helped me a lot by having fruitful discussions. And last but not least I would like to thank Karlijn Smits for all the energizing coffee breaks and lunches during the writing process of this thesis.

Table of Contents

List of figures

List of tables

1. Introduction

The aim of the present study is to gain insight how the sediment of the Haringvliet delta was redistributed after the construction of the Haringvliet dam. The Haringvliet used to be a system with considerable freshwater discharge and strong tides. The delta therefore bared similarities with a river delta and an ebb-tidal delta (Figure 1). River deltas develop due to sediment being transported by rivers to the coast, where the sediment is deposited. An ebb-tidal delta is a characteristic feature of a tidal inlet. Ebb-tidal currents and waves construct this accumulation of sediment seaward of the tidal inlet (Hayes, 1980). Due to fear of flooding, the river was cut-off from the Haringvliet delta in 1970, causing a change in the hydrodynamics and morphodynamics of the Haringvliet basin. Since 1970 both river discharge and tidal flow are greatly reduced at the Haringvliet delta which increased the relative importance of wave-driven erosion.

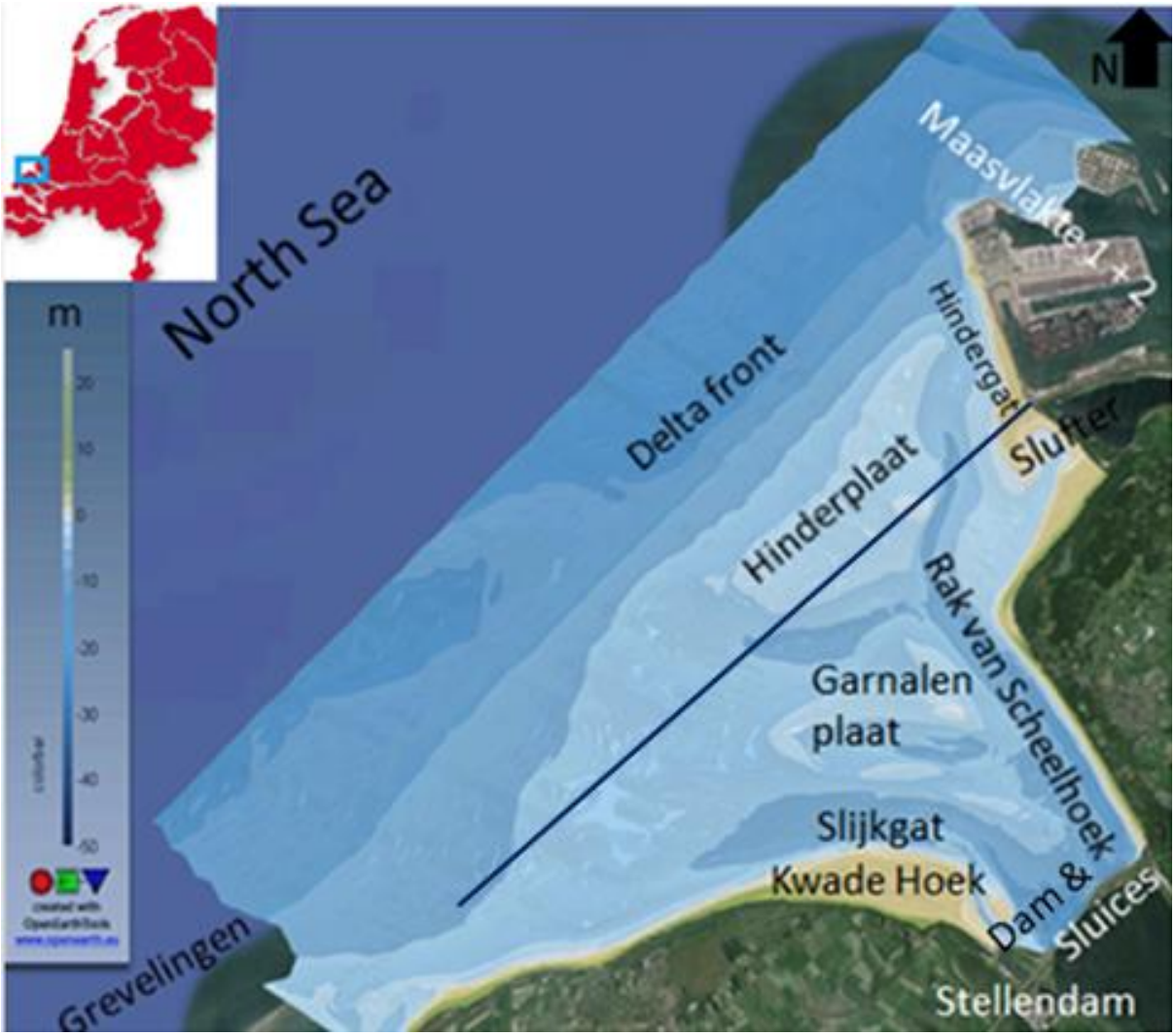

Figure 1. Indication of all main features in the Haringvliet tidal basin plotted on the bathymetry of 1970 (Google Earth, 2013; Rijkswaterstaat, 2015). The inner area is located south-eastward of the blue line.

Ebb-tidal delta behaviour after a change in tidal prism, such as experienced by the Haringvliet delta, is highly uncertain (de Jongste et al., 2013). The inner area of the Haringvliet experienced a total sedimentation of approximately 100 million m^3 in the period 1970 to 2000 (Dam et al., 2006). However, it is uncertain where this sediment originated from and what the involved transport processes were. Therefore, the focus of the present study is on the behaviour of a delta after human interference.

The Haringvliet is an ideal location to study the effects of human implementations on a delta. There is sufficient data before the building of the closure works as well as after 1970 when the closure works were completed. This makes it possible to learn about the underlying mechanisms and processes of ebb-tidal delta evolution, which will be helpful for future human interventions in similar areas.

A literature review is presented on the next pages. From this literature review the relevance of the present study, resulting research questions and hypothesis are drawn. To study the hydrodynamics and morphology of the Haringvliet delta over the period 1970 to 2012, a Geographical Information System (GIS) and a hydrodynamic computer model (Delft3D) were used. To research the relative influence of waves and tides, those were modelled both separately and combined. Velocity and sediment transport magnitudes and directions were calculated and behaviour during a storm was analysed. The sedimentation rates acquired with GIS were compared with the sedimentation rates acquired using the computer model.

2. Literature review

In this literature review first the morphology, the sediment distribution and hydrodynamics of the area are described. Secondly, the history of the delta influenced by humans is discussed. Thirdly, the morphological changes due to these human interferences are discussed.

2.1 Area description

The present study gives insight into a heavily moderated tidal basin. It shows how a delta behaves after its long tidal basin became a short tidal basin. With sea level rise and water safety issues high on the agenda, it is expected that other tidal basins will be subjected to similar changes induced by people. The ability to predict changes will give insight in the behaviour of deltas and could influence policy decisions. Furthermore, further knowledge of the Haringvliet specifically could shape policy decisions of Rijkswaterstaat (the Ministry of Infrastructure and the Environment of the Netherlands).

2.1.1 Morphology

2.1.1.1 Channels and shoals

The Haringvliet mouth consists of several shoals and channels (Figure 1). The main channels are the Rak van Scheelhoek and the Slijkgat. These channels appeared due to strong cross-shore tidal current velocities in the previous long tidal basin. They were also an extension of the river bed.

A shoal is defined as a zone with a bed level height above -3 meter Mean Sea Level (Louters et al., 1991). Shoals appear due to local patterns of wave induced currents and tidal currents. The most important process for redistribution of sediment of shoals is the interaction of waves and tidal currents. When waves proceed over the shoals and break, they create a set-up towards the coast. Waves that break on the shoal induce wave bores which travel shoreward as well. This shoreward moving wave energy interacts with tidal currents (Oertel, 1972).

Cross-shore shoals appear when tides are predominant in an area. In a long tidal basin the tide moves in and out of the tidal basin in cross-shore direction. The currents move around higher areas which causes several cross-shore shoals to appear. Longshore shoals mostly appear due to strong wave influence. Cross-shore approaching waves transport sediment towards the coast. They dissipate on shoals which creates longshore shoals. An example of a longshore shoal is the Hinderplaat in 1970 (Figure 1). In 1970 a cross-shore directed shoal is the Garnalenplaat.

2.1.1.2 Deltas

The morphology of a delta depends on the discharge regime, the sediment load and the grainsize of the river, the water depth of the standing body of water and the relative influence of waves, tides and currents (Seybold et al., 2007). Therefore, deltas appear in different forms (Figure 2). River deltas

develop when a river transports sediment towards the coast. The sediment is deposited when the rivers transport capacity suddenly decreases. Such a sudden decrease in transport capacity is apparent when a river reaches the coastline. The Haringvliet delta is partly a river delta. The river sediment accumulated in front of the coast. However, its appearance was not comparable with a typical river delta, such as the Mississippi river delta. The tides and waves had too much influence for the delta to extend far into the sea. The sediment transported to the shore by the river was redistributed and eroded by waves and tidal currents.

Wave dominated deltas do not extend far into the sea. This is due to the immediate mixing of fresh and salt water by breaking waves. The river sediment is transported along the coast. In appearance, a tide dominated delta is similar to an estuarine bay in which bars are formed in the direction of main tidal flow, mostly cross-shore (Seybold et al., 2007). The different types of deltas are shown in Figure 2. Before closure the Haringvliet delta showed similarities with a tidal and river dominated delta. Similar to a typical tide-dominated delta it had some cross-shore directed bars. The river influence caused the Haringvliet delta to extend into the sea.

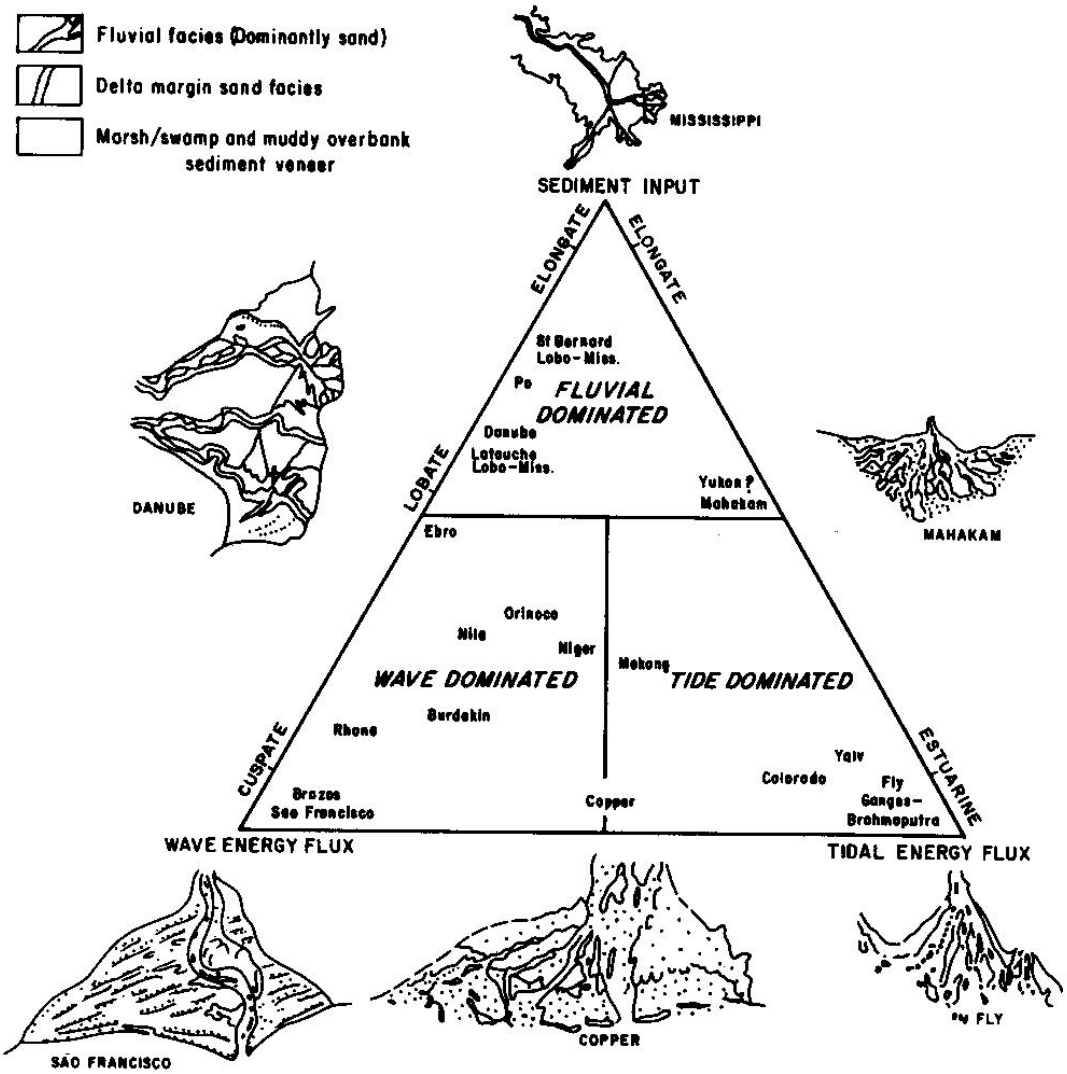

Figure 2. Original delta classification by Galloway (1975).

Many deltas in the world are abandoned due to delta lobe switching, river damming, sand mining and sea level rise. A delta is called abandoned when its deterioration was induced by a reduction in sediment supply (Nienhuis et al., 2013). The Haringvliet delta is an abandoned delta because the closure dam with sluices caused the river and tidal influence to decrease. The tidal influence

decreased since the previous long tidal basin became a short tidal basin after the dam was built in 1970. Sedimentation took place in the tidal channels and on the longshore bars on the seaward side of the delta (Mulder et al., 1990). There was insufficient water to transport enough sediment to the coast to maintain the delta. This resulted in a volume decrease of the Haringvliet delta.

An ebb-tidal delta is a shallow area on the seaward side of a tidal inlet (van der Vegt et al., 2009). An ebb-tidal delta is a typical feature of a tidal inlet system (Figure 3). The most important hydrodynamic processes for a tidal inlet system are tidal currents and wind waves. The relative influence of those two processes determines to a large extent erosion and deposition patterns of the tidal inlet. They therefore have a large impact on the morphology (de Swart and Zimmerman, 2009).

In Figure 3 the main processes influencing a typical tidal inlet are shown. Waves that don't propagate perpendicular to the coast generate longshore currents when they break close to the coast. Waves and tidal currents combined can create a littoral drift. When sediment is transported by the longshore currents it either passes by the ebb-tidal delta or it is transported into the inlet and is deposited there (de Swart and Zimmerman, 2009). Sediment from the inlet can be exported seaward due to asymmetry of the cross-shore tides, which can contribute to the maintenance of the ebb-tidal delta. This happens when the peak ebb currents are larger than the peak flood currents. On the seaward side of the tidal inlet, the tide induced residual current is the dominant factor transporting sediment (van der Vegt et al., 2009). In the tidal inlet tides prevail over waves in the deep channels. However, near tidal flats and other intertidal areas waves can cause significant erosion (de Swart and Zimmerman, 2009). On the inland side of the tidal inlet, the higher harmonics are the most important factor transporting sediment (van der Vegt et al., 2009). The sediment of which an ebb-tidal delta consists, originates mostly from other barriers in the area. However, the sediment can also be derived from river influx, the substrate of the inlet during formation or channel deepening (FitzGerald et al., 2004).

Since closure, the Haringvliet delta could be considered an ebb-tidal delta of an estuary. The Haringvliet tidal basin can be compared with a typical tidal inlet system (Figure 3). There is no narrowing passage confined by barrier islands in the Haringvliet tidal basin in which flow velocities would accelerate. Therefore, only the top part of a typical tidal inlet system can be recognized in the Haringvliet tidal basin. This divide is indicated by a red line in both images of Figure 3. Littoral drift due to the breaking of waves occurs close to the Haringvliet coast. Furthermore, an ebb-tidal delta lobe exists although it does not have two flood currents confining the delta. The Haringvliet delta does have a relatively deep ebb channel. However, the ebb-tidal delta is not folded around it. The cross-shore tidal current was more important before closure than after closure. The cross-shore tidal current could propagate far into the tidal basin, creating a large water level difference between the basin and offshore. This caused high cross-shore current velocities (de Swart and Zimmerman, 2009).

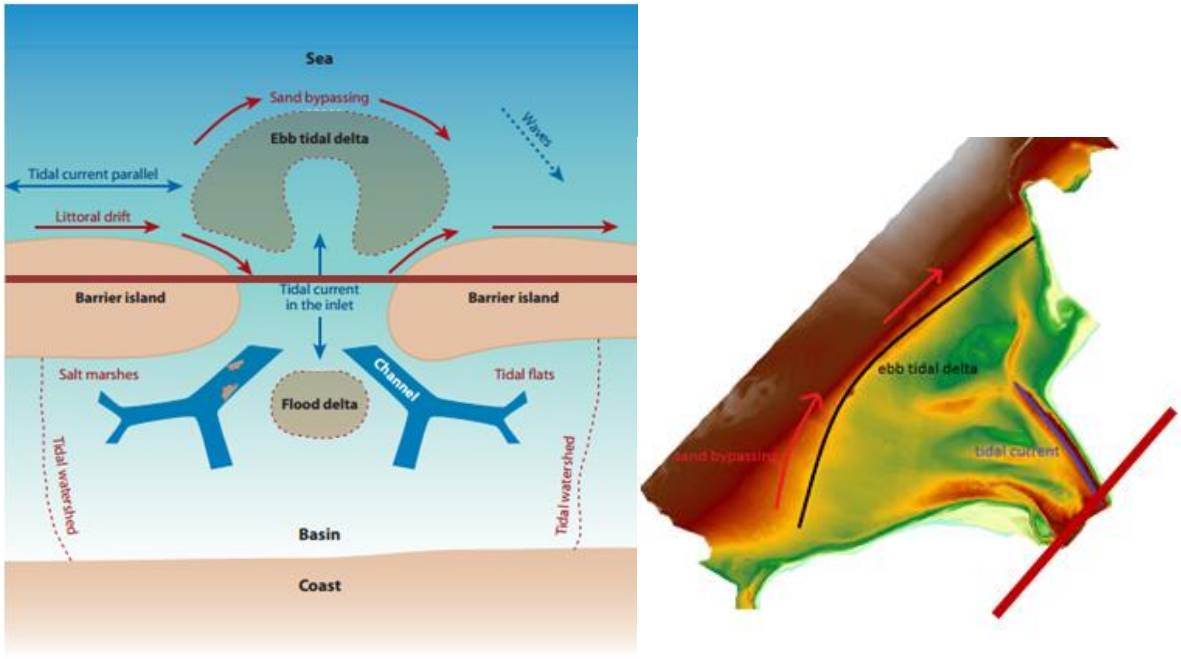

Figure 3. Typical tidal inlet system (de Swart and Zimmerman, 2009) and bathymetry of the Haringvliet mouth in 1970 (Rijkswaterstaat, 2015).

The volume of an ebb-tidal delta is dependent on the tidal prism (Sha and van den Berg, 1993; van der Vegt et al., 2006). Walton and Adams (1976) found a direct correlation between the tidal volume and the sediment volume of an ebb-tidal delta (Equation 1).

Equation 1

$$Vd = \alpha\, Vt^{\beta}$$

Vd = sediment volume of an ebb-tidal delta (m^3)
α = positive empirical constant
Vt = tidal prism (m^3)
β ~ 1.23

According to Ridderinkhof et al. (2014) the ebb-tidal delta volume is influenced by the length of the tidal basin. Namely, the back-barrier basin determines the tidal prism, which determines the volume of the ebb-tidal delta. For a long back-barrier basin, the net sediment transport is seaward which results in a large ebb-tidal delta. The Haringvliet was a long tidal basin before the closure dam was built in 1970. Therefore, it can be assumed that it had a large ebb-tidal delta. For a small back-barrier basin the net sediment transport is landward which results in a smaller ebb-tidal delta. Since closure, the Haringvliet has a small back-barrier basin. Therefore, it can be assumed that it has a small ebb-tidal delta (Ridderinkhof et al., 2014). A decrease in size of the ebb-tidal delta since 1970 was expected.

Although ebb-tidal delta morphology is not studied extensively, there are some 'rules of thumb' that can be applied. One of these rules is that the interaction of tidal currents with waves determines the morphology of the ebb-tidal delta (Hayes, 1980). If tides are relatively more important than waves, an almost symmetric delta results (with respect to the mid-axis through the centre of the inlet). This symmetry will evolve due to the different spatial patterns of ebb and flood currents. These form a tidal residual circulation pattern which consists of two cells: seaward of the tidal inlet the currents will be ebb dominant, whereas on the landward side of the inlet the currents are flood dominant. It is assumed that net sediment transport results from stirred up sediment transported by the residual

current. Therefore, it can be concluded that an ebb-tidal delta forms at the seaward end of an ebb-dominant channel. Tidal inlets will only be stable when the wave induced littoral drift is not very strong. This has the tendency to close the inlet. Tidal currents in the inlet increase the size of the inlet (de Swart and Zimmerman, 2009).

An ebb-tidal delta can be asymmetric due to the littoral drift. The ebb-dominant channel than bends in a down-drift direction. According to de Swart and Zimmerman (2009) ebb-dominant channels can also be asymmetric due to a phase difference between tidal currents offshore and tidal currents inside the basin. When this phase difference is small, the channel bends updrift of the tidal wave. When the phase difference is 90 degrees, a symmetric delta appears. However, Sha and van den Berg (1993) argue that the updrift orientation of the main ebb-dominant channel is caused by a large tidal prism.

Both the river Rhine and the Meuse transport part of their water via the Haringvliet. The Rhine has an average discharge of 2200 m^3/s. The Meuse has an average discharge of 230 m^3/s (van Wijngaarden et al., 2002). Therefore, the river Rhine has most impact on the Haringvliet. The exact discharge through the Haringvliet before 1970 is unknown. However, the discharge through the Haringvliet under normal conditions was 1000 m^3/s during a test with complete sluice opening (van Wijngaarden, 1998). Therefore, before 1970 the average discharge through the Haringvliet must have been over 1000 m^3/s because the cross-sectional area without the dam would have been even bigger.

The river discharge created a river delta. An ebb-tidal delta occurred because the Haringvliet mouth was a tidal inlet with relatively strong cross-shore tidal currents. The deltas of the other inlets of the province of Zeeland combined with the Haringvliet delta created one big delta stretching in front of the coast of Zeeland. This delta is called the Voordelta (Figure 4, Louters et al., 1991). These interlinked deltas had a cross-shore length of 10 to 15 km seaward of the coastline.

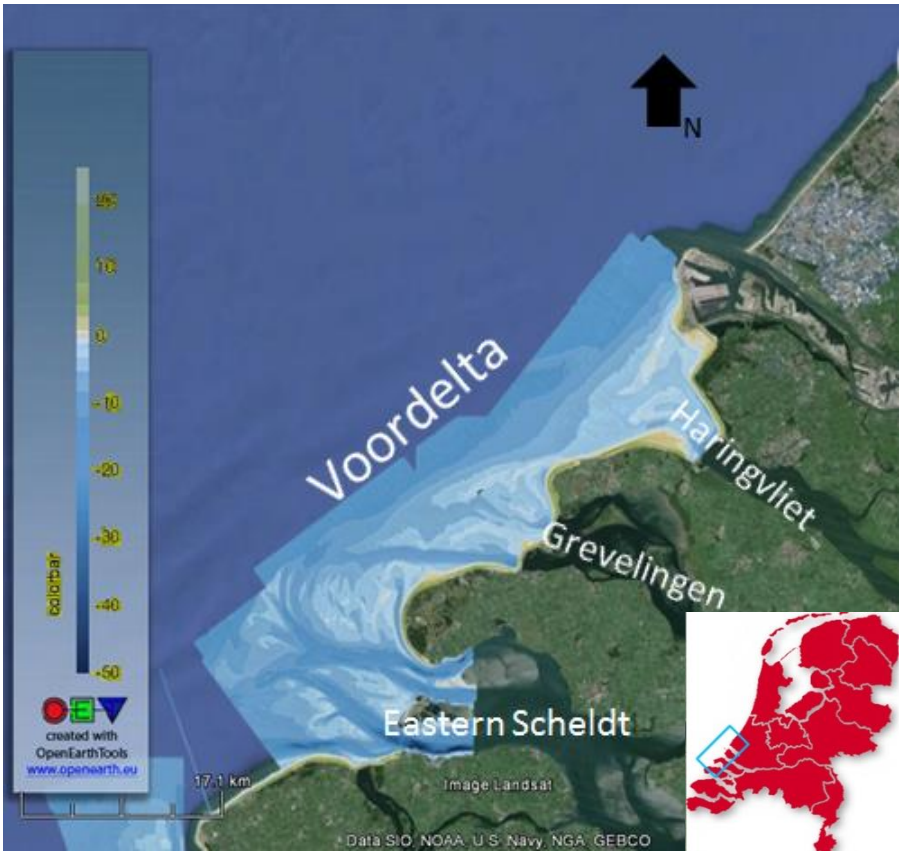

Figure 4. The deltas of the Eastern Scheldt, Grevelingen and Haringvliet combined are called the Voordelta. The bathymetry is of 1984 (Google Earth, 2013; Rijkswaterstaat, 2015).

2.1.2 Sediment distribution

Ebb-tidal deltas on the Dutch continental shelf consist primarily of sand (Eelkema et al., 2013). The median grain size in the Haringvliet mouth varies between 150 micrometer on the shoals to 350 micrometer in the channels (Eelkema et al., 2013; Louters et al., 1991). According to Dam et al. (2006) cohesiveness of sediment is important when modelling sediment transport in the Haringvliet. However, the sediment seaward of the shoal Hinderplaat consists for less than 20% of silt (Louters et al., 1991). Inland of this shoal, silt concentrations are larger (Koomans et al., 2001). Especially in the two main channels, Rak van Scheelhoek and Slijkgat, differences in sediment size and cohesiveness influence erosion patterns. More than 90% of the sediment in the upper 5 meter of the Rak van Scheelhoek is silt which is a cohesive substrate. The sediment in the Slijkgat is predominantly sand, which is more readily erodible than the silt of the Rak van Scheelhoek (personal communication, Bliek, May 7th, 2015). The present study focuses on the patterns of infilling and redistribution of sediment. The Rak van Scheelhoek did not erode heavily since 1970, because of which cohesive sediment was not taken into account.

2.1.3 Hydrodynamics

The morphology and bathymetry of deltas are largely determined by the local hydrodynamics (Ridderinkhof et al., 2014). The southwestern part of the Netherlands has a mixed energy shoreline (Louters et al. 1991). The tide has a mean range of 2.4 meter and is semidiurnal, implying that two high and two low tides pass by every lunar day (Louters et al., 1991; Tönis et al., 2002). The tidal wave propagates along the coast, during flood the tidal wave is directed northward and during ebb it propagates in southward direction (Louters et al., 1991).

The wave climate at the Goeree Lightvessel, situated 20 km of the coast of the Haringvliet at 21 meter water depth, shows mainly wave energy fluxes from the southwest to west. However, frequently waves with long periods arrive from the northwest (Tönis et al., 2002). An overview of the directions of waves arriving at Goeree Lightvessel and their occurrence and waveheight is given in Table 1.

Table 1. Wave characteristics reaching Goeree Lightvessel (Tönis et al., 2002).

Direction range (degrees)	Occurrence (%)	Average wave height (m)
338-22	10.3	1.05
22-67	11.2	1.09
67-112	4.2	0.93
112-157	2.7	0.78
157-202	5.8	1.05
202-247	27.8	1.49
247-292	13.5	1.41
292-337	24.6	1.28
000-360	100	1.27

Since closure in 1970, the sluices are partly opened from a Rhine discharge of 1500 m^3/s at Lobith onwards. Lobith is the location where the Rhine enters the Netherlands. Only when the river flow is larger than 1500 m^3/s, the remaining part will be discharged through the Haringvliet. Approximately 60% of the year the Rhine discharge is over 1500 m^3/s (van Wijngaarden et al., 2002). The mean discharge through the sluices is 550 m^3/s since the Haringvliet dam was implemented (Louters et al., 1991).

2.1.4 Ebb and flood channels

Van Veen (1950) was one of the first to analyse ebb and flood channels (Figure 5). Flood channels are mainly open to the flood current. They are deep at the seaward side and have a sill at the landward

end of the channel. An ebb channel on the other hand is mostly open to the ebb current and is a seaward extension of the river bed. It has a sill at the seaward end. The sills are formed at the location where ebb and flood channels meet. Typically, the dominant flood (ebb) current in a flood (ebb) channel results in flood (ebb) driven sand transport. The most important characteristic of ebb and flood channels is that they try to avoid each other (Robinson, 1960; van Veen, 1950).

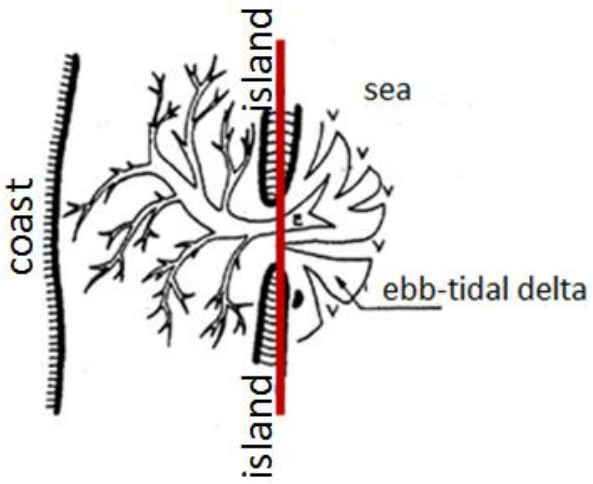

Figure 5. Ebb and flood channels in a typical ebb-tidal delta. E indicates an ebb channel, V a flood channel (edited after van Veen, 1950).

The red line in Figure 5 indicates that the features to the right are found in the Haringvliet mouth since closure in 1970. According to Tönis et al. (2002) the main channels in the Haringvliet mouth, Slijkgat and Rak van Scheelhoek, were both flood dominant before closure. The tidal current velocities were maximum during flood conditions. However, an internal report of Rijkswaterstaat argues that the Slijkgat was indeed a flood dominant channel but the Rak van Scheelhoek was an ebb-dominant channel (Snijders, 1998). There should have been at least one ebb channel before closure given the fact that river discharge through the area was high at the time. Namely, the ebb channel is the extension of the river bed in the tidal inlet (Robinson, 1960). Therefore, the Rak van Scheelhoek, was most probably an ebb channel before closure (Snijders, 1998).

2.2 Human interventions

The Haringvliet is situated in the southwestern part of the Netherlands (Figure 1). In this part of the Netherlands a delta system with tidal inlets and channels was formed due to transgression of the sea. The Haringvliet mouth has been influenced by human measures since the 13th century when dikes were erected in the Netherlands (van Wijngaarden et al., 2002). The storm flood of 1953 caused a lot of casualties and damage. After the storm flood it was decided that the Netherlands needed protection from flooding. The storm surge protection plan that was developed is called the Deltaworks. Two inlets in the southwestern part of the Netherlands were closed off, the Haringvliet and Grevelingen. The Eastern Scheldt was protected with a storm surge barrier and the Western Scheldt was kept open for shipping to Antwerp (Tönis et al., 2002).

From 1957 until 1970 the largest intervention took place: the closure works disconnecting the Haringvliet from the river Rhine and Meuse appeared. A large dam with sluices was implemented which enabled the Dutch control of the river discharge through the Haringvliet. The Haringvliet sluices are situated on the south-eastern side of the Haringvliet and were completed in 1970. At low tide they release fresh water into the channel Slijkgat, which transports it to the sea.

The Haringvliet sluices are a system of more than a kilometer in length. The sluice system consists of 17 sluices which are all 60 meter long. Every sluice has two closing mechanisms, one on the seaward

side and one on the inland side of the dam. During ebb conditions the closing mechanisms can be elevated and fresh water is able to flow out to the sea (Steenbergen, 2004).

Figure 6. The Haringvliet sluices (personal photograph, May 2015).

From 1964 to 1976 the port of Rotterdam was extended by the Maasvlakte 1, situated to the north of the Haringvliet delta. From 1986 until 1987 the Slufter was built. This was a smaller land reclamation project. The port of Rotterdam needed another extension. From 2008 to 2013 the Maasvlakte 2 was built. This land reclamation project is again situated to the north of the Haringvliet delta. Together the two Maasvlaktes extend 8 km into the North Sea. Since these projects had only a few years between them, it is generally assumed that the system did not reach equilibrium from a previous intervention before the next project was started. This makes it difficult to determine how the system responded to each implementation (Tönis et al., 2002).

The harbour of Stellendam to the southeast of the Haringvliet is connected to the North Sea by the channel Slijkgat. The Slijkgat became smaller due to the fresh water and tidal prism decrease after closure. Therefore, the Slijkgat has been dredged since 1983. Until 2004 dredging maintained the depth of the channel at 4.5 meter below Mean Sea Level (MSL) to keep the channel navigable. Since 2004 the depth and width of the Slijkgat were maintained at 5 meter below MSL and 100 m width. With the construction of Maasvlakte 2, the port of Rotterdam promised the harbour of Stellendam that they would keep the Slijkgat 100 m wide and at least 5.5 meter deep. Over the last 20 years the dredging volumes are on average 250.000 m^3 per year, with a variance of several hundred thousands of cubic meters (Figure 7, Bliek and de Gelder, 2014).

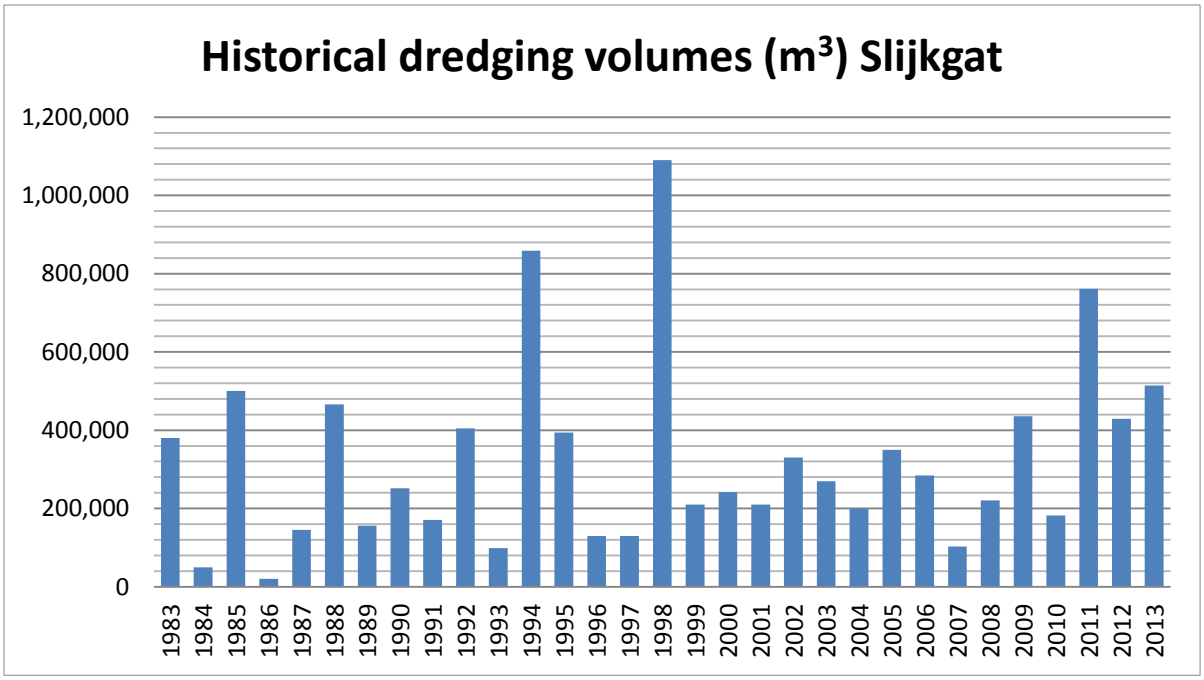

Figure 7. Historical dredging volumes (m^3) of the Slijkgat (Bliek and de Gelder, 2014).

Currently, there is no salt water inflow through the sluices to the inland area of the Haringvliet. For almost 15 years the option of opening the sluices during flood is studied. This opening during flood could have positive ecological responses. The downside of this partial opening would be a reduction in drinking water. Furthermore, salt intrusion will be unbeneficial for agriculture (de Jongste et al., 2013).

2.3 Morphological changes

2.3.1 Changes in hydrodynamics

Several changes took place after the building of the closure works in 1970. According to Louters et al. (1991) the hydrodynamic changes that took place since 1970 are a direct consequence of the civil engineering works in the area. The dam caused the tidal prism to decrease by 70% (Dam et al., 2006; Louters et al., 1991). Before closure the tidal prism had a volume of 73 million m^3. Since closure the tidal prism is only around 22 million m^3 (Tönis et al., 2002). Furthermore, the cross-shore tidal current velocities in the tidal channels have decreased by 45%. Moreover, the maximum current velocities in the proximity of the dam have even decreased from 1.5 m/s to 0.3 m/s (Louters et al., 1991).

Not much research has been done into the change in wave influence in the Haringvliet mouth due to human implementations in the past 50 years. However, waves do have a large impact on the ebb-tidal delta. Wave breaking creates a set-up which induces currents that transport sediment. Furthermore, they stir up sediment, which leads to high sediment concentrations available for transportation (Eelkema et al., 2013).

It could be argued that due to land reclamation projects to the north of the system, there is less influence from waves coming from the north(west). The Haringvliet tidal basin is protected from these wave directions by the Maasvlaktes. This could be important because the highest waves often come from the northwest because they have the longest fetch length. When waves are interrupted by the Maasvlakte land reclamation projects, the morphology of the delta could change.

2.3.2 Tidal current patterns

The tidal current patterns changed in the Haringvliet mouth due to the dam. Before the Haringvliet was dammed it could be considered a long tidal basin. The salt intrusion and tides reached up to 50

kilometer inland. The length of the basin caused a phase difference between tidal velocities inside the estuary and the longshore tidal velocities offshore.

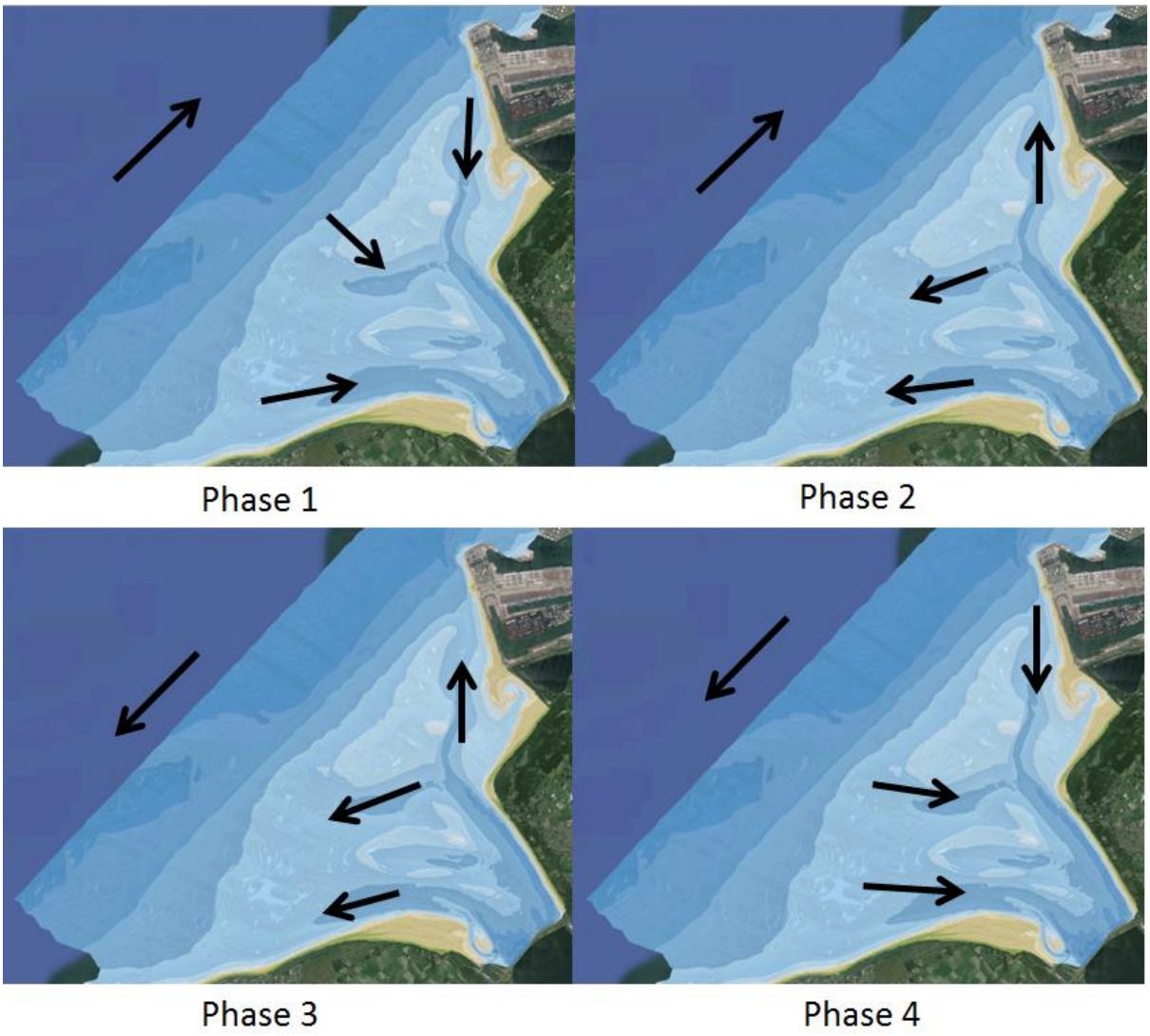

Figure 8. Phases over a tidal cycle in the Haringvliet tidal basin before closure. The bathymetry is of 1970 (Google Earth, 2013; Rijkswaterstaat, 2015). The arrows indicate current directions, not current magnitude (edited after Tönis et al., 2002).

As analysed by Sha and van den Berg (1993), a tidal cycle before closure had four phases (Figure 8**)**. With flood (ebb) currents in the basin, a current from the sea (tidal basin) into the tidal basin (sea) is described. With flood (ebb) currents offshore, a tidal current directed to the northeast (southwest) is described. Phase 1: Before closure at high tide, flood currents occurred inside as well as outside the estuary at the same time. Phase 2: Approximately three hours after high tide there was a difference noticeable. Offshore, the current is still in flood direction. However, inside it is already in the ebb direction which caused the water to flow from the tidal basin into the sea. Phase 3: At low tide the ebb currents occur both offshore as well as inside the tidal basin. Phase 4: Approximately three hours after low tide the current offshore is still in ebb-direction whereas inside the tidal basin it is already in flood direction again. This caused water from the sea to enter the tidal basin. There was a phase difference of less than 90 degrees between tidal velocities inside the basin compared to tidal velocities outside the basin before closure (Tönis et al., 2002). The currents show a standing wave pattern offshore and a progressive wave propagating into the long tidal basin. This caused a three hour difference between flood and ebb currents inside and outside the basin.

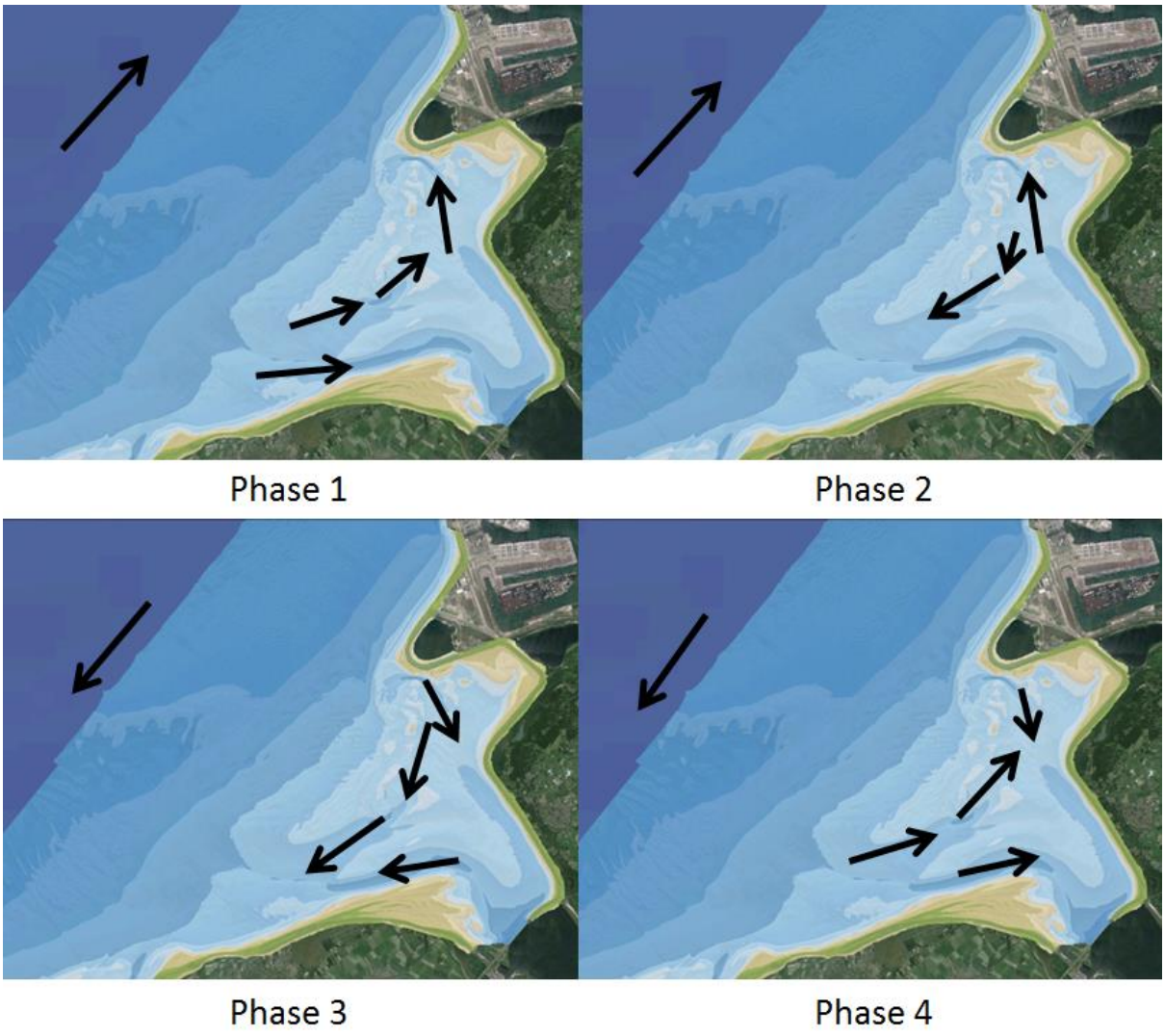

Figure 9. Phases over a tidal cycle in the Haringvliet tidal basin after closure. The bathymetry is of 1984 (Google Earth, 2013; Rijkswaterstaat, 2015). The arrows indicate current directions, not current magnitude (edited after Tönis et al., 2002).

Since closure the Haringvliet tidal basin is a short tidal basin. A standing wave pattern appeared inside the basin. Still, four different phases can be identified (Figure 9**)**. Phase 1: During high tide the water moves into the Haringvliet from the south side and leaves via the northern side. Phase 2: Approximately three hours after high tide the current offshore is in flood direction. Inside the Haringvliet tidal basin the current is already in ebb direction, longshore towards the southwest. Phase 3: During low tide, water from the sea enters at the northern side of the tidal basin and leaves on the southern side. Phase 4: Approximately 3 hours after low tide the current offshore is in ebb direction whereas inside the tidal basin it is already in flood direction (Sha and van den Berg, 1993; Tönis et al., 2002). Since closure the currents inside and outside the estuary are almost in phase. The phase difference is approximately 0 degrees.

2.3.3 Morphological adaptation

Morphology is an agent with strong feedbacks. The morphology determines to a large extent the tidal currents and waves inside the system, which by their own means modify sediment transport (de Swart and Zimmerman, 2009). The influence of the morphology of the Haringvliet tidal basin on waves, tides and currents and with that sediment transport will be analysed. Therefore, bathymetry data of 1957, 1970, 1984, 1998 and 2012 were analysed.

The bathymetry of 1957 clearly showed ebb and flood channels (Figure 10). The Rak van Scheelhoek was an ebb channel with the sill on the seaward side. In this ebb channel a fork like pattern appeared due to a flood channel approaching from the seaward side. The 'delta' of this flood channel created the sill of the ebb channel. The Haringvliet consisted of a long tidal basin in 1957. Large river discharges combined with strong tidal influence, created a delta to which terrestrial sediment is supplied by the river and reshaped by tidal currents. Tidal currents were predominant, which caused waves to have minor influence on the system. The relatively large tidal and river influence caused most bars to be directed cross-shore. Due to incompleteness of the bathymetry, the morphology of 1957 was not used for further analyses by GIS and computer modelling.

Figure 10. Bathymetry of 1957 (Google Earth, 2013; Rijkswaterstaat, 2015).

In 1970 the Haringvliet dam was finished, which caused the Haringvliet tidal basin to become a short tidal basin. The bathymetry of 1970 did not have time to adapt to this major change (Figure 11). Still, the fork like appearance of the Rak van Scheelhoek was found. However, the flood channel in the centre of this fork of the Rak van Scheelhoek disappeared. This is the first indication that tidal influence decreased, tidal channels were filled with sediment. The land extension to the northeast of the Haringvliet, Maasvlakte 1, was finished in 1970.

Due to the change from a long tidal basin to a short tidal basin in 1970 the north-south directed tidal currents became more important than the east-west directed tidal currents. The tidal currents could not travel as far into the tidal basin (Louters et al., 1991). After closure the tidal wave had a standing wave pattern in the tidal basin. The contour lines of the delta follow the coast, which is caused by relatively strong longshore tidal currents (Sha and van den Berg, 1993). The channels Rak van Scheelhoek and Slijkgat are still deep. However, especially the deep parts of the channels are effective sediment traps because the tidal current velocities strongly decreased in the channels which decreased the sand transport capacity (de Jongste et al., 2013; Louters et al., 1991).

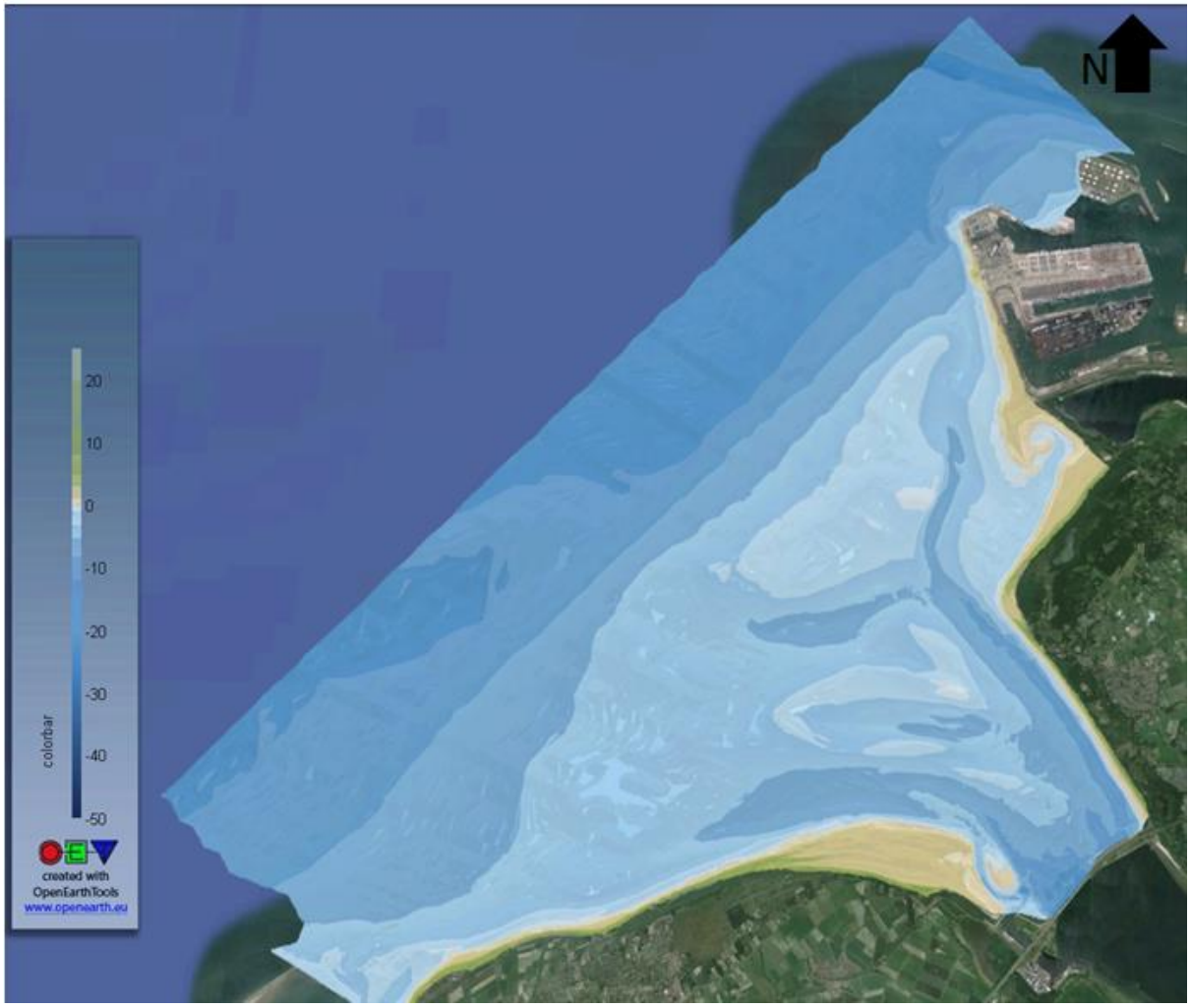

Figure 11. Bathymetry of 1970 (Google Earth, 2013; Rijkswaterstaat, 2015).

After closure, channels became shallower whereas shoals extended (Tönis et al., 2002). That was caused by the Haringvliet dam, which decreased cross-shore tidal current velocities and fresh water discharge through the system. This can be recognised in the bathymetry of 1984 (Figure 12). Almost all shoals were directed longshore from 1984 onwards. This is due to the increase in relative influence of waves. The landward directed asymmetric wave orbital motion is responsible for creating those longshore bars (Louters et al., 1991). The shoal on the north-western side, the Hinderplaat, was almost attached to the coast and part of its bed level was above MSL. Even very small waves will dissipate on this shoal.

According to Tönis et al. (2002), the change in phase due to the change from a long tidal basin into a short tidal basin caused the previous fork shaped ebb channel system of the Rak van Scheelhoek to change to a more southwards directed main ebb channel, the Slijkgat. The increased influence of the Slijkgat could be found in the following bathymetries as well. This increase in importance of the Slijkgat was accelerated by dredging.

The decrease in ebb-tidal delta volume due to the decrease in tidal prism after closure caused the transport of a significant part of the sand from the delta front. The landward directed sand transport was not compensated anymore by seaward directed ebb-tidal currents (Louters et al., 1991). Some of the sand of the delta front fills its channels whereas the rest forms a large bar complex consisting of the Hinderplaat and the Garnalenplaat in the Haringvliet (Fitzgerald, 1982). There was overall sedimentation and the inner area became shallower. Therefore, the tidal wave lost even more of its

influence in the inner area. It could be argued that since the Haringvliet dam was erected in 1970, a redistribution of sediment took place (Arends, 1997).

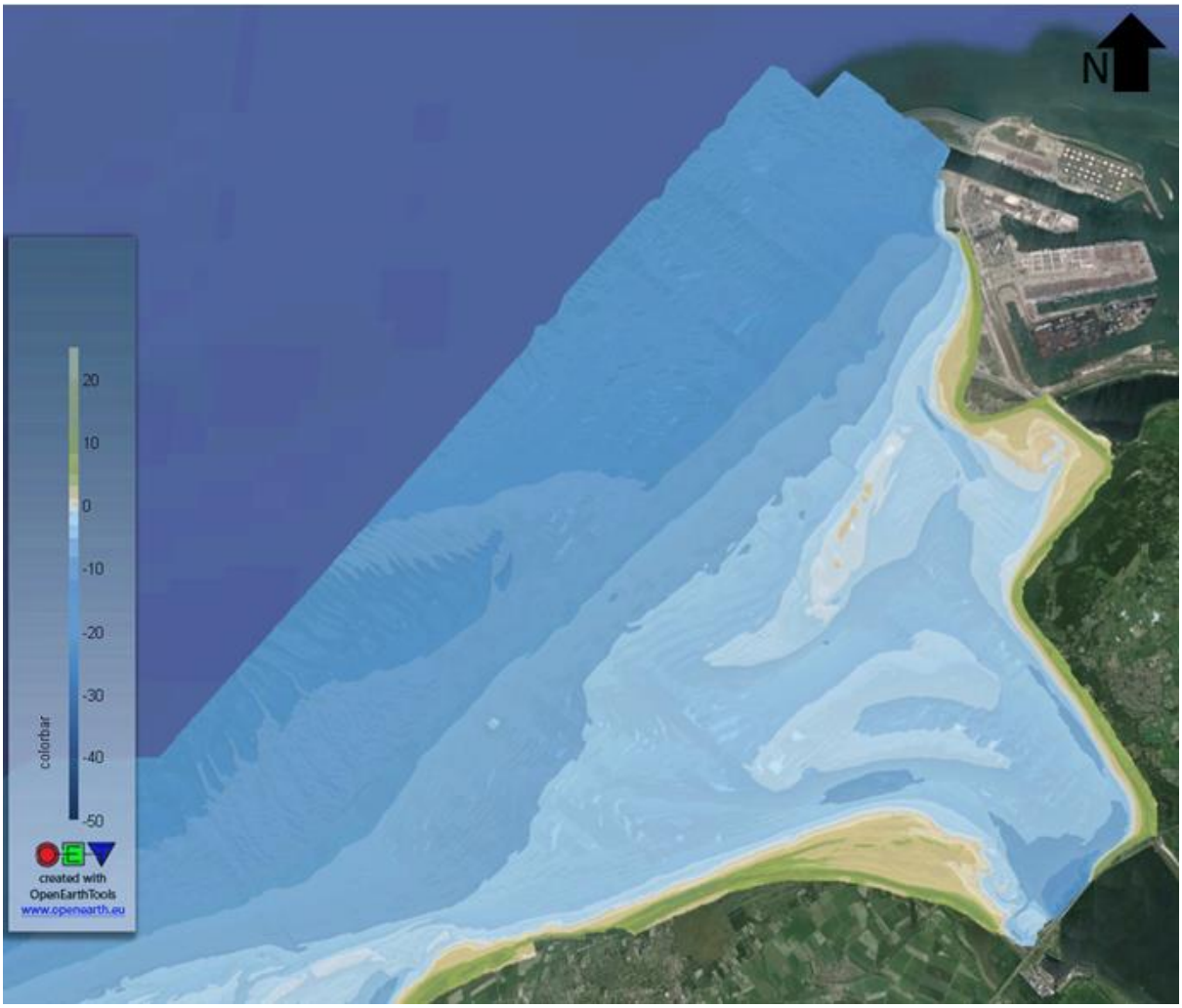

Figure 12. Bathymetry of 1984 (Google Earth, 2013; Rijkswaterstaat, 2015).

The bathymetry of 1998 showed an increase in bed level height over almost the entire inner area (Figure 13). This implied that only at high water currents could proceed over the shoals and bars into the area, but that at low water currents could only flow through the deeper parts of the estuary (Louters et al., 1991). The Hindergat seemed to have created its own small ebb-tidal delta. The channel Slijkgat maintained its depth, probably due to dredging and release of fresh water from the southern side of the sluices. Furthermore, the shoal Hinderplaat migrated landward and fragmentised in several pieces. This fragmentation might be caused by the tidal current moving over the shoal. The Hindergat became too small to transport all the water coming in via the Slijkgat out of the inner area. During flood, the current flows over the Hinderplaat shoal out of the inner area. The water prefers the slightly deeper areas on the shoal which are then further deepened and cause the fragmentation.

Spits attached to the coast and one extending from the Hinderplaat developed in the Haringvliet tidal basin, see the blue boxes in Figure 13. A spit is an accumulation of sediment visible at the surface, which grows due to a sediment source in the direction of a water body (Kraus, 1999). Spits form because of breaking waves, which cause littoral transport (Simeoni et al., 2007). The behaviour of a spit is such that there is predominantly growth in one direction. They have the shape of a long narrow bar and run mostly alongshore. When a spit grows it usually protects a bay (Wheeler, 1902). Spit formation indicates that there is an abundance of sediment (Simeoni et al., 2007).

This abundance of sediment for spit formation might have been present in the Haringvliet due to the ebb-tidal delta volume reduction which represented a large sand reservoir (Fitzgerald, 1988). However, spit formation only started after 1984. Apparently, there was extra sediment that induced spit formation after 1984. The storm surge barrier of the Eastern Scheldt resulted in its ebb-tidal delta volume reduction in 1986. Part of this sediment could be transported alongshore into the Haringvliet. Especially the spits in the south attached to the shore are most possibly formed because the tidal inlet is an interruption of the longshore sediment transport system (Fitzgerald, 1982). The longshore currents carrying capacity decreases and therefore an accumulation of sediment is the result.

Overall, the Haringvliet delta decreased in size again and seemed to have migrated updrift. This updrift behaviour of the delta is explained by Sha and van den Berg (1993). They argue that the phase difference between shore parallel tidal currents and inlet currents are the cause of this updrift behaviour. When this phase difference is small, the ebb-tidal delta will show a more updrift behaviour (de Swart and Zimmerman, 2009).

Figure 13. Bathymetry of 1998 (Google Earth, 2013; Rijkswaterstaat, 2015).

The most significant change was that the land extension Maasvlakte 2 was almost completed in 2012. Furthermore, the delta front migrated more inland. The spit features attached to the shore on the southern side of the Haringvliet estuary became more pronounced in 2012. The Hinderplaat including its spit feature migrated inland since the dominant flow over the Hinderplaat was landward. Waves break across the shoal and retard ebb-tidal currents in the cross-shore whereas they enhance flood-tidal currents in the cross-shore (Fitzgerald, 1982). The spits on the southern side force the channel Slijkgat to migrate in the direction of spit migration. For the spit at the end of the Hinderplaat, the cross-shore directed flood current combined with wave-induced longshore currents around the tip of

the spit cause the spit to curve in direction of the sluices (Kraus, 1999). The focus of wave energy due to refraction over the shoal increased the probability of a spit becoming a recurved spit. The attachment of the Hinderplaat to the shoreline is a typical end product of sediment bypassing (Fitzgerald, 1982).

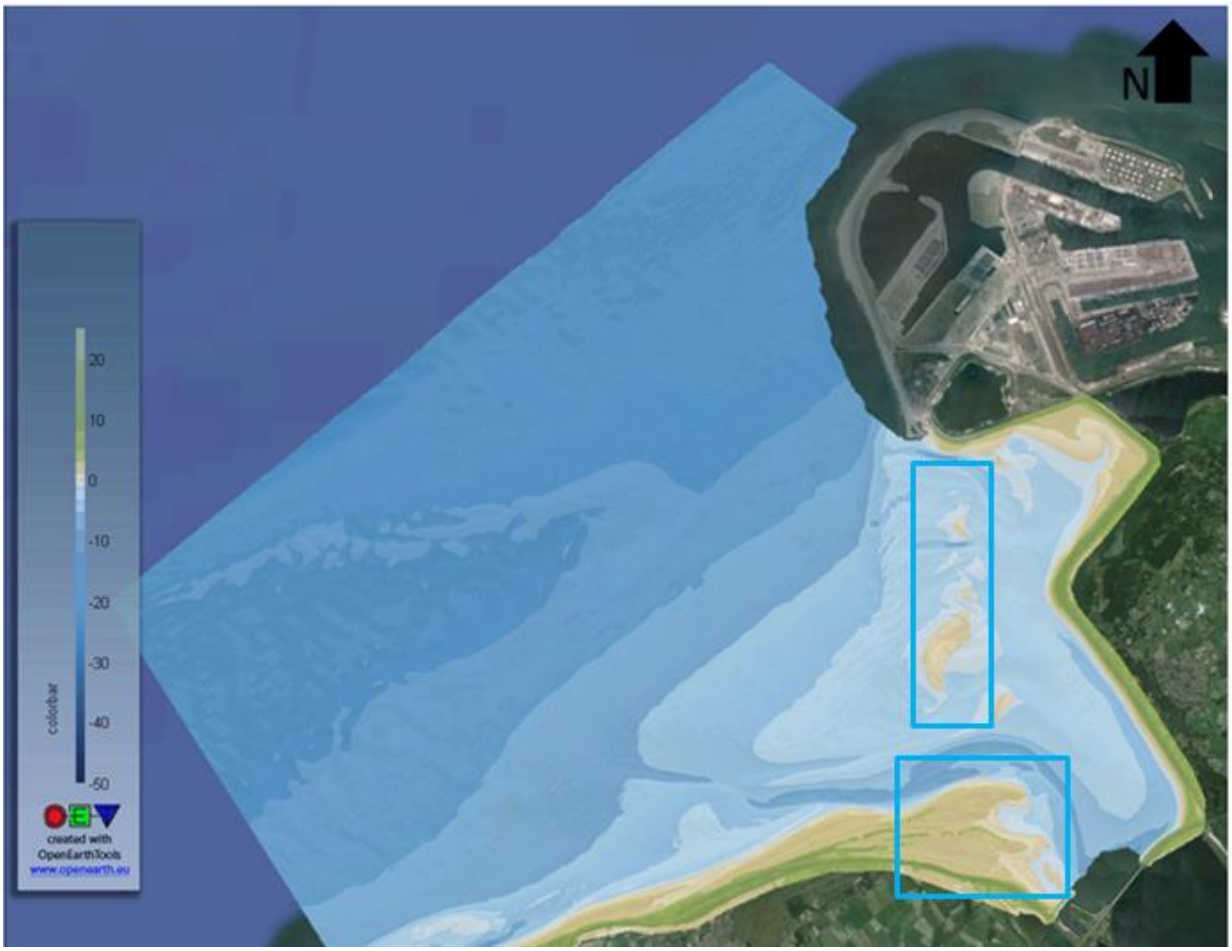

Figure 14. Bathymetry of 2012 (Google Earth, 2013; Rijkswaterstaat, 2015).

It can be concluded that the change from a long tidal basin to a short tidal basin in 1970, caused sediment to be redistributed landwards. Furthermore, the delta front is eroding and migrating inland (Louters et al., 1991). The tide-induced flow velocities decreased in the Haringvliet tidal basin due to the shortening of the tidal basin whereas the relative influence of waves increased (Dam et al., 2006; de Jongste et al., 2013). Bars were cross-shore directed before closure. After closure there were mainly longshore directed bars due to the increased relative influence of waves. The channels became effective sediment traps due to the smaller tide-induced flow velocities and low river discharge (Tönis et al., 2002).

Which bed level heights in the Haringvliet tidal basin increased in area and which bed level heights have decreased in area from 1970 to 2012 was visualised by a hypsometric curve (Figure 15, de Winter, 2008). A hypsometric curve shows the cumulative area on the x-axis and bed level height on the y-axis. It was shown that the mean height for areas with a bed level below -4.5 m decreased in the period 1986 to 2002/2003. The areas with a bed level above -4.5 m increased in average bed level height. From this hypsometric curve it can be concluded that deeper areas in the Haringvliet lost sediment whereas shallower areas gained sediment over the period 1986 to 2002/2003.

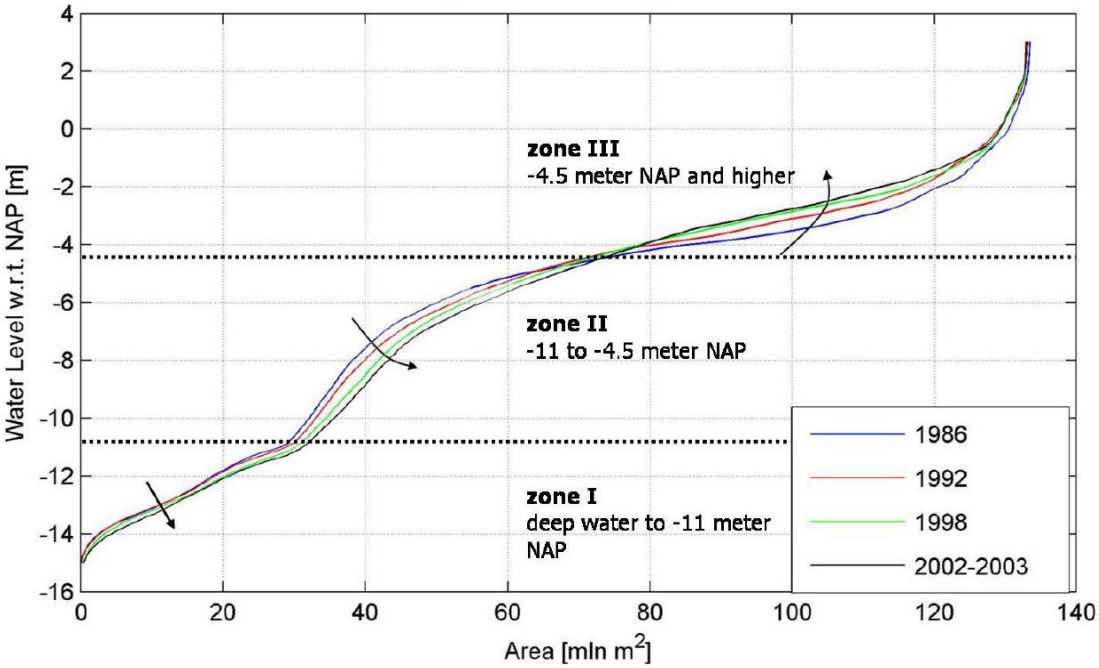

Figure 15. Hypsometric curve of the Haringvliet area (de Winter, 2008).

2.3.3 Dominant channels

The function of the channel Rak van Scheelhoek changed after closure by the dam in 1970. The Rak van Scheelhoek degraded from a main channel to a side stream which is currently incapable of transporting large amounts of water (Arends, 1997). It was covered by a 5 meter thick layer of silt. The Slijkgat became the dominant sandy channel after closure (Dam et al., 2006). This difference is probably caused by fresh water being transported through the sluices on the southern side. Roughly all of the fresh water flows via the Slijkgat to the sea. Furthermore, the Slijkgat is the channel dredged because it is the most convenient channel for navigation to the harbour of Stellendam (Bliek and de Gelder, 2014).

2.3.4 Mechanisms reworking deltas

There are few quantitative studies focussing on the redistribution of sediment after delta abandonment (Nienhuis et al., 2013). Since the closure dam was erected in 1970 the delta front migrated inland, the shoals became more longshore directed and the channels filled. The delta volume became smaller because of (relative) increasing onshore wave energy (Walton and Adams, 1976). The processes of erosion of the delta front by wave dissipation that cause a cross-shore current landward and longshore transport in downdrift direction by littoral drift, are similar as during stable conditions. However, the replenishment of sediment decreased because almost no sediment is transported by the cross-shore tidal current anymore from the back-barrier basin. Furthermore, input of river sediment decreased (Louters et al., 1991). Therefore, the sediment of the delta front is redistributed in the cross-shore direction by waves and in the longshore direction by littoral drift.

The rotation of the shoals in longshore direction and the inland migration of these shoals was caused by the relative increase in wave influence. When waves propagate over a shallow area, their skewness and asymmetry change. This causes the wave crest to be dominant over the wave trough. An overall landward transport of the shoal in longshore direction is the result. Refraction is the more parallel alignment of waves with the coast when they are approaching the coast. When a wave approaches the coast with the crest at an angle to the bottom contours, the depth varies along the wave crest. The parts in deeper water propagate faster than the part in shallower water. This causes the waves to refract and the wave crest to become more aligned with the coast and the bed level contours

(Masselink and Hughes, 2003). Therefore, most wave energy on the shoals is transported in cross-shore landward direction.

Furthermore, the heightening of the shoals is largely dependent on the interaction between the shoal and the adjacent channel. With a standing wave pattern in the inner area high water levels coincide with maximum flow velocities. This is when shoals inundate as well. The large flow velocities cause sediment concentrations to be high. On the shoals flow velocity decreases due to friction. This causes sediment to be deposited. Therefore, especially the parts of the shoal close to the channel increase in height quickly. During lower water heights and ebb-flow the flow is concentrated in lower lying areas on the shoal and is due to its lower flow velocities less capable of transporting sediment. Therefore not all sediment can be eroded and the shoals gain height (Louters and Gerritsen, 1994). This system was the same before the closure of the dam. However, due to more river outflow and stronger ebb velocities before closure the sediment on the shoals was eroded again.

The tidal channels filled due to the decrease in strength of the cross-shore tidal velocities. Tidal current velocities decreased due to the decrease in tidal prism after closure. This caused the sediment transport capacity to decrease as well. Especially the deep parts of channels are effective sediment traps. This trend is counteracted by dredging of the channel Slijkgat in the Haringvliet.

2.4 Research questions

The literature study has indicated what is known of the Haringvliet tidal basin and of the transition from a long tidal basin to a short tidal basin. The hydrodynamic forcing that caused the bathymetry changes in the area are not fully understood yet. One gap that stands out is that in a lot of studies of ebb-tidal deltas, wave forcing is not taken into account. Waves on the Dutch coast transport the sediment towards the coast and cause higher sediment concentrations than situations without waves. They do this by enhancing bed shear stress and stirring. In shallow areas, waves are of great importance. The relative influence of waves has increased in the Haringvliet, which can give insight in the ebb-tidal delta behaviour after such change. Some 2D modelling has been done considering the Haringvliet area. However, cross-shore transport has mostly been neglected (Tönis et al., 2002). Due to the increased importance of waves after closure, it is expected that cross-shore transport is an important sediment transport direction in the area.

Furthermore, the land reclamation projects Maasvlakte 1 and 2 block waves coming from the northwest. Storms might also have changed in impact at the Haringvliet due to the land reclamation projects and the closure dam. To be able to reproduce such situations, wave modelling is needed. How waves add to the removal of ebb-tidal deltas is still largely unknown and this research can contribute to that knowledge (Eelkema et al., 2012).

The main question of this research is: How is sediment of the Haringvliet delta redistributed and eroded after construction of the Haringvliet dam?

The sub questions are:

1. What is the influence of waves on the hydrodynamics of the Haringvliet delta?
    a. How are wave height and near bed orbital velocity spatially distributed?
    b. How did these patterns change over the period 1970 to 2012?
2. What is the influence of tides on the hydrodynamics of the Haringvliet delta?
    a. What are the patterns of tidal currents?
    b. How did these patterns of tidal currents change over the period 1970 to 2012?
3. What are the sediment transport patterns and erosion and deposition trends over the period 1970 to 2012?

To enhance the impact of the present study a comparison study was done between the Haringvliet delta and other similar deltas in the Netherlands. This comparison can be found in the Discussion section.

2.5 Hypothesis

The delta volume of the Haringvliet became smaller from 1970 onwards. This could have been caused by a relative increase in onshore wave energy (Walton and Adams, 1976). It was expected that the majority of the 100 million m^3 sediment filling up the inner area of the Haringvliet area came from the removal of the delta front. This would imply that cross-shore transport induced by waves was predominant. It was expected that the relative influence of waves on hydrodynamics and sediment transport in the area increased over time.

Storms from the northwest would have had less impact on the inner area of the Haringvliet in 2012 than in 1970. This expectation was based on the extension of the harbour of Rotterdam by the Maasvlakte 1 and 2 to the northwest of the Haringvliet. Before north-western storms could have severe impact on the inner area of the Haringvliet they would damp out.

3. Methods

First, the way by which the research questions were studied will be discussed. Secondly, the data that were needed to conduct the present study will be explained. Thirdly, the way in which GIS and the hydrodynamic model were used will be set out. Lastly, the analysis done with GIS and the hydrodynamic model will be explained.

3.1 Methodology of handling the research questions

The present study aimed to reveal trends in behaviour of a delta by using a process-based model and bathymetry data. This was done using two techniques: 1. Morphological changes and sedimentation rates were studied using bathymetry maps. 2. Wave and tidal influence on the system were modelled using the programme Delft3D with SWAN incorporated for wave modelling.

1. *What is the influence of waves on the hydrodynamics of the Haringvliet delta?*

To answer research question 1, the computer model Delft3D with built-in SWAN (**S**imulating **Wa**ves **N**earshore) was used in stand-alone mode as well as with implementation of a tidal signal. Those were compared and the influence of waves on the hydrodynamics of the Haringvliet delta was researched. This modelling was conducted for the bathymetries of 1970, 1984, 1998 and 2012 to study the changes in wave induced current patterns over the period 1970 to 2012.

2. *What is the influence of tides on the hydrodynamics of the Haringvliet delta?*

Research question 2 was studied using a similar methodology as research question 1. In the computer model Delft3D only tides were implemented on a grid. The results were compared with the outcomes of a simulation of both tides and waves. This modelling was conducted for the bathymetries of 1970, 1984, 1998 and 2012 to study the changes in tidal current patterns over the period 1970 to 2012.

3. *What are the sediment transport patterns and erosion and deposition trends over the period 1970 to 2012?*

Bathymetry data of the years 1970, 1984, 1998 and 2012 and a GIS program (ArcMap 10.2.2) were used to calculate sediment budgets of the Haringvliet delta and study morphological changes over time. This was done by subtracting the bed level heights of consecutive bathymetries and calculating sedimentation over time. The results gave insight in the erosion and deposition trends 1970 to 2012.

The computer model Delft3D with SWAN incorporated for wave modelling was used to study the sediment transport over profile lines over the period 1970 to 2012. The outcomes of the research conducted with the GIS program (ArcMap 10.2.2) and the computer modelling were compared to validate the computer modelling.

Figure 16 shows the zones to which will be referred in the rest of this thesis. The total area consists of zone 1, zone 2 and zone 3 together. The inner area consists of zone 1 and zone 2. The outer area is zone 3. Zone 3 is the outer boundary of the total area because all four bathymetries had bathymetry information up to this line.

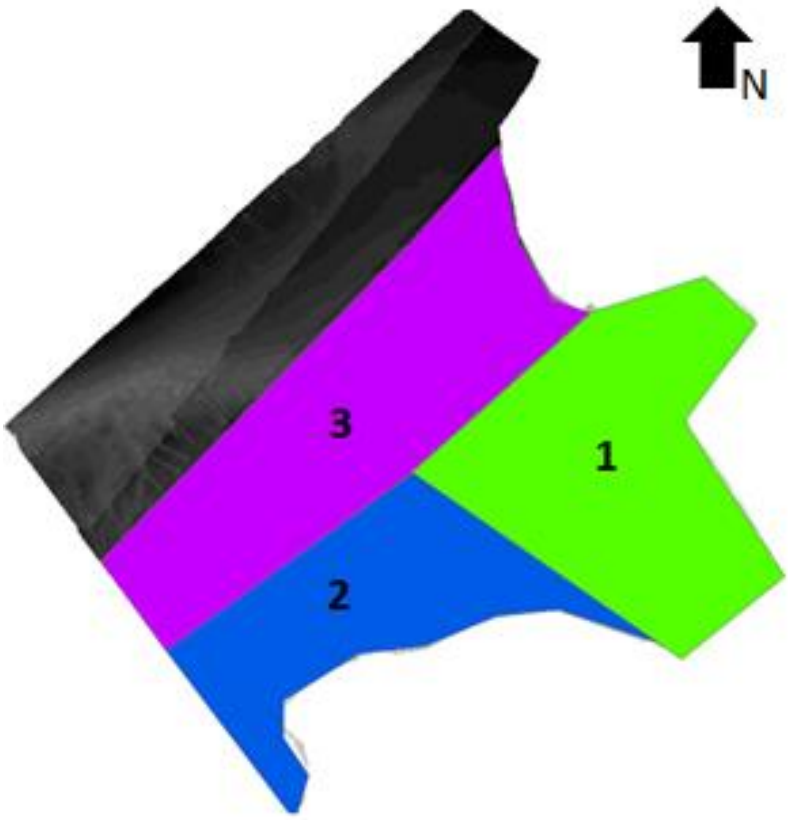

Figure 16. Division of the Haringvliet area in three zones.

The present study was not conducted to reproduce reality as closely as possible. The relative changes between simulations were researched to be able to understand topography and geometry changes and how they have influenced wave and tidal behaviour and sediment transport.

3.2 Methodology of input

3.2.1 Bathymetry data

The bathymetry files used for the present study were acquired from Rijkswaterstaat (2015). From 1927 onwards, Rijkswaterstaat measured the coastal bottom topography every three to seven years. The frequency of the measurements depends on financial resources and the need for monitoring. In the early days the measurements were done with standard ships. These ships interpolated water depth measurements with the available water level data to acquire bathymetry. In 2002 all measurements were done with direct measurements using echomeasurements and laseraltimetry. According to a report of the NAM (a Dutch oil company) no significant differences between the two types of methods could be found (NAM, 2010). Rijkswaterstaat produced bathymetry data with a grid cell size of 20 meter x 20 meter. Furthermore, Rijkswaterstaat provided internal reports and online

water information on (tidal) water levels and wave heights of their measurement stations in the Dutch waters (Waterberichtgeving Rijkswaterstaat, 2015).

The present study worked with the bathymetry files of 1970, 1984, 1998 and 2012 because the period since 1970 up to as far as possible in the future were needed for this research. The bathymetries were selected on the basis of the extent of their coverage of the area of interest. Furthermore, it was convenient that they all had 14 years in between consecutive bathymetries for comparison of morphological changes.

3.2.2 Delft3D

The Delft3D-FLOW module was used in its 2DH depth averaged mode (Delft3D-FLOW User Manual, 2014). Six types of model simulations were performed per bathymetry that could be grouped into three scenarios (Table 2). The simulations were all modelled as short-term models. The first scenario is the only wave scenario. In this scenario no tidal influence was modelled. The second scenario is the only tide scenario, in this scenario only the mean tidal range and realistic phase of the tide was modelled for four M_2-tidal cycles. The third scenario is the wave and tide combined scenario. Lastly, a storm scenario is modelled, which is a combined wave and tide model as well.

Table 2. Model simulations per bathymetry.

Bathymetry	Wave	Wave	Tide	Wave and Tide	Wave and Tide	Storm
1970	Wave direction 220°	Wave direction 310°	M_2 tidal simulation	Wave direction 220° and Tide	Wave direction 310° and Tide	North-western storm
1984	Wave direction 220°	Wave direction 310°	M_2 tidal simulation	Wave direction 220° and Tide	Wave direction 310° and Tide	North-western storm
1998	Wave direction 220°	Wave direction 310°	M_2 tidal simulation	Wave direction 220° and Tide	Wave direction 310° and Tide	North-western storm
2012	Wave direction 220°	Wave direction 310°	M_2 tidal simulation	Wave direction 220° and Tide	Wave direction 310° and Tide	North-western storm

For the Delft3D modelling three grids were implemented per bathymetry (Figure 17). Several grids had to be used to properly simulate the tidal propagation along the coast. These three grids were nested into each other. First, the simulation with the outer grid was completed. The water levels and sediment transport results from this outer grid were implemented on the seaward boundary of the middle grid. Then, the middle grid simulation was completed. Again, the water levels and sediment transport results from the middle grid were implemented on the seaward boundary of the inner grid. Finally, the inner grid simulation was completed.

Figure 17. The nested grids for the 1970 simulation.

The largest bathymetry for the outer grid was acquired via the European Marine Observation and Data network (EMOD). This grid and its bathymetry were based on bathymetry data of 2013 (EMOD, 2015). The grid cell size was enlarged from 189.5 meter x 189.5 meter to 379 meter x 379 meter to decrease computation time. The total size of the grid was 44.0 kilometer in longshore direction and 44.3 kilometer in cross-shore direction. The medium sized grid used the same bathymetry as the outer grid. However, the grid cells were kept at their original size of 189.5 meter x 189.5 meter. This extra middle grid was implemented since the refinement factor from one grid to the next had to be below 5 (Delft3D-FLOW User Manual, 2014). The longshore stretch of this grid was 34.3 kilometer whereas the cross-shore length was 24.4 kilometer. Only the bed level of the smallest (inner) grid therefore changed per scenario according to the bathymetry of 1970, 1984, 1998 and 2012. The dimensions of the smallest grids are given in Table 3.

Table 3. Dimensions of the inner grids used in the computer modelling.

Bathymetry of year	Longshore length (m)	Cross-shore length (m)
1970	26360	14640
1984	26400	15360
1998	26040	15680
2012	18600	18800

To define the accurate grid cell size for the finest grid several considerations had to be taken into account. First of all, the bathymetrical and geographical features which were important for the modelling had to be covered by 5 to 10 grid cells. Secondly, the bottom steepness had to be taken into account. SWAN needs smaller grid cells in areas with steep slopes to be able to compute the wave transformation in the form of shoaling, refraction and bottom friction accurately over steep slopes. Lastly, the computation time was considered. Refining the grid cells once results in squaring the computational time (Delft3D-FLOW User Manual, 2014). All these points were considered and resulted in a fine grid with a grid cell size of 40 m x 40 m (Table 4). For the parameters and their values used in Delft3D, see Appendix C – Parameters.

Table 4. Characteristics of the three grids used in the computer modelling.

Model bathymetry	Model size	Grid resolution	Simulation time step	Simulated physical processes
EMOD (outer grid)	44.0 km x 44.3 km	379 m	1 min	Tidal flow Sediment transport Waves Wave-induced flow
EMOD (middle grid)	34.3 km x 24.4 km	189.5 m	7.5 s	Tidal flow Sediment transport Waves Wave-induced flow
Rijkswaterstaat (inner grid)	Depends see Table 3	40 m	1 s	Tidal flow Sediment transport Waves Wave-induced flow

3.2.3 Wave simulations

To model the evolution of waves in the Haringvliet area the SWAN model was used. It solves the spectral action balance equation. SWAN accounts for a wide range of wave related properties such as wave generation by wind, dissipation due to white capping, bottom friction and depth-induced breaking. Waves always propagate down wave in SWAN. This results in up-wave values being imposed on down-wave grid cells (Delft3D-WAVE User Manual, 2014). The standalone wave model set-up was the same as for the nested tidal simulation. The same three grids were used because the area of interest was supposed to be sufficiently far away from the outer boundaries of the wave grid (Holthuijsen, 2007). Boundaries are fully absorbing for waves that propagate towards the open sea or those running into the coast unless defined differently. Therefore, no reflection of short period waves was apparent in the present study. For an in-depth review of the wave formulas used and the interactions in SWAN, the reader is referred to Booij and Holthuijsen (1999), the Delft3D-WAVE Manual (2014) and Holthuijsen (2007).

The influence of waves was studied by implementing two types of waves, waves from the northwest (310 degrees) and waves from the southwest (220 degrees). These waves account for over 50% of the waves currently reaching the Goeree Lightvessel (Table 1, Tönis et al., 2002). In SWAN the waves from the northwest were modelled from the seaward boundary (orientation northwest). The waves from the southwest could originate from both the seaward longshore and the southern cross-shore boundary of the outer grid (northwest and southwest orientation). The waves were modelled using realistic values for wave height, peak period and directional spreading (Table 5).

Table 5. Wave characteristics of the two types of waves modelled, information provided by Tönis et al. (2002).

Wave direction (degrees)	Wave height (m)	Peak period (s)	Directional spreading (degrees)
310	1.28	5	10
220	1.49	5	25

3.2.4 Tidal simulations

Harmonic analysis strives for separating the harmonic components of an extensive set of tidal data. The assumption is that a tidal signal can be reproduced by a known number of harmonic terms (Pugh, 1987). In the present study only the M_2-tide is prescribed to the open boundaries of the grid because it is the most important tidal component along the Dutch coast. The Europlatform dataset of 2014

provided the mean tidal amplitude for the seaward boundary of the model grid (Waterberichtgeving Rijkswaterstaat, 2015). The mean amplitude on the southern side of the outer grid is 0.8364 m.

A common way to describe the behaviour of the tidal wave propagating along the coast is by implementing a water level boundary on the seaward side of the model and Neumann boundaries on the lateral sides. The Neumann boundaries were used to accommodate the alongshore water level gradient. Neumann boundary conditions were implemented on the northern and southern boundaries for all flow models for numerical stability reasons (Roelvink and Walstra, 2004).

The lengths of the seaward open boundary and the lateral boundaries were used to calculate the alongshore water level gradient. The corner points of the seaward boundary were called A and B (Figure 18). The southern lateral boundary consisted of corner point A, and the point closest to the coast, A'. The northern lateral boundary consisted of corner point B, and the point closest to the coast B'. The distances for the largest (outer) grid are given in Table 6.

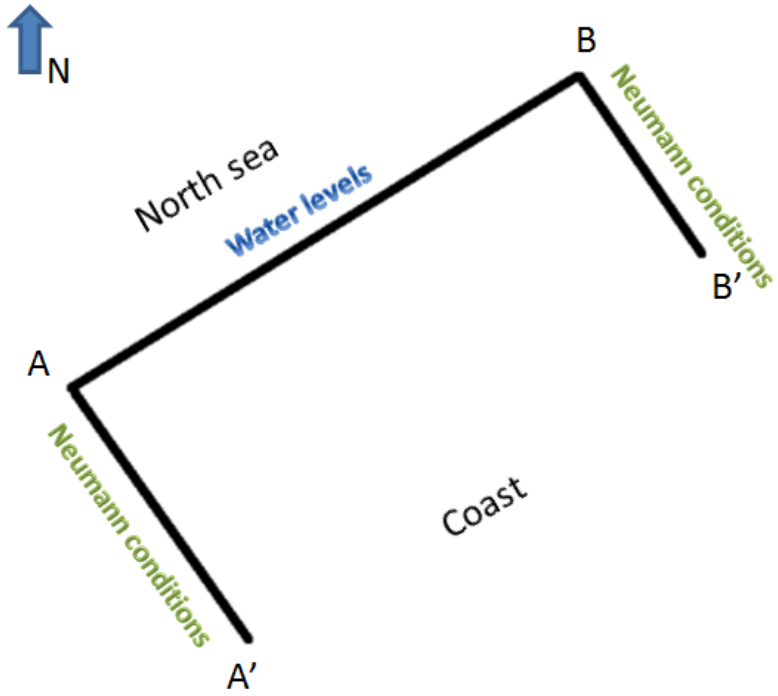

Figure 18. Conceptual drawing of the tidal implementation in Delft3D.

Table 6. Lengths of the segments of the outer grid.

Segment	Length (m)
Seaward boundary (A – B)	43964
Southern boundary (A – A')	33352
Northern boundary (B – B')	33352

The wave celerity at the seaward boundary and the wave celerity at the coastline were calculated by the water depth at the seaward boundary and at the coastline. These were respectively 25 m and 1 m for the outer grid.

Equation 2

$$c = \sqrt{gH}$$

c = wave celerity (m/s)
g = gravitational constant (9.81 m^2/s)
H = water depth (m)

The period of the M_2-tide (s) was used to calculate the frequency. The wave celerity was used to calculate the wave length.

Equation 3

$$L = \frac{2\pi c}{f}$$

L = wave length (m)
f = frequency (rad/s)
c = wave celerity (m/s)

The wave length was necessary to calculate the wave number at both the seaward boundary and at the coastline.

Equation 4

$$k = \frac{2\pi}{L}$$

k = wave number
L = wave length (m)

The wave number was used to calculate the phase at every corner point of the grid. For example, the phase at B was calculated as given below.

Equation 5

$$\varphi b = kdAB + \varphi a$$

φb = phase at B (degrees)
φa = phase at A (degrees)
k = wave number
dAB = Distance between A and B (m)

The amplitude at the Neumann boundaries at both corner points is given by the formula:

Equation 6

$$a = \frac{(\boldsymbol{\varphi a} - \boldsymbol{\varphi b})}{dAB\pi/180} * Z$$

a = amplitude on Neumann boundaries (-)
φa = phase at A (degrees)
φb = phase at B (degrees)
dAB = Distance between A and B (m)
Z = amplitude of tidal signal (m)

For a detailed description of the processes and the other equations used in the modelling with Delft3D, the reader is referred to the Delft3D-FlOW User Manual (Deltares, 2014), Lesser et al. (2004) and van Rijn et al. (2004).

3.2.5 Waves and Tidal simulations combined

The combination of waves and tides and their relative influence determines the morphological and sedimentological response in mixed-energy tidal systems (Herrling and Winter, 2014). In this research due to time constraints it was chosen to only let the waves influence the flow simulation and not the other way around. This is called offline coupling. Stationary wave forcing is added to the flow simulation. This caused wave-induced currents, enhanced turbulence, enhanced bed shear stress and set-up by waves to be included in the simulation (Holthuijsen, 2007). This type of modelling had some disadvantages. Namely, the effect flow has on waves via set-up, current refraction and enhanced bottom friction was not taken into account. The coupling interval between the wave model and the hydrodynamic (tidal) model was set to 10 minutes to reduce computation time.

3.2.6 Storms

The present study simulated one specific storm and analysed its impact on the Haringvliet tidal basin. Specifically, the differences between the impact over the period 1970 to 2012 were analysed. The highest waves occur during north-westerly storms since those storms have the longest fetch length. Therefore, the so called Sinterklaasstorm of 5 December 2013 was the storm chosen to be reproduced in the present study. This storm induced a maximum significant wave height of 5.4 meter. The waves were predominantly coming from the northwest (wave direction 310 degrees, Figure 19).

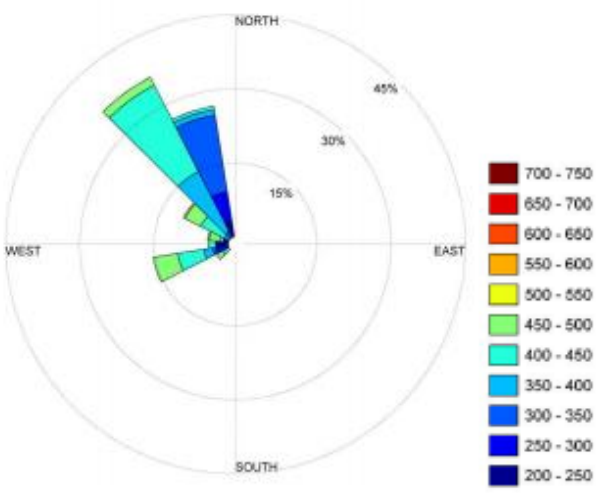

Figure 19. Wave height (cm) and direction of the Sinterklaasstorm at the Europlatform (de Kort, 2015).

At the Goeree Lightvessel, wave heights were roughly between 4 and 4.5 meter. Modelling the significant wave height as 4.5 m was preferred. The storm surge was around 3 meter (de Kort, 2015). The storm surge was implemented in the model by lowering the bottom topography by 3 meter. This caused water depths to increase, which caused tides to propagate faster over the grid and waves to break more inland. The peak period of the waves was 9.1 seconds (Gautier et al., 2014). The spring tide condition present during the Sinterklaasstorm was not taken into account.

3.2.6 Hypsometric curve

Hypsometric curves were calculated for the separate zones (Figure 16). The hypsometric curves were calculated using GIS (ArcMap 10.2.2). With the integer function every value was converted into a round value. The attribute table could then be used to display the number of cells which had a bed level with a range of 0.5 m above and 0.5 m below that value. The accuracy of this method is therefore 0.5 meter. The size of the grid cells was for every bathymetry 20 meter x 20 meter. Therefore, starting

at a bed level height of -15 meter the areas were cumulatively added to obtain the hypsometric curve. The total area was translated into a hypsometric curve for that particular part of the grid showing the area with a bed level height below a certain bottom depth.

3.2.7 Sediment transport

Sediment transport is induced by the increase of bed shear stresses due to a moving fluid over a bed (Masselink and Hughes, 2003). In reality, sediment transport is a feedback mechanism of the morphology of an area. The present study did not include bed level updating but incorporated the redistribution of sediment fractions only (Herrling and Winter, 2014). This was decided because modelling was conducted over four tidal cycles, with only four bathymetries. The median grain size chosen for the computer model was 200 micrometer. With a median grain size of 200 micrometer and without modelling of cohesive sediment the particles are free to behave individually. Therefore, single grain properties are most important for sediment transport in the simulations (Masselink and Hughes, 2003).

Several different transport formulas could be chosen for non-cohesive sediment in Delft3D. In the present study the van Rijn et al. formulas (2004) are used to predict sediment transport. One of the reasons to choose the formulas of van Rijn is that they distinguish between bed load transport and suspended load transport. Bed load transport is taken into account for sediment transport below the reference height and suspended load transport for transport above the reference height. The depth averaged sediment transport is the combined bed load transport vector and the suspended load vector (Equation 7).

Equation 7

$$\vec{q} = \overrightarrow{qb} + \overrightarrow{qs}$$

$\vec{q}$ = depth-averaged sediment transport ($m^3/s/m$)
$\overrightarrow{qb}$ = depth-averaged bed load transport ($m^3/s/m$)
$\overrightarrow{qs}$ = depth-averaged suspended load transport ($m^3/s/m$)

Furthermore, the van Rijn formulas et al. (2004) were chosen because they can predict sediment transport for waves and currents combined. The parameter settings for sediment which were used in the simulations are given in Table 7. For a clear overview of the sediment transport in Delft3D the reader is referred to the Delft3D-Flow User Manual (2014), van Rijn and Walstra (2003) and van Rijn et al. (2004).

Table 7. Sediment parameter settings.

Sediment type	Sand
Specific density (kg/m^3)	2650
Median sediment diameter (D_{50}) (m)	0.0002 (fine sand)
Dry bed density (kg/m^3)	1600
Reference density for hindered settling calculations (kg/m^3)	1600

3.3 Methodology of the analysis

3.3.1 Wave simulations

The two scenarios of stand-alone wave simulations were modelled for all four bathymetries. The significant wave height is the mean wave height of the largest 1/3 of the waves. The decrease in significant wave height indicated where in the grid waves lose most energy. Wave energy is lost due to bed friction and wave breaking. The wave height initially decreases in shallower water after which the

wave height increases rapidly, this is called wave shoaling. The decrease in wave height due to friction may exceed the increase in wave height due to shoaling. This can be recognized by the gradual reduction of the significant wave height over the grid. This results in breaking wave conditions with less energy than offshore wave conditions (Masselink and Hughes, 2003). The results of the orbital velocity near bottom gave an indication of where waves interact with the bed. The orbital motion near bottom stirs the sediment from the bed. This stirred sediment could then be transported by currents. Shortly before waves break, the orbital velocity near bottom is largest. The patterns of significant wave height and near bed orbital velocity gave an overview of the wave behaviour in the area for the period 1970 to 2012.

3.3.2 Tidal simulations

A common way to analyse tides is by calculating tidal ellipses. A least squares harmonic analysis was performed on the tidal current velocities (Pawlowicz et al., 2002). This harmonic analysis resulted in the tidal constituents with their amplitude, frequency and phase. M_2 tidal ellipses were calculated using the amplitude and phase of the M_2 tidal velocity that resulted from the harmonic analysis (Xu, 2000).

A tidal ellipse is calculated by two opposite rotating circular radial vectors. The circular radial vector with the longest diameter defined the rotation direction of the elliptical radial vector. Half of the angle spanned by the two circular radial vectors is the phase angle (Figure 20, Xu, 2000). For the tidal ellipses in the present study the x-axis defined the u-component of the current vector (geometrically) and the y-axis defined the v-component of the current vector. This resulted in a longshore current if the tidal ellipse is directed to the northeast (linear relation between u- and v-component). A dominant cross-shore current was apparent if the tidal ellipse is directed to the northwest (inverse relation between u- and v-component).

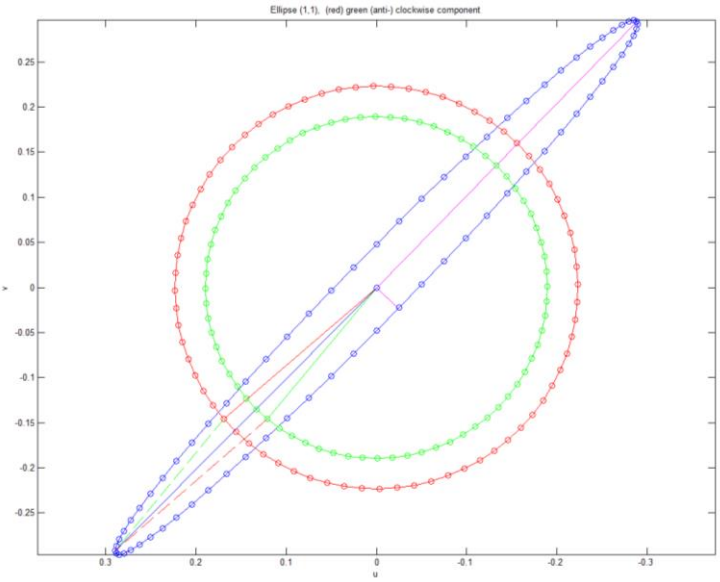

Figure 20. An example of a tidal ellipse. The red circle shows the anticlockwise circular radial vector, the green circle shows the clockwise circular radial vector. The blue ellipse shows the elliptical radial vector. The longest purple vector indicates the maximum current velocity (or semi-major axis). The shortest purple vector indicates the semi-minor axis (Xu, 2000).

The rotation direction of the current vector depends on reflection, the Coriolis effect, topographical and geometrical effects. However, the rotation direction in deep water is mainly controlled by reflection and the Coriolis effect. The locations for which the tidal ellipses were calculated are given in Figure 21. Furthermore, the tidal ellipse parameters semi-major axis, eccentricity and inclination were plotted over the total area. The semi-major axis (SEMA) is the maximum current velocity at a specific location. In deeper waters tidal current velocities are higher than in shallow waters. The ellipse

parameter eccentricity (ECC) is the ratio of the semi-minor axis over the semi-major axis. The smaller the eccentricity the more elliptical the ellipse. Negative eccentricity values mean that the ellipse is rotating in a clockwise direction, whereas positive eccentricity values indicate a counterclockwsie rotation. The inclination is the angle between the semi-major axis and the x-axis (Xu, 2002). At an inclination of approximately 45 degrees the SEMA is directed alongshore. An inclination of approximately 135 degrees indicated a SEMA in the cross-shore direction.

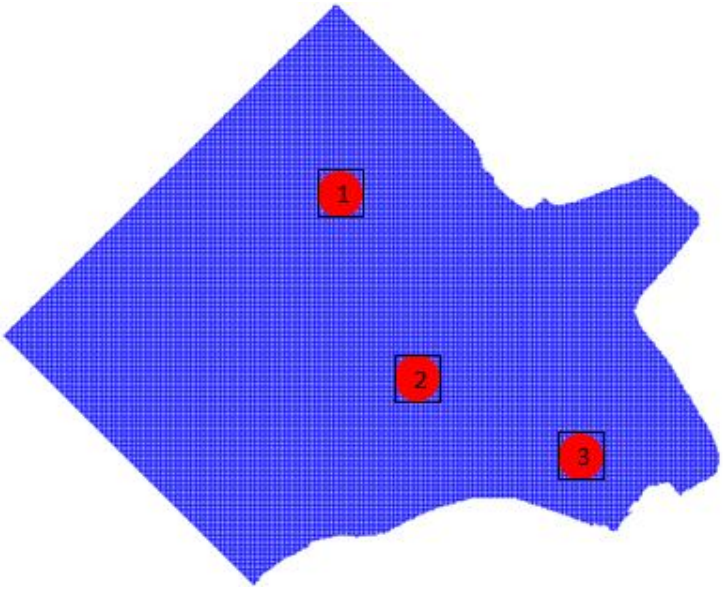

Figure 21. Locations of the tidal ellipses for 1970 (left).

The water level is moving up and down with a period of 12.42 hours when considering only the M_2-tide. Therefore, if the flood and ebb duration and strength are equal, it would appear that there is no net velocity and therefore sediment transport due to tides. However, the tidal sinusoid can be distorted due to topography or geometry. This is called tidal asymmetry. Tidal asymmetry would cause a net (tide averaged) velocity in a specific direction which could then cause net sediment transport. This net velocity is called the residual velocity.

A residual current is apparent when the tidal ellipse is not closed. The residual current could also be affected by density driven and wind-driven flow and therefore by waves. The residual current is normally smaller than 0.1 m/s, but can be important for transport of fine particles. In the end, residual currents are driven by the interaction of the flow with the bathymetry and the coastal geometry (Van Rijn, 2011). When flood tidal currents are larger than ebb tidal currents mainly bed load transport responds. However, when the periods of slack water differ the fine suspended load residual transport is most influenced. The fine sediment has more time to settle to the bottom when slack periods are longer. This results in less suspended sediment in the water column. In the present study mainly coarse fractions (200 micrometer) are taken into account. Because with tidal current velocity differences mainly the coarser fraction (> 100 micrometer) and bed load responds, the residual transport by tides will be mainly caused by tidal asymmetry (Dronkers, 1986).

3.3.3 Wave and Tidal simulations combined

To compare the influence of waves and tides on the resultant velocity vector in the tidal basin the velocity vectors of the wave and tidal simulations were plotted together with the combined wave and tidal simulations. The mean velocities over a tidal cycle on a particular spot on the grid were calculated (Eulerian mean velocity). For the only wave simulations the tidal cycle as such did not exist and the wave induced currents were equal for every time step of 10 min. The magnitude and the direction of the velocity vectors of wave and tidal simulations were analysed.

3.3.4 Sedimentation rates

The bathymetries of 1970, 1984, 1998 and 2012 were used to calculate sedimentation rates using GIS (ArcMap 10.2.2). First of all, the bathymetries were resized in such a way that they all represented the same part of the Haringvliet tidal basin and could be compared (Figure 16). Deliberately, the Maasvlaktes 1 and 2 were left out of the sediment budget calculations to prevent them from disturbing the sedimentation rate results.

After resizing the images from two consecutive bathymetries, the older bathymetry was subtracted from the younger one. This resulted in an image of the change in height over the period covered by the two bathymetries. Secondly, the mean grid cell height of the resultant image after subtraction was multiplied by the grid cell size. The number of grid cells was multiplied by the mean grid cell height and the grid cell size. This resulted in the total sediment gained or lost over the fourteen years in between the two bathymetries. To be able to compare with the computer modelling, the total sediment volume gained over 14 years was recalculated to the sedimentation rate in a particular area in m^3/s.

To research if there were large yearly variations, a more dense set of bathymetries needed to be considered. The years of which a complete bathymetry image of the Haringvliet tidal basin was available were: 1970, 1972, 1976, 1979, 1980, 1984, 1986, 1989, 1992, 1998, 2003 and 2012. The same method was used to research the trends of erosion and sedimentation.

Extensive dredging has taken place in the Slijkgat. Part of this dredged sediment was dumped again in the area covered by the white rhombus in Figure 22. The dredge and dump values were provided by Rijkswaterstaat and are given in Appendix A – Dredging and dumping. The dumping location where the dredged material is released was not included in zone 1 + 2. Therefore, only the dredging values were added when calculating the sedimentation rates in the inner area.

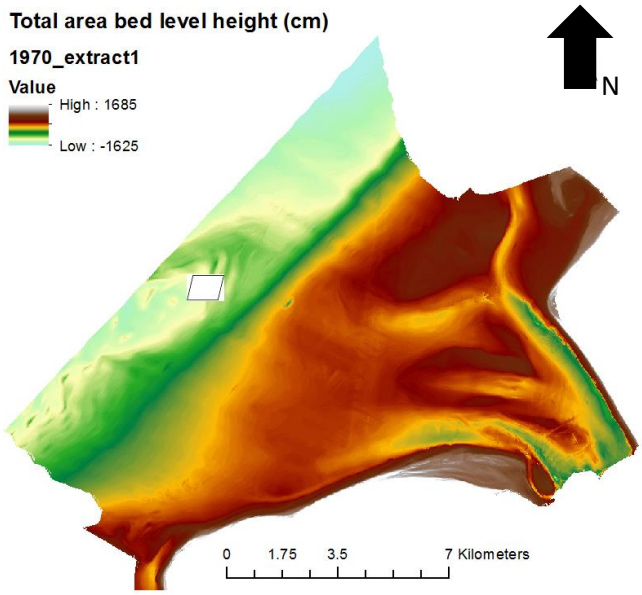

Figure 22. The bathymetry of 1970. The dump location was indicated by the white rhombus (Rijkswaterstaat, 2015).

The Delft3D model was also used to calculate the mean total transport in m^3/s in both the total area and the inner area. The results from GIS could be compared with the modelling results. The sediment transport simulated by Delft3D was calculated by looking at sediment transport over profile lines for one tidal cycle. The profile lines used were the outer boundaries of the total area and the outer boundaries of all three zones separately. The sediment transport rate was calculated in $m^3/s/m$ over the profile line. The mean over this profile line was then multiplied by the number of grid cells over which that profile line was drawn. The result was multiplied by 40 because of the grid cell length in the

inner grid. The total net output or input of sediment per zone was compared with the values obtained from the analysis of the bathymetry data.

The sedimentation rates per bathymetry were calculated for the tidal and wave combined simulations and the storm simulations. The sedimentation rates per situation were accounted for by their relative occurrence of their normal appearance over a year. Therefore the tidal simulation combined with waves with wave direction 220 degrees accounted for 52.5% of the time, the tidal simulation combined with waves of wave direction 310 degrees accounted for 46.5% of the time and the storm accounted for 1% of the time. The total sediment transport into or out of a zone was then calculated per bathymetry.

The influence of waves and tides separately on sediment transport was calculated by the sediment transport over profile lines of the wave only simulations with wave direction 220 degrees and wave direction 310 degrees and the tide only simulations. These results were compared with the results of the combined wave and tidal simulations. The influence per zone of waves and tides on transport could then be compared.

4. Results

4.1 Wave simulations

The significant wave height in the total area of waves with wave direction 310 degrees was compared to waves with wave direction 220 degrees. It was found that the 310 degrees simulations have higher wave heights in the inner grid than the simulation with waves with wave direction 220 degrees (Figure 23 and Figure 24). Even though, the implemented wave height for waves with wave direction 220 degrees was 21 cm higher than for waves with wave direction 310 degrees. Apparently, the waves with wave direction 220 degrees lose almost all their energy before reaching the inner area. Since waves from the southwest encounter the shallow Grevelingen part of the Voordelta, wave energy is lost. The 310 degrees waves maintain most of their energy because they propagate over deeper parts of the grid. The water depth on the seaward boundary of the inner grid is between 15 and 20 meters. The wave length is around 30 meters. Waves interfere with the bottom at a water depth which is approximately half their wave length. This interference with the bottom and the simultaneous loss of energy is therefore already taking place on the seaward side of the inner grid. When waves dissipate they decrease in height, which was shown by the decrease in significant wave height over the inner grids.

The resultant significant wave heights close to the Haringvliet sluices were up to 0.4 meter for the 310 degrees waves. The simulations with wave direction 220 degrees showed a significant wave height of only 0.3 meter close to the Haringvliet dam. In 1983 the significant wave height at the Haringvliet sluices was between 0.6 and 1.0 meter according to wave measurements of Rijkswaterstaat (Waterberichtgeving Rijkswaterstaat, 2015). The exact significant wave heights for the wave directions that were implemented in the present study could not be found. However, the real wave height is significantly higher than the only wave data of the models show. This might be due to lack of hydrodynamic coupling of waves with tides, lack of winds or simply a misrepresentation of reality by the model. Furthermore, the waves were implemented on the outer grid 44 kilometer of the sluices. The wave characteristics used were measured at the Goeree Lightvessel, 20 kilometer of the coast of the Haringvliet. This difference might have influenced the resulting significant wave height at the sluices as well.

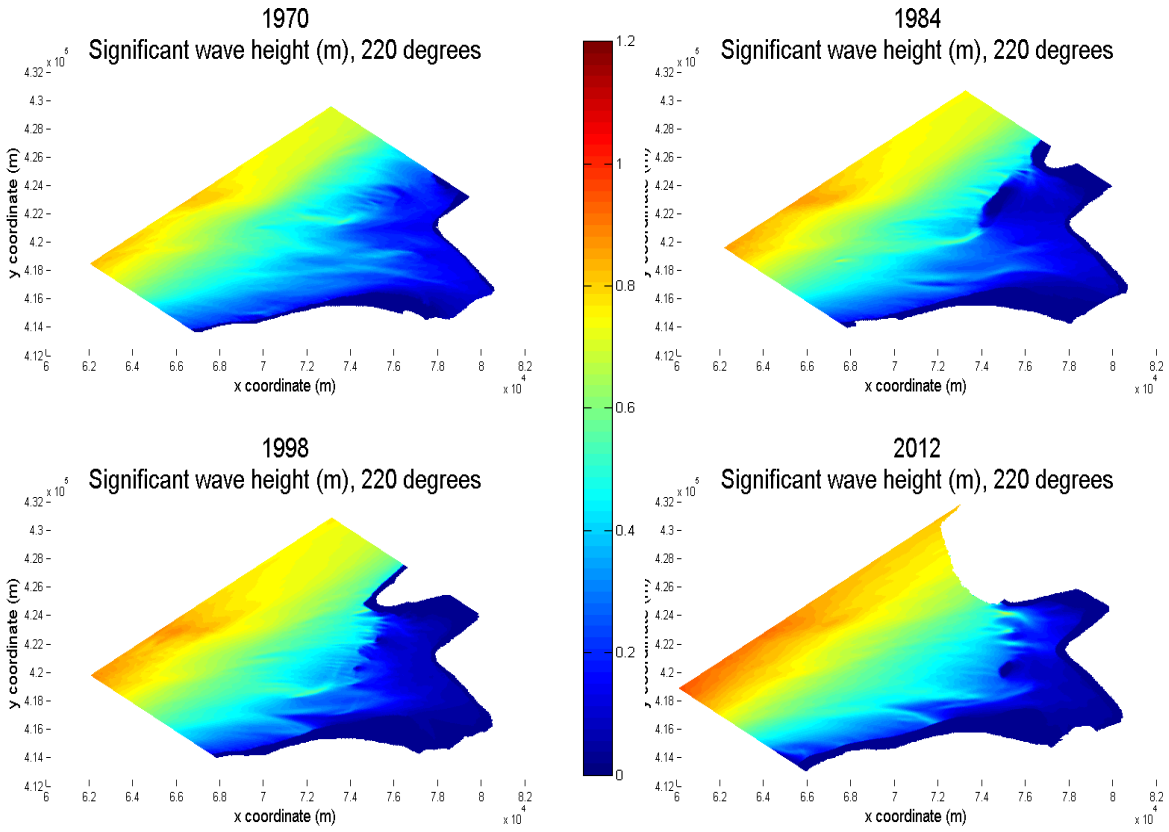

Figure 23. Significant wave height (m) modelled per bathymetry year for wave direction 220 degrees.

The significant wave height in the inner grid for waves of both directions changed significantly over time. First of all, the inland migration of the delta front could be recognised by the higher significant wave heights at the seaward boundary of the grid from 1970 to 2012. Especially for waves with wave direction 220 degrees. This is due to the water depth increase close to the seaward boundary of the grid when the delta front migrates inland. Waves dissipated less and therefore maintained a larger part of their significant wave height.

Secondly, the evolution of the shoal Hinderplaat is clearly recognisable. In 1970 the shoal Hinderplaat is not very pronounced yet. The waves dissipate over a large area and far into zone 1. In 1984 the shoal Hinderplaat increased in bed level height and became elongated. This is clearly visible in the sudden decrease of the significant wave height, due to all waves breaking on this shoal. This was concluded because the significant wave height inland of the shoal became 0 meter. In 1998 the shoal Hinderplaat fragmentised in several parts and migrated landward. Therefore, waves do break in the proximity of the shoal Hinderplaat, but not all on the same longshore stretch. In 2012 the shoal Hinderplaat turned landward. Due to the migration of the Hinderplaat inland the significant wave height in the inner area increased. Waves could penetrate further into zone 1, even though the bed level height was in general higher than for previous years.

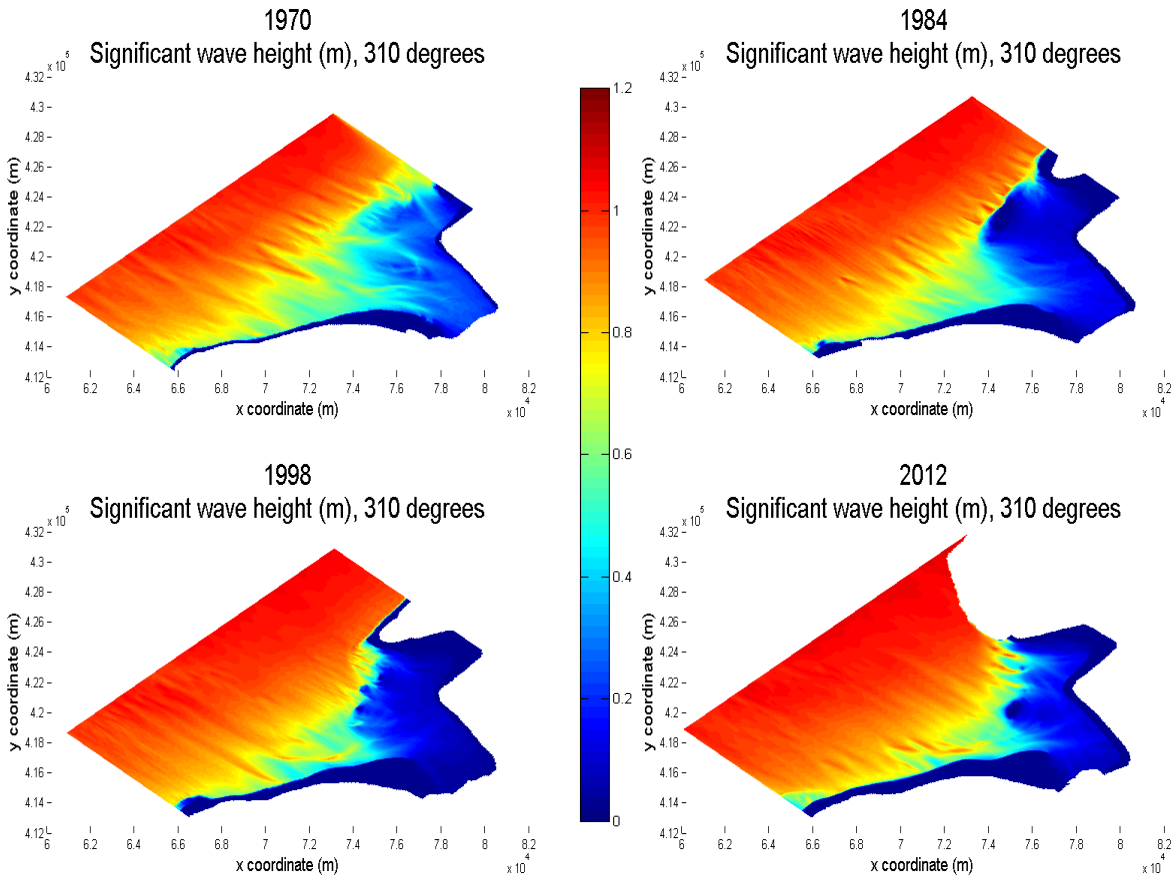

Figure 24. Significant wave height (m) modelled per bathymetry year for wave direction 310 degrees.

For waves with a wave direction of 220 degrees the orbital velocity near bottom results are presented in Figure 25. Orbital velocity near bottom indicates where the waves interact with the bed. The waves stir the sediment from the bottom, which can then be transported by the currents. There is a lot of widespread orbital velocity near bottom for the simulation with the bathymetry of 1970. In 1984 and 1998 the orbital velocity near bottom is highly concentrated on the Hinderplaat shoal. In 2012 orbital velocity near bottom decreases slightly, moves inland and appears more fragmentised. This is caused by the heightening of the inner area in general in 2012. Waves dissipate more gradually over the inner area.

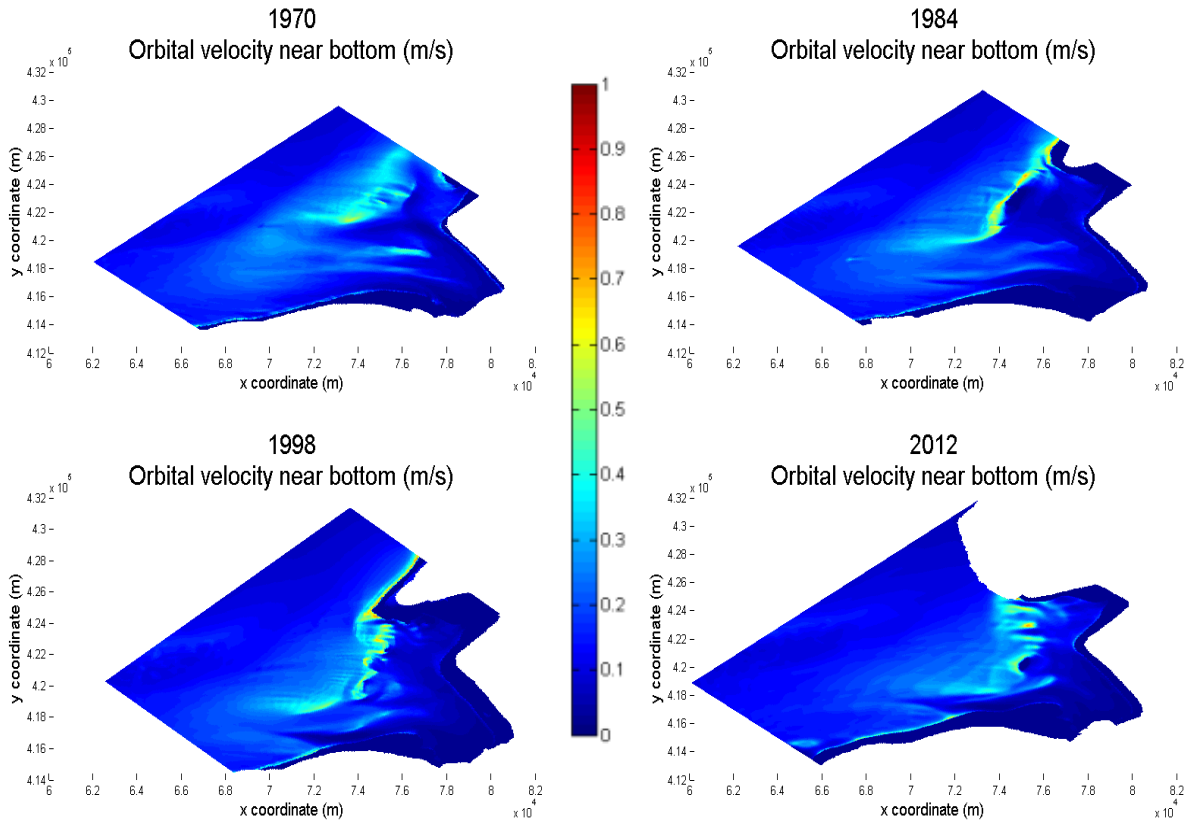

Figure 25. Orbital velocity near bottom (m/s) for standalone wave simulation with a wave direction of 220 degrees.

The orbital velocity near bottom for waves with a wave direction of 310 degrees is presented in Figure 26. Similar trends are noticeable as for the simulations with waves coming from the southwest (220 degrees). They differ mainly in magnitude. Where the waves with wave direction 220 degrees had orbital velocity magnitudes around 0.4 to 0.5 m/s, the orbital velocity near bottom for waves with wave direction 310 degrees reached magnitudes of around 0.8 m/s. This was probably caused by the maintenance of energy as described for the significant wave height as well.

The large orbital velocities on shallower areas with magnitudes as high as 0.8 m/s were caused by relatively high waves arriving at areas with low water depth (water depth ~ 0.5 m). Due to the grid cell size of 40 meter x 40 meter the water depth can greatly differ between two consecutive grid cells, there is a large slope. A wave travelling from on grid cell to the next suddenly experiences a large water depth decrease and breaks. This breaking caused a wave induced set-up, which then created a wave induced current.

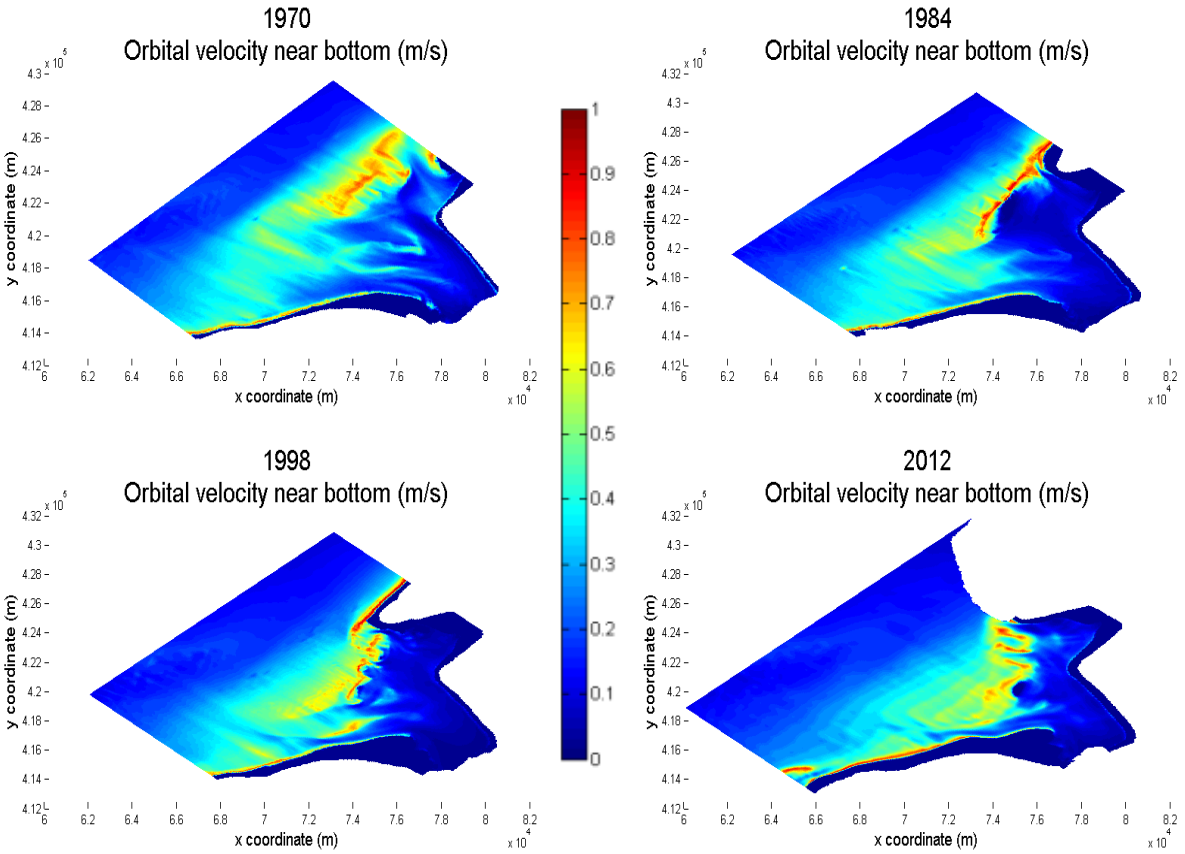

Figure 26. Orbital velocity near bottom (m/s) for standalone wave simulation with a wave direction of 310 degrees.

4.2 Tidal simulations

First of all, the tidal ellipses at the three locations were compared. In Figure 27 the tidal ellipses are given for location 1, which is the most offshore location. All three tidal ellipses are directed to the northeast which indicates longshore behaviour. At the most offshore location, longshore behaviour was expected because the tidal wave propagates along the Dutch coast. There is no confinement of the tidal flow by shallower areas. For all years there is a small residual current apparent of a few cm/s.

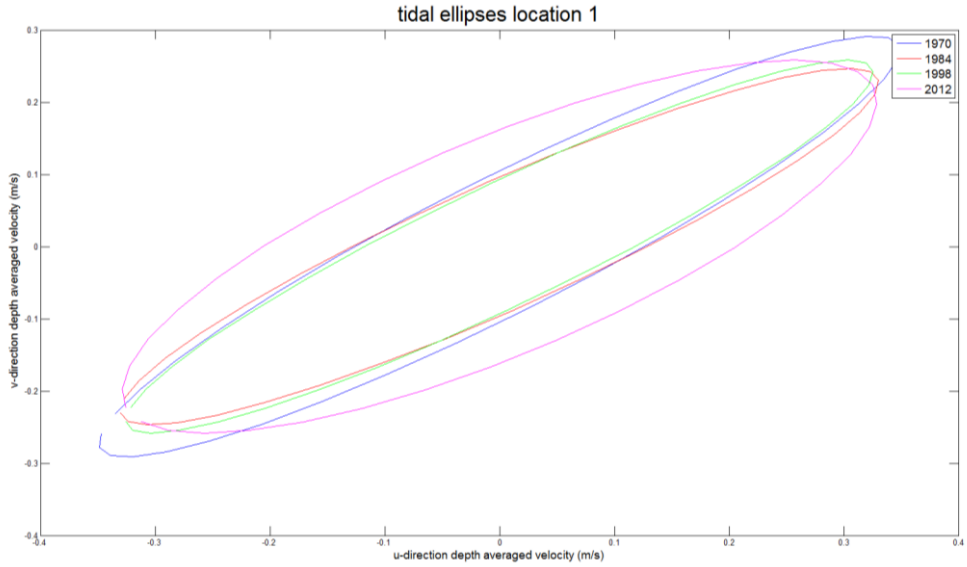

Figure 27. Tidal ellipses at location 1.

In Figure 28 the tidal ellipses for location 2 can be found. All ellipses showed lower velocities in v-direction compared to the tidal ellipses at location 1. The semi-major axis of the tidal ellipses of 1970, 1984 and 2012 were again longshore directed. The main current velocities were in the u-direction. In 1998 the tidal current direction was mainly in the cross-shore direction at location 2.

Location 2 is westward of the shoal Hinderplaat for the bathymetries of 1970 and 1984 with a height below MSL of approximately 4 meter. However, due to movement of the Hinderplaat location 2 was situated on top of the Hinderplaat for the bathymetry of 1998. The height below MSL was only 2 meter. In 2012 location 2 was situated seaward of the shoal Hinderplaat due to inland migration of the Hinderplaat. In 1970 the channels were mostly directed in u-direction. In 1984 the channels became more longshore directed due to influence of waves. However, the channel westward of the Hinderplaat was still directed in the u-direction. In 2012 the littoral drift seaward of the Hinderplaat was directed in the u-direction. Therefore, the inclinations of the 1970, 1984 and 2012 ellipses were almost horizontal. In 1998 the tide moves over the shoal Hinderplaat at location 2. It is not confined by a channel or littoral drift. Therefore, the tidal ellipse has a lower eccentricity and its semi-major axis is cross-shore directed.

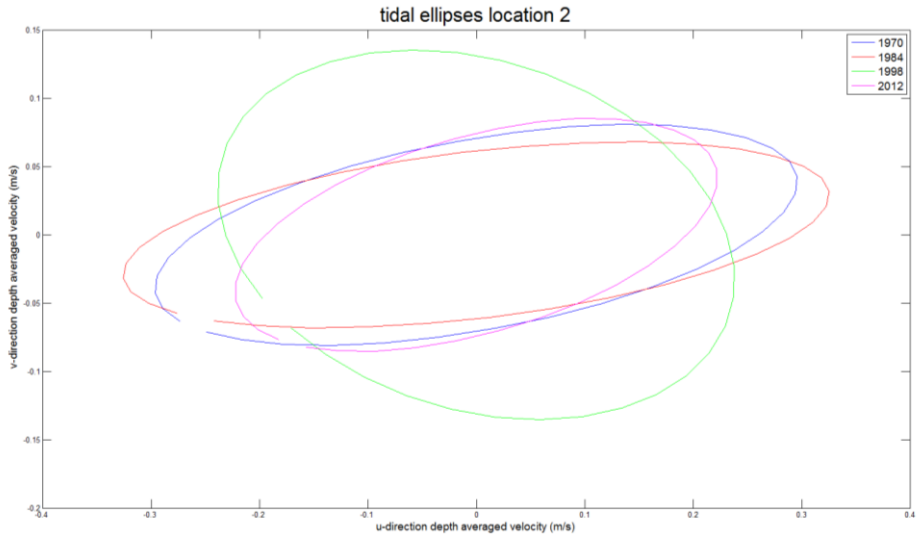

Figure 28. Tidal ellipses at location 2.

The tidal ellipses calculated for location 3 all had an inclination of 6 to 11 degrees (Figure 29). Location 3 is located in the main channel Slijkgat. These tidal ellipses show that for the bathymetry of 1970 the current velocities in the u- and v-direction at location 3 in the Slijkgat were approximately only halve of the velocities met in 1984, 1998 and 2012. Furthermore, the inclination angle is somewhat lower than for the 1984, 1998 and 2012 tidal ellipses. This could be caused by the land extension and spit growth in the southern Haringvliet tidal basin. De Kwade Hoek extended from 1984 onwards and forced the currents to propagate around it. That caused a more longshore behaviour of the tidal currents.

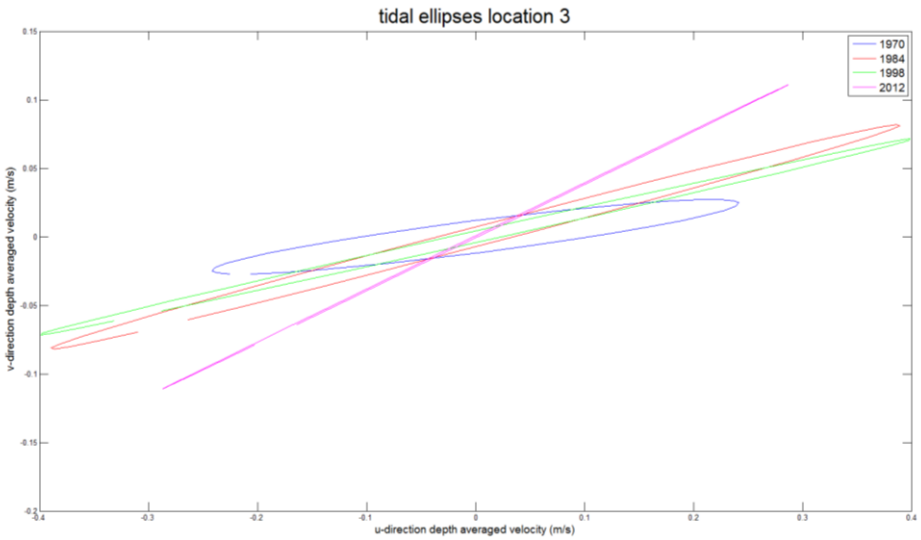

Figure 29. Tidal ellipses at location 3.

The above three figures gave an indication of what tidal ellipses are and how they differ over several locations in the Haringvliet tidal basin. The M_2 tidal ellipse parameters semi-major axis (SEMA), eccentricity (ECC) and inclination (INC) are shown in Figure 30, Figure 32 and Figure 33.

In 1970 the maximum tidal current velocities are approximately 0.5 m/s. In the inner area and at the shoal Hinderplaat maximum velocities barely reach 0.2 m/s. The shoal Hinderplaat is easily recognisable because it is confined by two channels. Furthermore, there is a sharp transition zone from the deeper waters to the shallower waters defined by the 0.3 m/s maximum velocity line. The SEMA in 1984 showed a similar pattern as for 1970. However, there are some distinct differences. First of all, the shoal Hinderplaat became a lot thinner and elongated, which is recognisable by the low SEMA-values on the Hinderplaat. Furthermore, only the channel to the southwest of the Hinderplaat with larger SEMA's than the surroundings was still apparent. The channel Slijkgat became the main channel. That is shown by the larger SEMA of the Slijkgat. The tidal current could propagate deep into the Slijkgat.

In 1998 the shoal Hinderplaat fragmentised into several smaller bars. This caused the tidal current to accelerate on the channels in between those small bars. This resulted in large SEMA's in between the higher areas. Even though the areas on which acceleration took place were not significantly deeper than other areas in the Haringvliet tidal basin. Due to the forcing of flow through these small depressions the SEMA increased. The Slijkgat was dredged, which caused higher SEMA here as well. The channel to the southwest of the Hinderplaat almost completely filled. In 2012 the entire inner area became shallower, which could be concluded from the maximum SEMA becoming lower. Furthermore, the inland migration of the shoal Hinderplaat is recognisable. The SEMA accurately responded to the bed level changes.

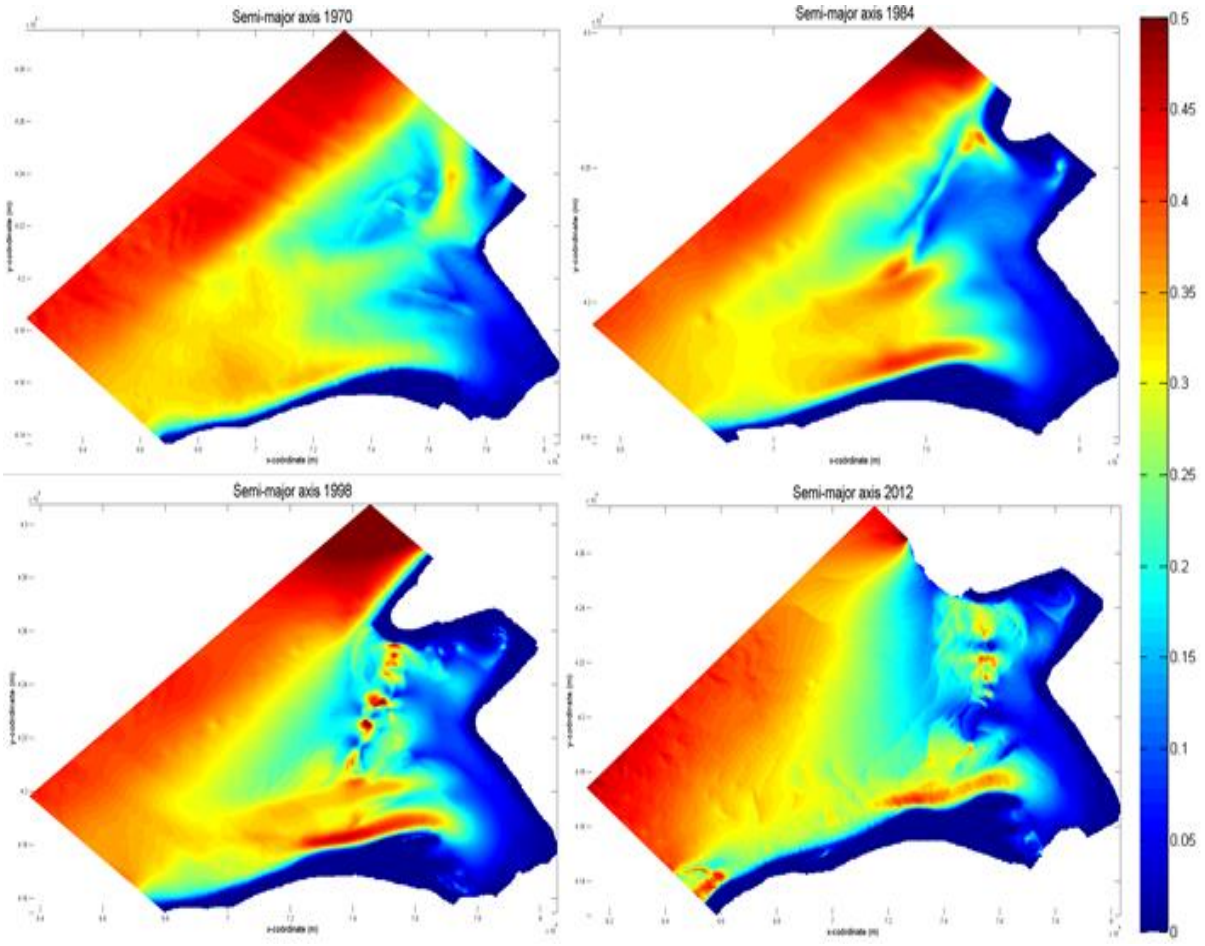

Figure 30. Semi-major axes (m/s) of the tidal ellipses per year.

Tidal current vectors rotated in a counter clockwise direction in the Haringvliet area (Figure 32). Only south-eastward of the Kwade Hoek, some clockwise rotation of the tidal current vector was found. In 2012 inland of the spit features of the Hinderplaat clockwise rotation was found as well. This is probably caused by the appearance of recirculation cells behind the spits. These recirculation cells appear because the tidal current could not propagate neatly around the bar. The angle was too large. Therefore, the current 'shoots' past the bar. That caused a difference in water level height behind the bar. This could result in a recirculation cell in the opposite direction as the dominant current (Figure 31).

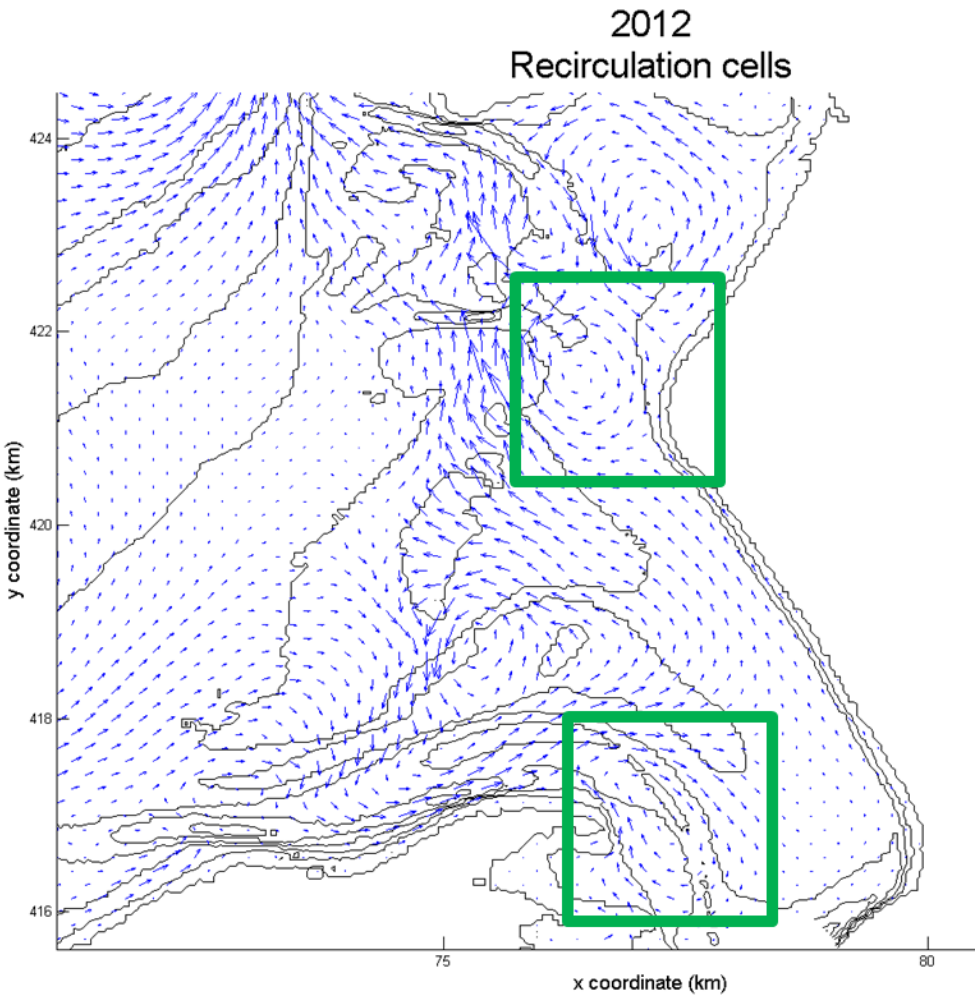

Figure 31. Recirculation cells in 'tide only' simulation 2012.

The eccentricity plots for the four tidal simulations are shown in Figure 32. From the eccentricity in 1970 it seems that the eccentricity increased on shallower areas, such as the shoal Hinderplaat and the area between the channel Rak van Scheelhoek and the Slijkgat. The semi-major axis was smaller on shallower areas. Therefore, it could be assumed that the semi-major axis on shallower areas was smaller, whereas not necessarily the semi-minor axis increased as well.

Similar trends could be found in 1984. The same features showed a large eccentricity. The eccentricity plot showed that the eccentricity is less instantaneous than the SEMA. It showed a more gradual transition from low eccentricity values towards higher eccentricity values. It could therefore be argued that the semi-minor axis increased more continuously than the semi-major axis decreased. Therefore, the semi-minor axis should become smaller more gradually than the SEMA. Furthermore, a clockwise rotation behind the developing spit feature on the southern shore was more pronounced. The blue areas with clockwise rotation reveal recirculation cells. In 1998 the eccentricity was highest on shallow areas. The eccentricity of 2012 showed a slightly different pattern. The lines of equal eccentricity were not parallel to the shoal Hinderplaat anymore. This was probably caused by change in direction of the tidal current due to the land extension Maasvlakte 2. Furthermore, clockwise rotation was found behind the spit attached to the Hinderplaat as well.

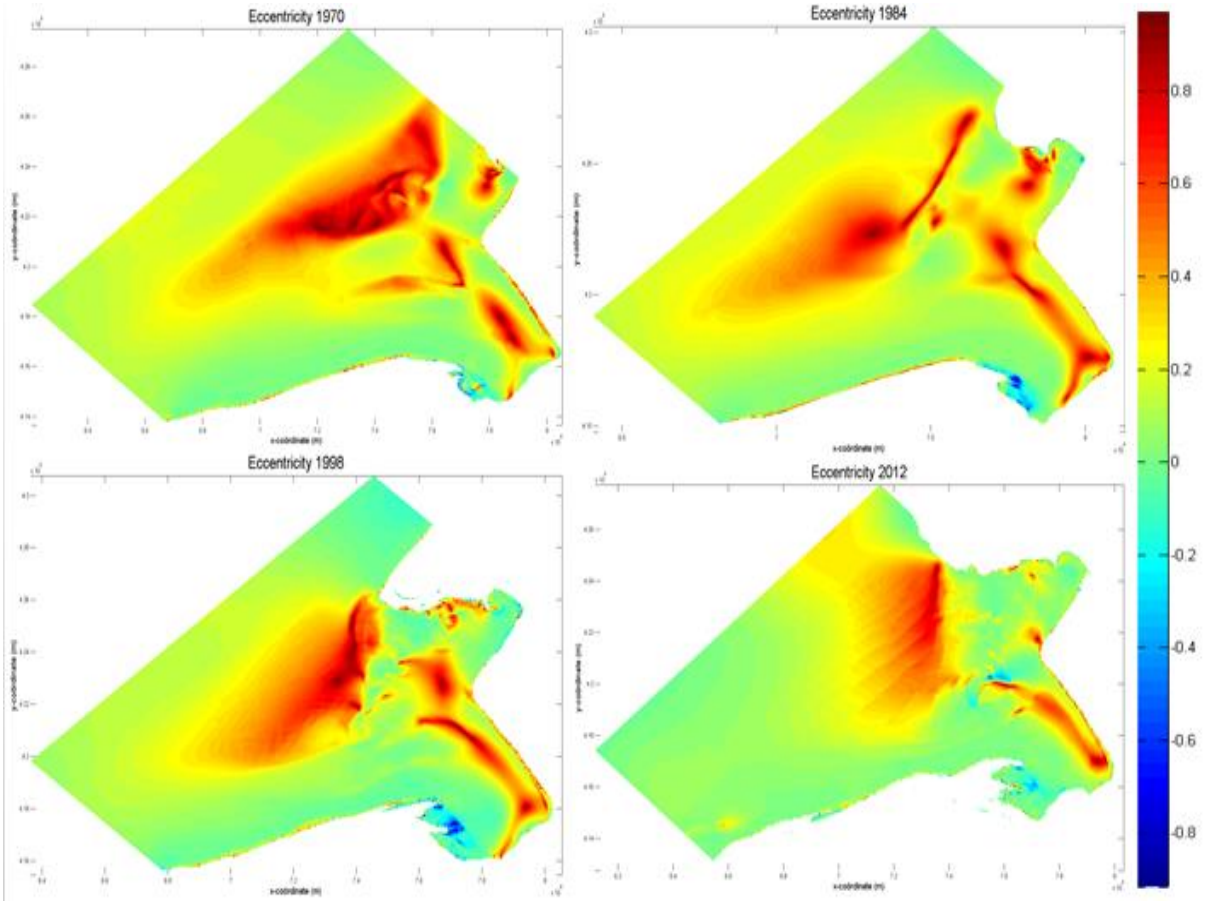

Figure 32. Eccentricity of the tidal ellipses per year.

The inclination colourplots showed the angle of the SEMA with the x-axis (Figure 33). In 1970 in deep water seaward of the shoal Hinderplaat, the tidal ellipse was approximately directed alongshore. On shallow areas the inclination was red or very dark blue indicating a SEMA parallel to the x-axis. In 1984 the Hinderplaat shoal had an almost horizontal inclination (INC of 160 to 20 degrees). The land extension above the Slufter forced the tidal currents to move around it, thereby adjusting the inclination in those areas. In 1998 the Hinderplaat had a more widespread influence which caused inclination values to differ more over the inner area. Furthermore, the shoal Garnalenplaat became more pronounced which is visible in the inclination values. The migration of the shoal Hinderplaat inland is visible as well in the inclination values in 2012. High spatial inclination differences were apparent in zone 1 and 2.

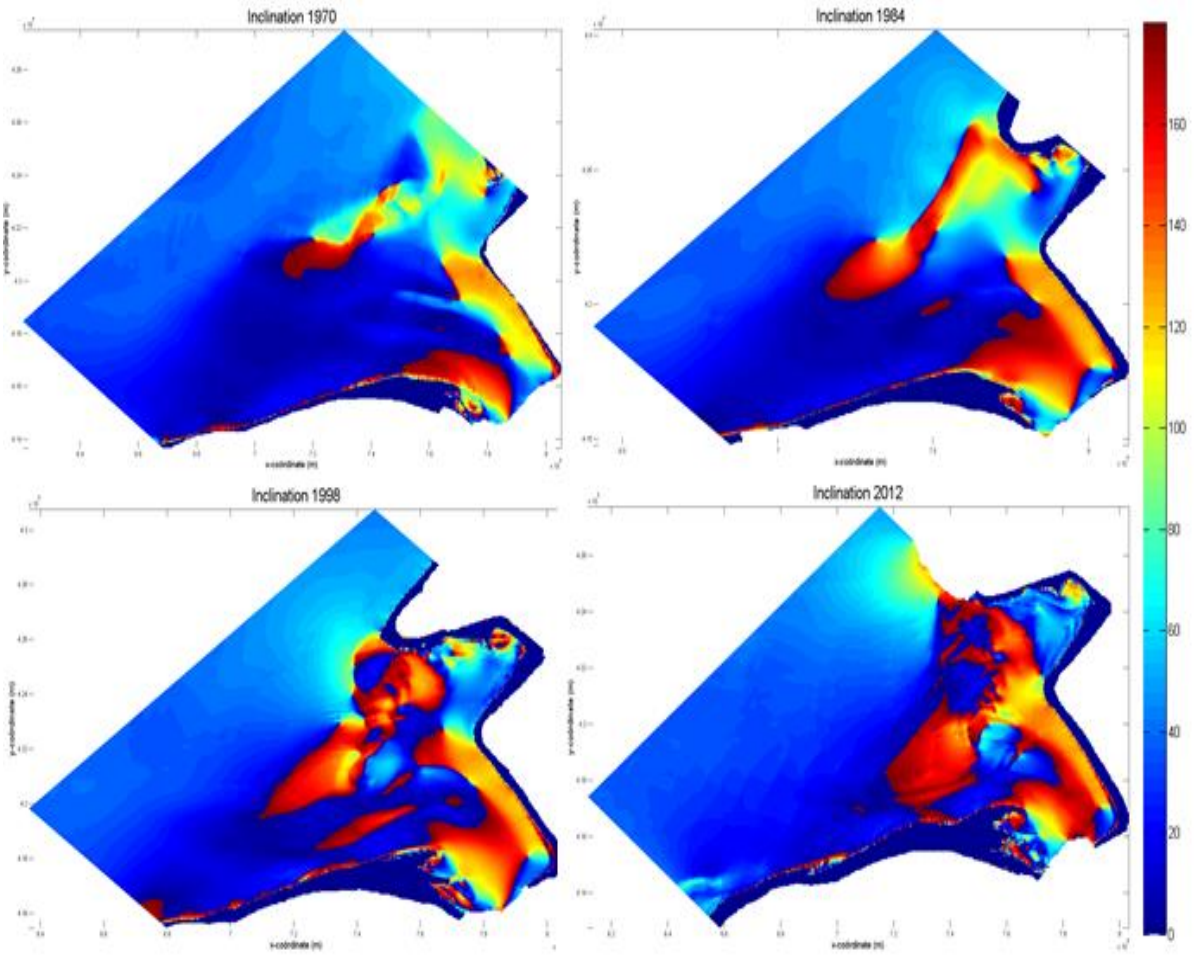

Figure 33. Inclination (degrees) with respect to the x-axis of the tidal ellipses per year.

4.3 Waves and Tidal simulations combined

For five types of computer simulations the direction of the mean velocity will be discussed (Figure 34 and Figure 35). The simulations depicted here were the standalone wave (wave direction 220 degrees and 310 degrees), standalone tide and the combined simulations. Only every 30th grid cell was shown in Figure 34 and Figure 35 to show general transport directions.

The wave only simulation with wave direction 220 degrees showed largest velocities up to 0.05 m/s on the Hinderplaat shoal. This was caused by the breaking of waves which cause wave induced set-up. This resulted in a current cross-shore in landward direction. In general most wave energy in 1970 is directed towards the eastern boundary of the Haringvliet. This caused the landward turning of the shoal Hinderplaat. For the bathymetry of 1984 the wave only simulation showed largest velocities directed towards the sluices. Maximum velocities for the only wave simulation were up to 0.07 m/s. The wave only simulation of 1998 showed similar velocity magnitude as in 1984. However, there were very high velocities found on the north-eastern side of the grid as well. In 2012 the velocity vectors of the only wave simulation were maximum around 0.04 m/s. In the inner area of the grid they were mostly directed to the northeast.

The tide only simulation with the bathymetry of 1970 resulted in a downdrift pattern. During flood the tide entered the Haringvliet basin from the southwest and left from the northeast (Tönis et al., 2002). Apparently, the flood directed currents downdrift are stronger than the ebb-directed currents directed updrift. This could be the result of the alongshore water level gradient to the northeast apparent along the southern Dutch coast (Sha and van den Berg, 1993). Strongest flow velocities are found on the north-eastern side of the Haringvliet inner area where it had to move around Maasvlakte

1. The tidal current was forced through a very small Hindergat. These could have caused the small ebb-tidal delta formation at the end of the Hindergat noticed in the bathymetries. The 1984 only tides simulation showed a similar pattern. The 1998 only tides simulation had more difficulty to move around the extended land extension seaward of the Slufter. In 2012 the tides only simulation showed slightly smaller mean velocities. Especially in the midsection of the grid. This is probably caused by the lower lying bed levels in this midsection due to the landward migration of the delta front. This deepening of the bed caused less tidal asymmetry. In general a decrease in tide induced currents in the most landward part of the inner area was found.

The simulation combining waves with wave direction 220 degrees and a tidal simulation showed approximately a combination of the two separate simulations. For 1970 this combination was found over the entire grid. Largest velocities were found at the north-eastern part of the grid. It was expected that the eastern boundary received a lot of sediment. The combined simulation for the bathymetry of 1984 did not always represent the wave only and tide only simulations evenly. Especially, the high wave velocities were not reproduced in the combined simulation. This was caused by higher friction due to tides, which resulted in smaller velocities for the combined simulation. The spit of the Hinderplaat was forced inland and low flow velocities were simulated in both main channels, Rak van Scheelhoek and Slijkgat. These low flow velocities caused sedimentation in those channels. The bathymetry of 1998 showed the same behaviour for its combined simulation. There were only small mean velocities in the inner area of the grid. Probably due to the infilling of the inner area. A further infilling of the inner area was therefore expected. The 2012 combined simulation showed relatively small mean velocities. The velocity vectors became smaller moving from the southern boundary into the grid. That resulted in sedimentation in the grid. The main flow direction on the western boundary is out of the grid which resulted in some sediment transport out of the grid.

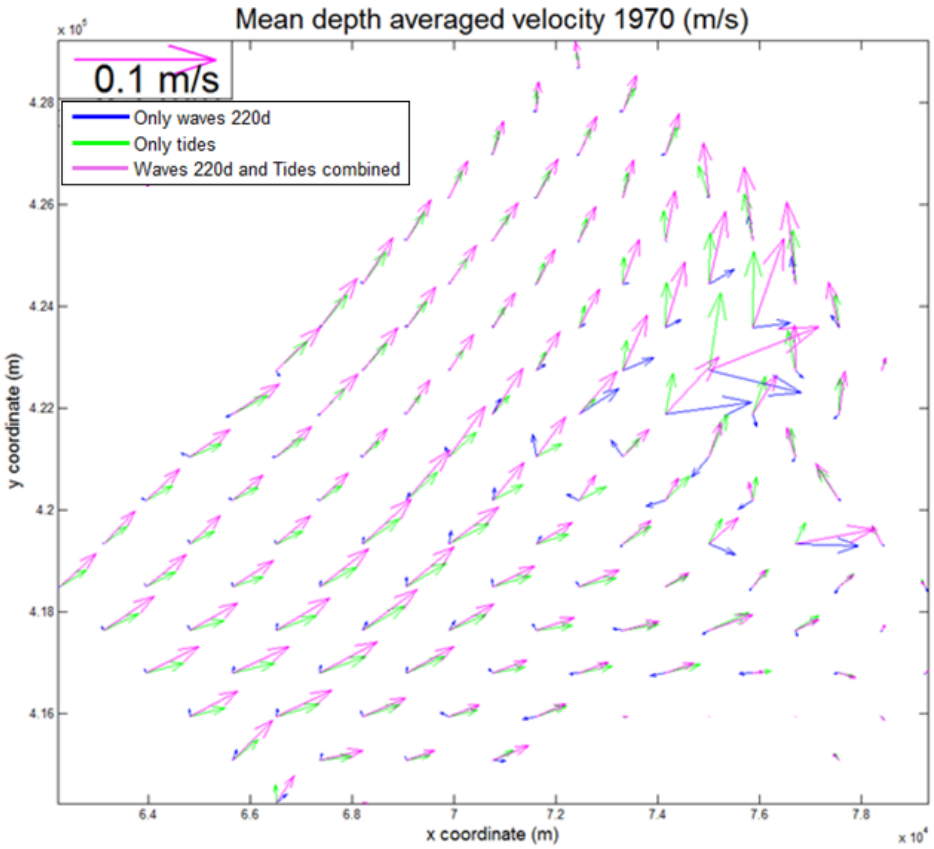

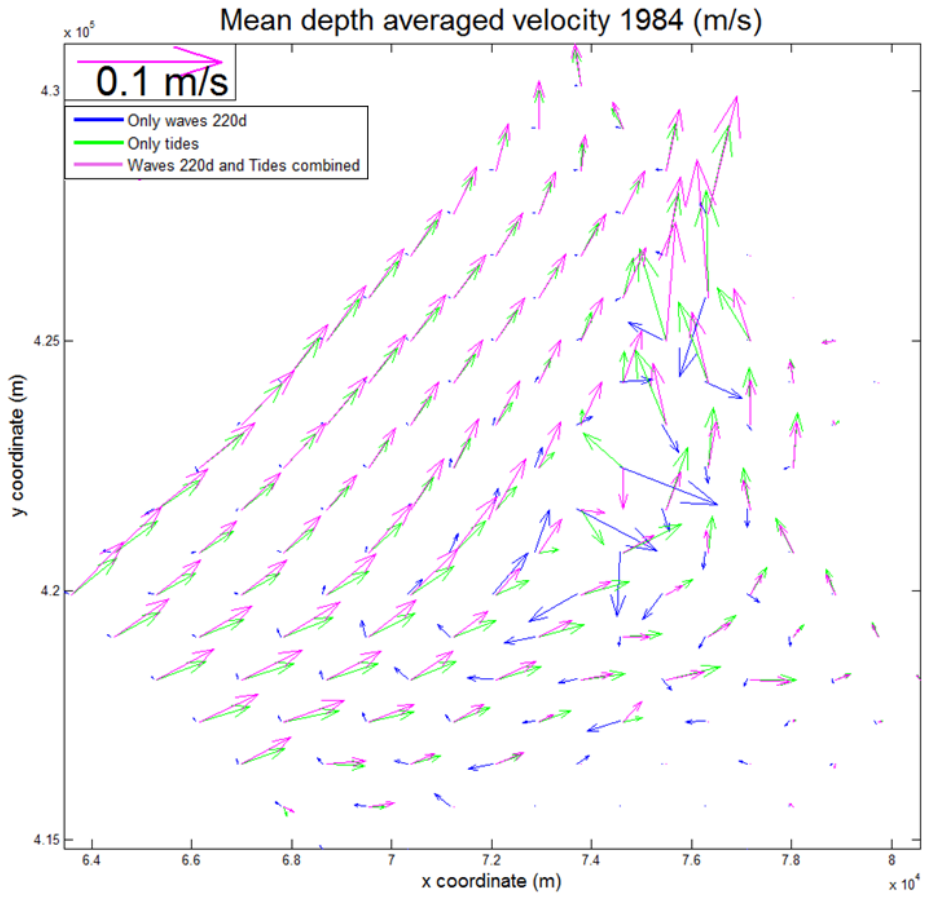
Mean depth averaged velocity 1984 (m/s)
0.1 m/s
Only waves 220d
Only tides
Waves 220d and Tides combined
y coordinate (m)
x coordinate (m)
x 10^5
x 10^4
4.3
4.25
4.2
4.15
6.4
6.6
6.8
7
7.2
7.4
7.6
7.8
8

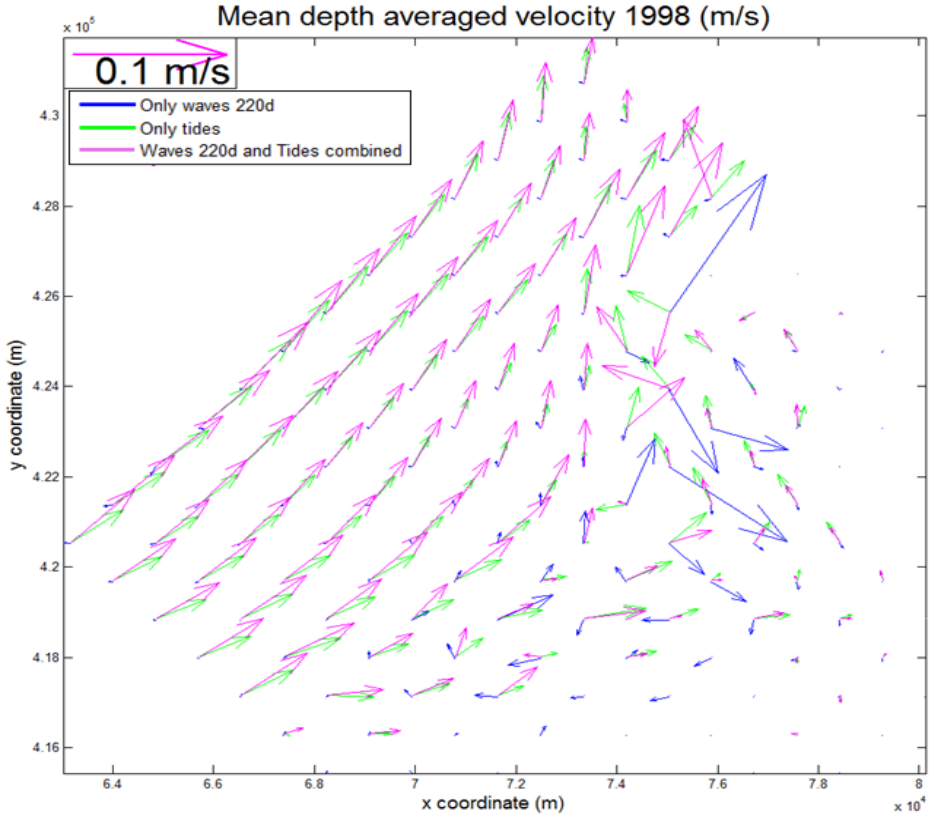
Mean depth averaged velocity 1998 (m/s)
0.1 m/s
Only waves 220d
Only tides
Waves 220d and Tides combined
y coordinate (m)
x coordinate (m)
x 10^5
x 10^4
4.3
4.28
4.26
4.24
4.22
4.2
4.18
4.16
6.4
6.6
6.8
7
7.2
7.4
7.6
7.8
8

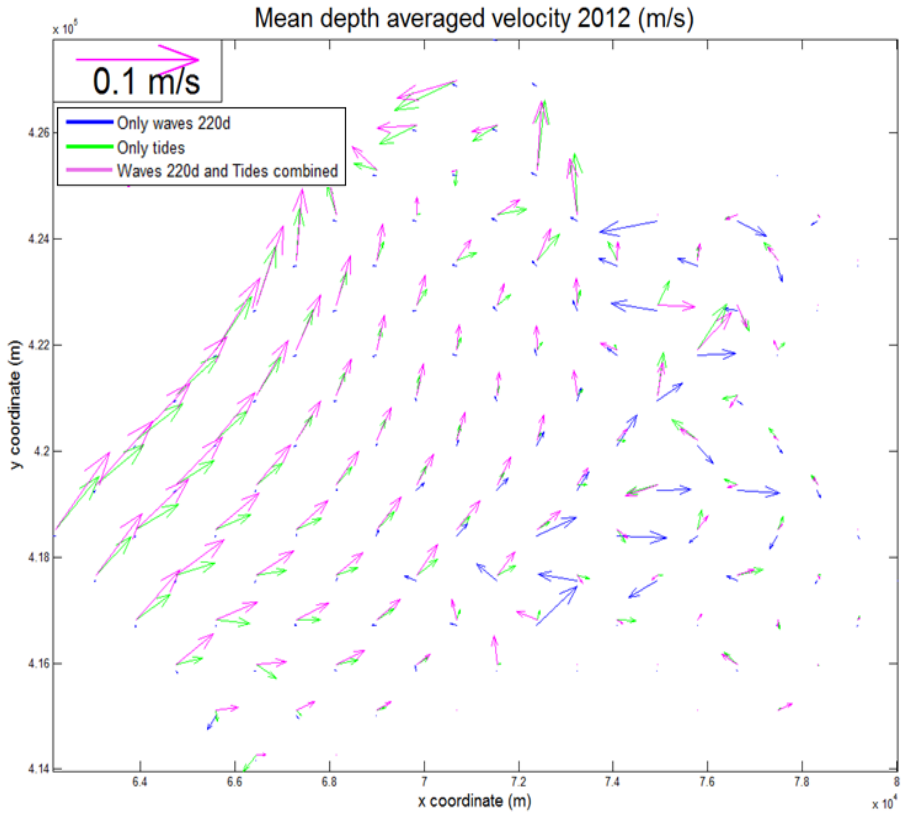

Figure 34. Mean velocity vector plots of the four bathymetries (wave direction 220 degrees).

The wave only simulation for waves with wave direction 310 degrees showed the interesting pattern that those waves stimulate an ebb-directed flow direction. Especially for the simulations 1970 and 1984. They moved into the Haringvliet tidal basin from the north-eastern side and left the inner area from the southwestern side. In 1984 the velocities for the wave simulation were very large, approximately 0.15 m/s. In 1998 and 2012 probably due to the land extensions on the north-eastern side, the updrift behaviour of the wave induced currents is less apparent. Waves could not easily move into the inner area from wave direction 310 degrees because it was sheltered by the land extensions.

From 1984 onwards a littoral drift due to the breaking of waves could be seen on the southern shore in the direction of zone 1. These velocity vectors were linked to the formation of spits from 1984 onwards. The bathymetry of 1998 caused only one very large velocity vector on the Garnalenplaat. The 2012 simulation showed a different pattern. The mean wave induced currents were all directed towards the seaward boundary, whereas the other simulations had some wave energy directed to the inner area. Probably, in 2012 those waves were blocked by Maasvlakte 2.

The tidal simulation combined with waves (wave direction 310 degrees) resulted in downdrift behaviour in the outer area. Therefore, it could be argued that in the deeper areas tidal influence is larger than wave influence. Smaller mean velocities were found in the Slijkgat and Rak van Scheelhoek than for the combined tide and wave simulation with wave direction 220 degrees. Waves (wave direction 310 degrees) approached from the seaward boundary and could therefore not propagate as easily into the Slijkgat. In 1970 there is landward directed mean velocity on the shoal Hinderplaat which is why in 1984 this shoal migrated inland. The mean velocities in the Rak van Scheelhoek were relatively large in 1970 due to its relative depth. In 1984 the mean velocity vectors were in general a lot larger. From 1984 onwards a large velocity vector on the coast on the southwestern side of the grid was found. The only wave simulation (wave direction 310 degrees) showed this velocity vector as well. This could have caused the spit feature clearly recognisable in the bathymetry of 1998. Furthermore,

there was still a landward movement of the shoal Hinderplaat. In 1998 there is some updrift behaviour visible from the Maasvlakte 1. This was probably caused by the recirculation cells in the area which appeared due to the fragmentation of the Hinderplaat (Appendix D - Mean velocity). In 1998 the shoal Hinderplaat was still migrating inland. In 2012 the Hinderplaat consisted of a few bars, which is why the mean velocity vectors pointed in different directions. The overall direction in 2012 was towards the western boundary due to the Maasvlakte 2 interrupting longshore behaviour.

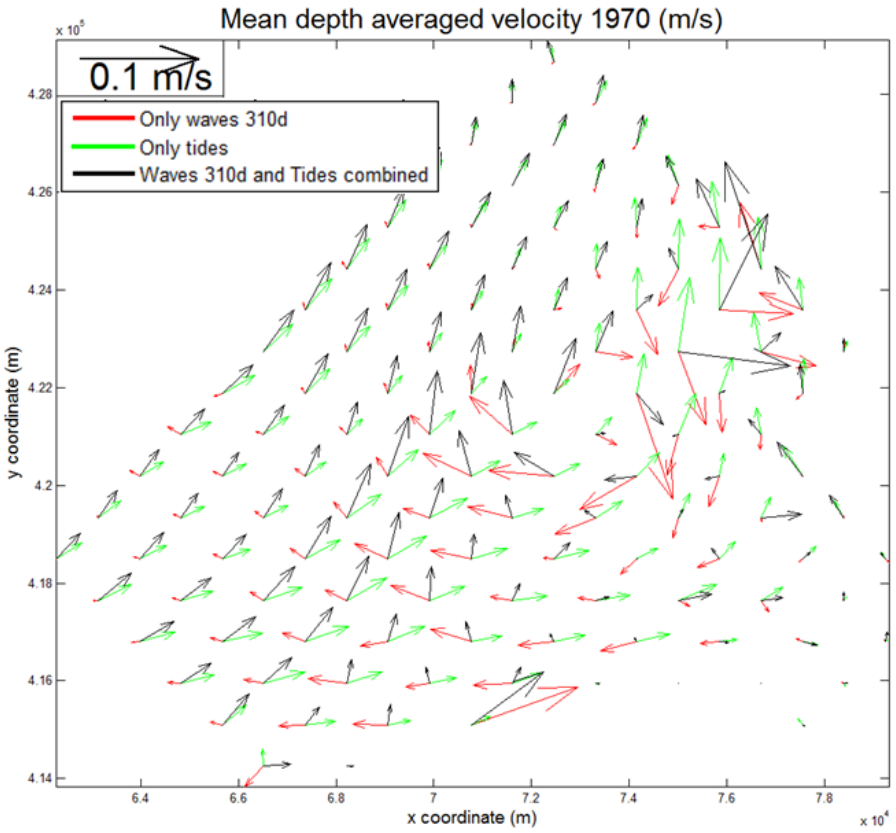

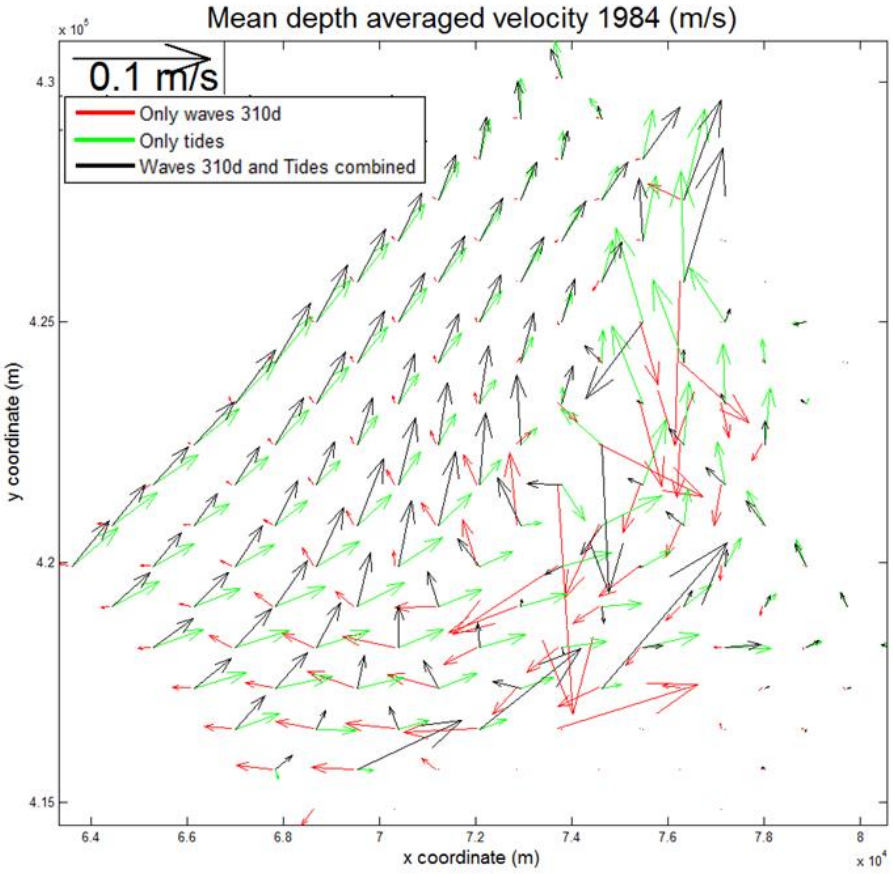
Mean depth averaged velocity 1984 (m/s)
0.1 m/s
Only waves 310d
Only tides
Waves 310d and Tides combined
y coordinate (m)
x coordinate (m)
x 10^5
x 10^4
4.3
4.25
4.2
4.15
6.4
6.6
6.8
7
7.2
7.4
7.6
7.8
8

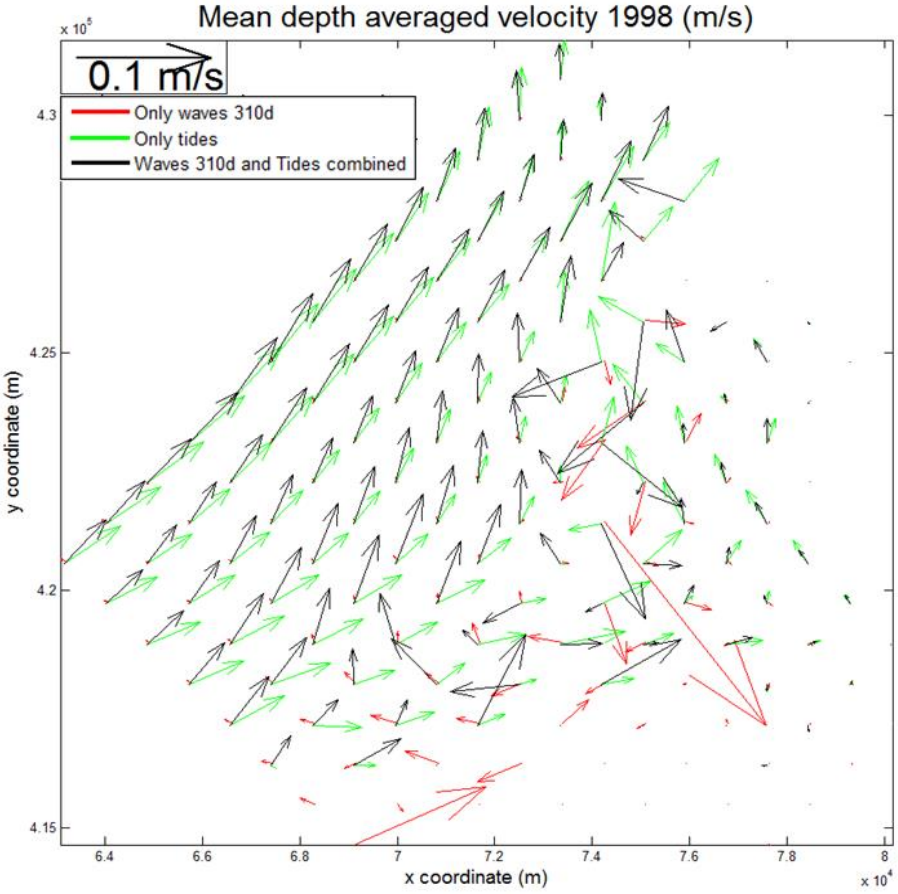
Mean depth averaged velocity 1998 (m/s)
0.1 m/s
Only waves 310d
Only tides
Waves 310d and Tides combined
y coordinate (m)
x coordinate (m)
x 10^5
x 10^4
4.3
4.25
4.2
4.15
6.4
6.6
6.8
7
7.2
7.4
7.6
7.8
8

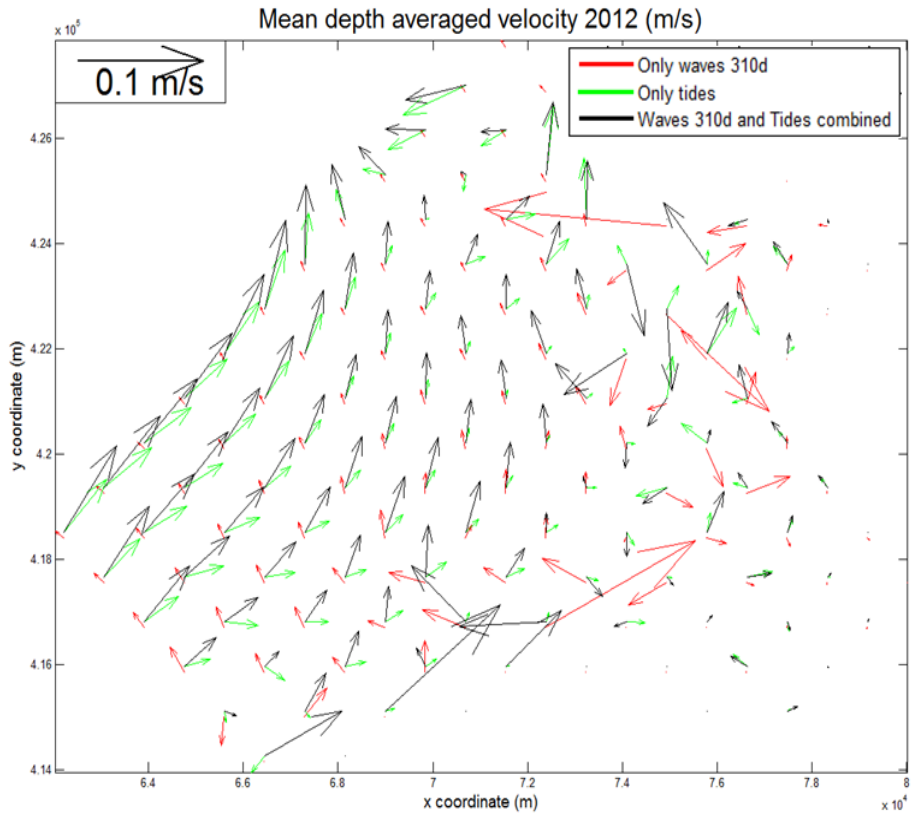

Figure 35. Mean velocity vector plots of the four bathymetries (wave direction 310 degrees).

The velocities induced by waves on the shoals were probably larger than they were in reality. This was caused by a too coarse grid on the shoal fronts because of which wave transformation could not be modelled properly. A wave propagated into the basin and could maintain a large part of its energy until it reached the shoal. Suddenly, the water depth is only ~ 0.5 m which resulted in wave breaking. This resulted in wave induced set-up, which caused high wave induced flow. In reality, those waves would have dissipated more gradually resulting in smaller velocities.

The waves with wave direction 220 degrees stimulated the mean velocity of the tide in the outer area (downdrift). However, the waves with wave direction 310 degrees propagated approximately perpendicular to this mean velocity direction. Therefore, although the maximum velocities of those waves are larger than for waves with wave direction 220 degrees, they contribute less to the mean velocity vector of the waves and tides combined.

The combined wave and tide direction seemed to be mostly influenced by the wave induced velocity on the shoals. However, in the deeper areas and in the channels tidal influence was largest. It could be argued that currents were dominant longshore directed on the seaward side of the grid, mainly due to tides. More inland the cross-shore landward direction of the velocity vector were predominant, caused by waves.

4.4 Storm simulations

For the storm modelling the significant wave height offshore was 3.4 m at location 3 for all simulations. The relative wave influence was expected to increase during storm conditions. The resultant velocity during a storm is depicted in Figure 36. The mean velocity increases during storm conditions (Masselink and Hughes, 2003). In the present study mean velocities of up to 10 times larger than for normal conditions were modelled. Furthermore, for the storm simulations of 1970, 1984 and 1998, in the outer area an ebb-dominated mean velocity pattern was found. The storm waves had a

wave direction of 310 degrees, similar to one of the tidal and wave combined simulations. Because waves are relatively more important during storm conditions than during normal conditions, the updrift wave induced currents caused an overall updrift behaviour. Only the storm simulation of 2012 showed a downdrift pattern in the outer area. Similar as during normal conditions, Maasvlakte 2 sheltered the total area from waves in 2012. This caused the downdrift trend of the tides to be predominant in the area. All simulations showed a strong littoral drift on the south-western coast. High flow velocities from zone 2 into zone 1 are found. Therefore, these storm conditions might have increased the spit features at the Kwade Hoek.

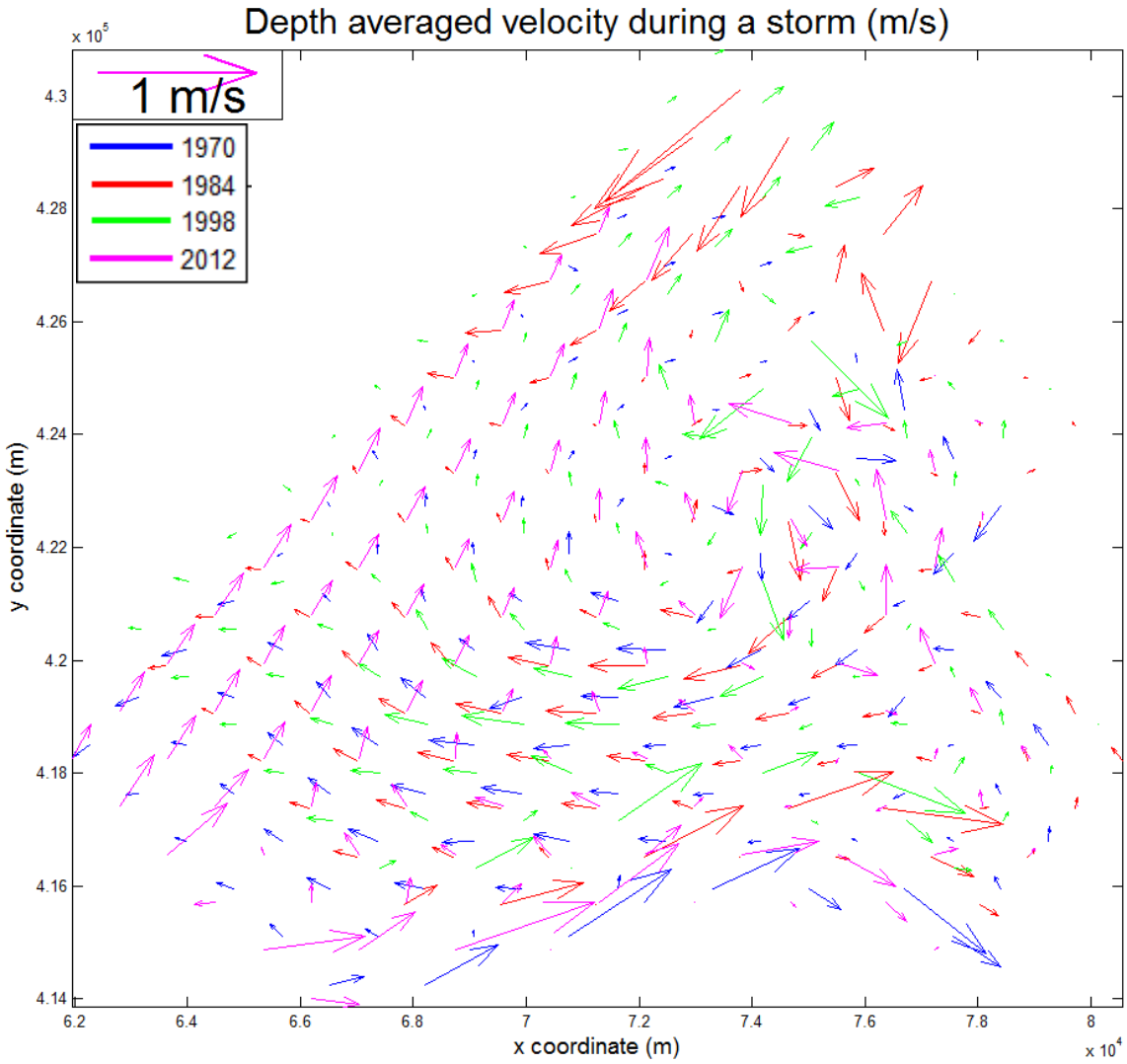

Figure 36. Storm mean velocity plots.

4.5 Sedimentation and Erosion

4.5.1 Sedimentation and Erosion GIS

4.5.1.1 Bathymetry calculations GIS

In Figure 37 the sedimentation rates for the total area and the inner area could be found. Those were calculated with GIS for twelve different bathymetries. The sediment volume increase can also be found in Appendix E – Sediment volume changes GIS, table 14. The results showed a slightly decreasing trend. Furthermore, it was found that for the period 1984 up to 1986 there was an erosive trend in the inner area. This sudden erosive phenomenon was also noticed by Tönis et al. (2002). The

reason for this erosion is not clear yet. It might be related to the land reclamation project the Slufter that was completed in 1986 and to the Eastern Scheldt flood defence that was finished in 1986. Since then, no significant sediment exchange of the Eastern Scheldt with the North Sea occurred. If normally a significant amount of sediment is transported with the longshore current up to the Haringvliet tidal basin, this could have influenced the Haringvliet. A decrease in the longshore sediment supply could then have caused a sudden erosive trend (de Winter, 2008). However, after 1986 sedimentation rates stabilized again, which did not support this theory. Furthermore, the spit formation since 1984 indicated an abundance of sediment from updrift. This was explained by the decrease in ebb-tidal delta volume of the Eastern Scheldt, which would have been transported by longshore currents up to the Haringvliet. Therefore, the temporary increase in sediment availability in the Haringvliet mouth due to the decrease in ebb-tidal delta volume of the Eastern Scheldt seemed more likely.

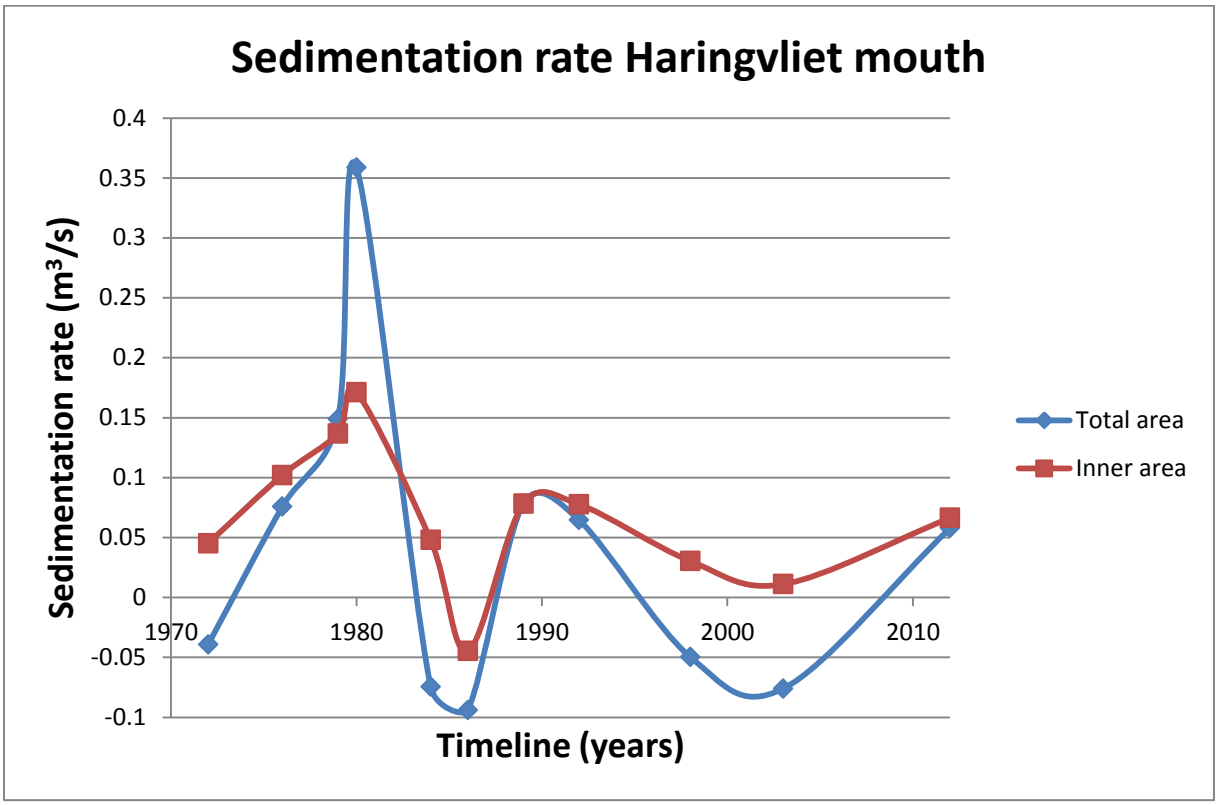

Figure 37. Sedimentation rates in the Haringvliet tidal basin considering 12 bathymetries. Positive numbers represent import of sediment whereas negative numbers indicate a loss of sediment.

It has been argued that due to large differences in discharge through the sluices of the Haringvliet the sedimentation values showed large differences between years (Arends, 1997). When using larger timespans these differences are levelled out.. This method of using only four bathymetries might therefore be more reliable. The system could have been in a dynamic equilibrium in 2000, as was argued by Louters et al. (1991) and Tönis et al. (2002). The sedimentation rates were approximately 0 in 2000.

4.5.1.2 Hypsometric curve

The part of the Haringvliet area closest to the sluices (zone 1) consisted of several channels and bars. The average depth was approximately -4 meter. The hypsometric curve of zone 1 can be found in Figure 38. The total area above or of -2 meter height stayed more or less the same over the period 1970 to 2012. However, the surface area below -2 meter height in general increased in average height. However, from 1998 until 2012 there is a lowering in the average bed level height when considering only bed levels below -2 meter. The total area having a bed level height between -2 meter and 2 meter decreased slightly over the period 1970 to 2012. Therefore, it can be argued that the

total intertidal area decreased. The total area with a bed level height higher than 2 meter stayed more or less the same over the period 1970 to 2012.

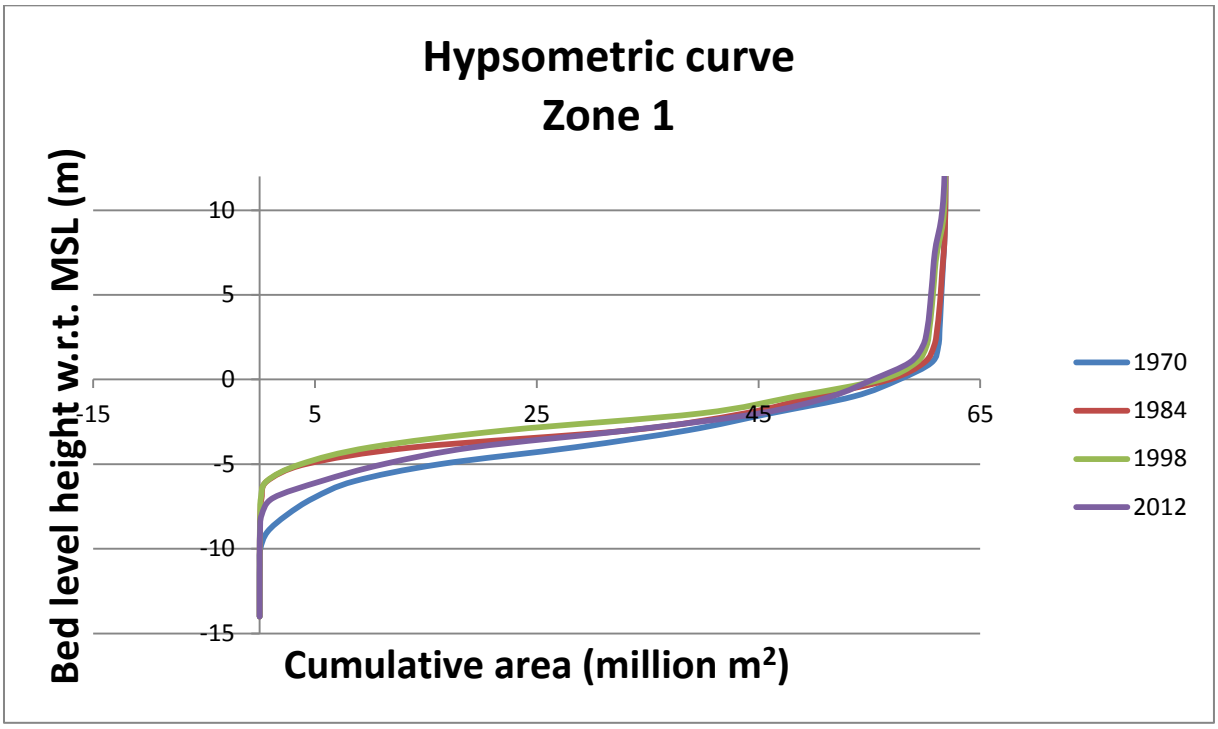

Figure 38. Hypsometric curve of zone 1.

The hypsometric curve of zone 2 can be found in Figure 39. In zone 2 the area below -4 meter was very stable up to the bathymetry of 1998. The cumulative area below -4 meter was for 2012 almost the same as it was for the older bathymetries. However, the area with a bed level height below -4 meter is on average lower for the 2012 bathymetry than it was for the other three bathymetries. The cumulative area that had a bed level height above -4 meter was less constant. On average the total area above -4 meter had a higher mean bed level in 1984 and 1998 than it had in 1970. In 2012 this mean bed level height increased even more.

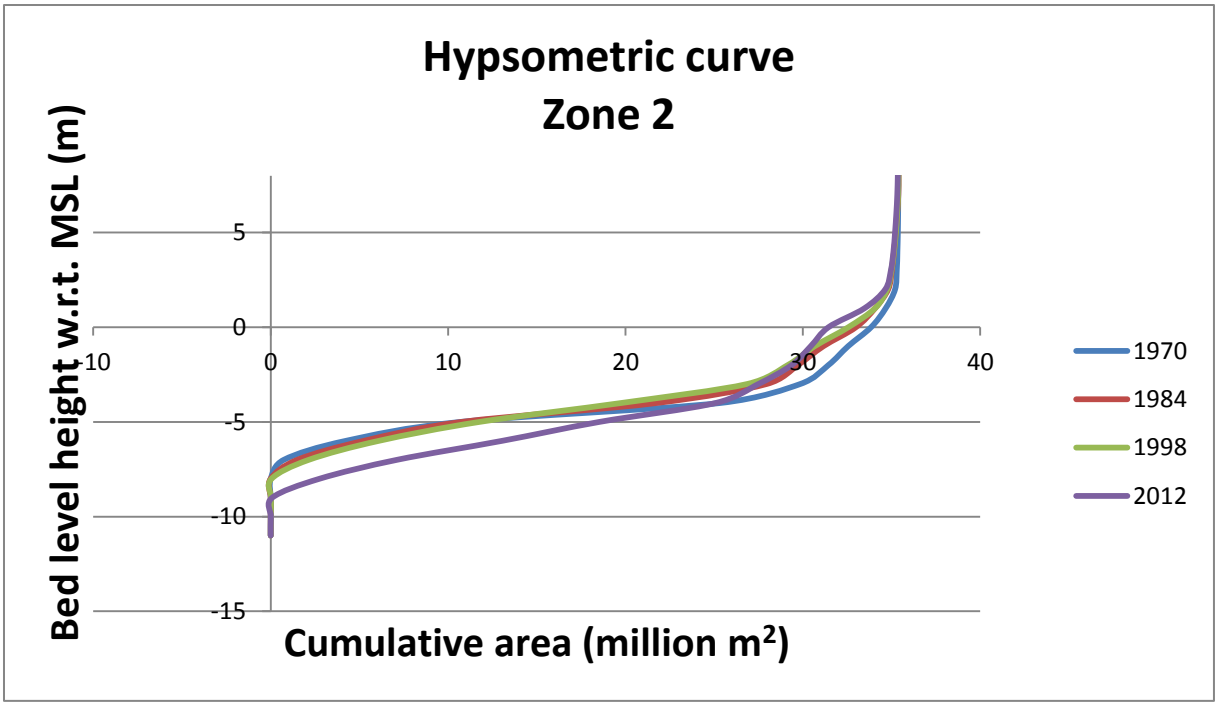

Figure 39. Hypsometric curve of zone 2.

Figure 40 shows the hypsometric curve of the outer area, zone 3. Zone 3 decreased the most in height of all three zones of the Haringvliet. Over the period 1970 to 1998 there was no change in total area below -12 meter. However, for the bathymetry of 2012 the total area below -12 meter increased with approximately 15 million m^2 compared to the other three bathymetries. For the period 1970 to 1998 the area with a bed level height between -12 meter and -6 meter made up a larger extent of the total area of zone 3 than in 2012. Overall, the bed level height of the entire zone 3 decreased several meters over the period 1970 to 2012.

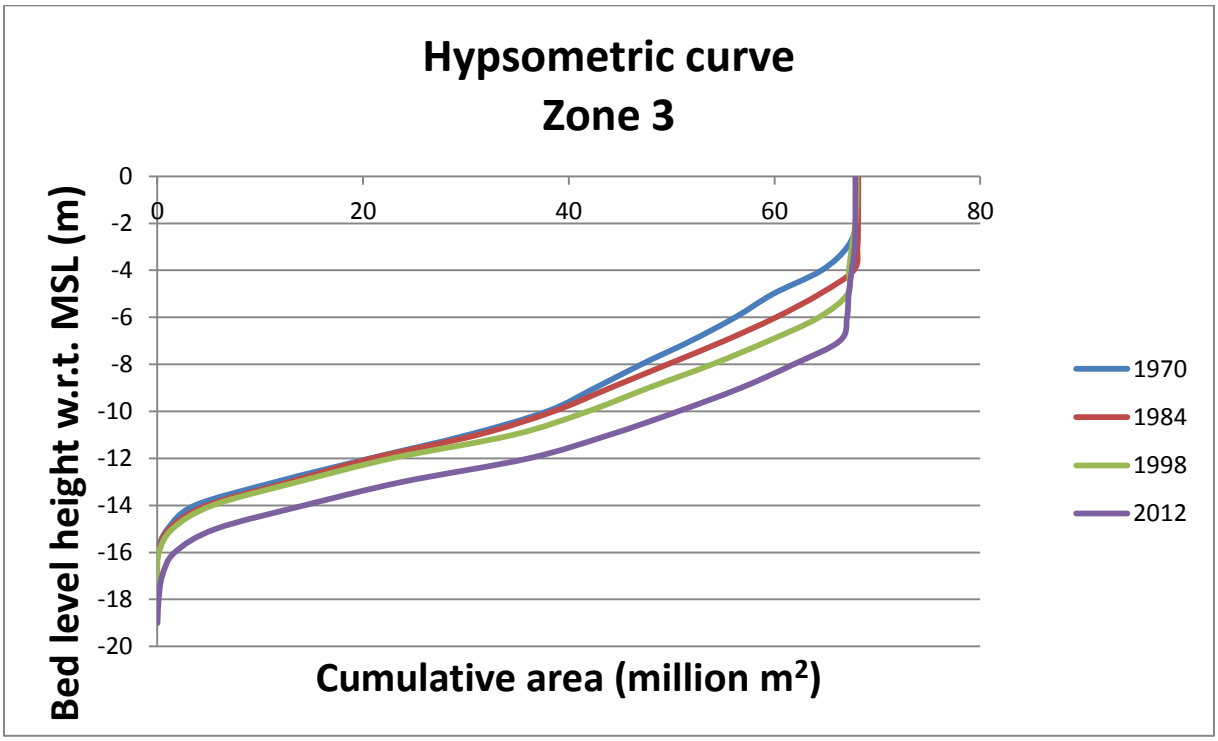

Figure 40. Hypsometric curve of zone 3.

Therefore in general, bed levels lower than -4.5 meter had a lower mean bed level in 2012 compared to 1970 and thus lost sediment. Bed levels above -4.5 meter had a higher mean bed level height and thus gained sediment. This was also found by de Winter (2008). However, the division in zones showed some additional details. The highest erosion was found in the outer area, zone 3.

4.5.2 Sedimentation and Erosion Delft3D

4.5.2.1 Storm sediment calculations

During a storm the mean velocities were higher than during normal conditions, which resulted in much higher sediment transport rates. This was caused by the nonlinear relation between velocity and transport (Eelkema et al., 2013). The higher mean velocities were expected because the larger significant wave height and wave period waves cause more sediment stirring. Therefore, during a storm suspended sediment transport is dominant (Steetzel, 1990).

In Figure 41 the mean sediment transport for all four simulations during a storm are shown. The sedimentation rates were 15 to 30 times larger than sedimentation rates during normal conditions. There was sedimentation in zone 1 and zone 2 and erosion in zone 3. For the storm simulations the transport into the total area was still relatively small. This was caused by large erosion rates in zone 3, compensating the sedimentation in zones 1 and 2. This erosion of the ebb-tidal delta during storm events was also encountered by de Swart and Zimmerman (2009). In general, zone 2 received relatively more sediment during storms than during normal conditions. This was caused by stronger littoral drift from updrift, as was shown in the storm mean velocity plots as well.

The simulations of 1970, 1984 and 1998 showed fairly similar sedimentation rates. However, the 2012 simulation showed higher sedimentation rates. This must be caused by the different velocity patterns in the total area for the 2012 simulation. The total area received more sediment, zone 2 received more sediment whereas zone 3 eroded more. Only zone 1 showed more or less stable sedimentation.

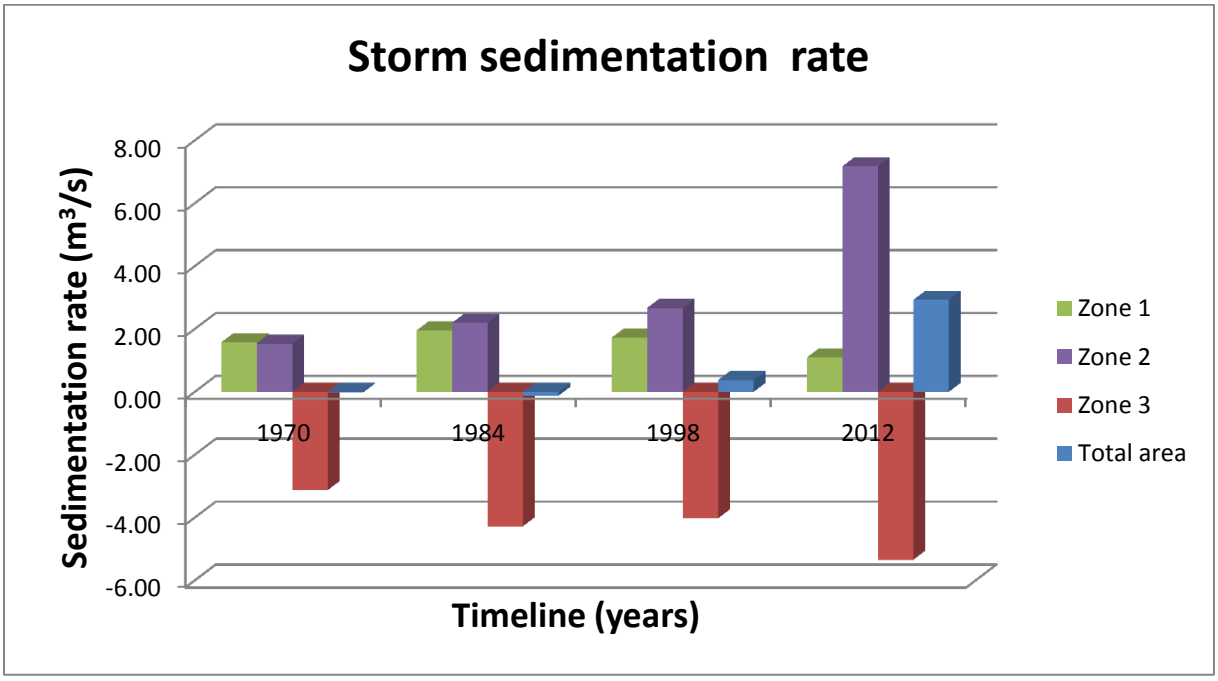

Figure 41. Storm transport divided per zone. Positive numbers represent import of sediment whereas negative numbers indicate a loss of sediment.

4.5.2.2 Mean Sedimentation and Erosion Delft3D

The mean transport directions for the combined wave and tidal simulations together with the storm simulations resulted in Figure 42. They were similar for all bathymetry simulations. The longshore

current in zone 3 was mainly induced by the tides. Along the Dutch coast the flood tide rises faster than the ebb tide lowers. Therefore, flood transport of coarse sediment normally exceeds ebb transport (Dronkers, 1986). The tidal simulation caused part of the sediment transport of zone 3 and transported it mainly in longshore downdrift direction. There was a small amount of sediment leaving zone 3 on the seaward boundary. Most sediment from area three was transported landward into zone 1 and zone 2 by wave induced currents. Landward cross-shore transport was larger than the longshore transport induced by tides in zone 3. Zone 2 received almost all of its sediment from zone 3. Almost no sediment came into zone 2 from the up-drift direction. This was probably caused by the Grevelingen delta. This is a low lying area reducing tidal and wave energy which is why almost no sediment is transported into zone 2 from the up-drift side. Only during storms the Grevelingen is inundated due to the water depth increase, which caused large sediment transport from the Grevelingen into zone 2. Zone 2 transported part of its sediment to zone 1 which net only receives sediment.

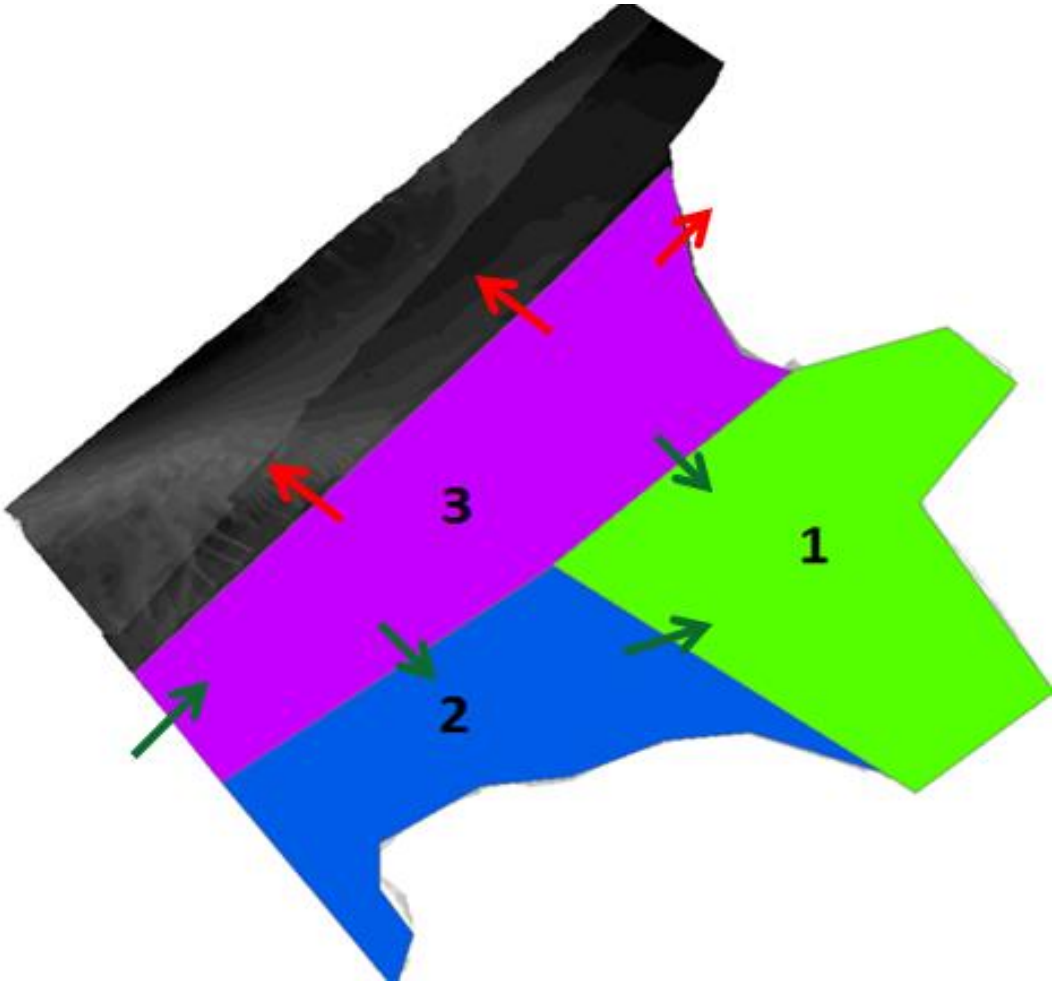

Figure 42. Mean transport directions.

In all simulations there is sedimentation in zone 1 and zone 2 and there is erosion in zone 3 (Figure 43). Furthermore, the general trend is that the sedimentation rates into zone 1 decrease over time. The erosion rates in zone 3 decrease as well. Zone 2 net transports the least of all three areas. The computer modelling with the bathymetry of 2012 showed an increase of sediment transport into zone 2. Probably, because zone 1 is sheltered from waves by Maasvlakte 2 most sediment is transported cross-shore into zone 2. Furthermore, the bed level height in zone 1 is on average higher than the bed level height of zone 2, which is why currents transporting sediment could penetrate more easily into

zone 2. From these modelling results it could be concluded that in 2012 sediment transport over all areas was smallest. However, considering the total area most sedimentation takes place. Furthermore, the storm results indicated a stronger response of the bathymetry of 2012 to storms from the northwest. It therefore depends on the occurrence frequency of storms whether there is more or less sedimentation for the bathymetry of 2012 than for the other areas.

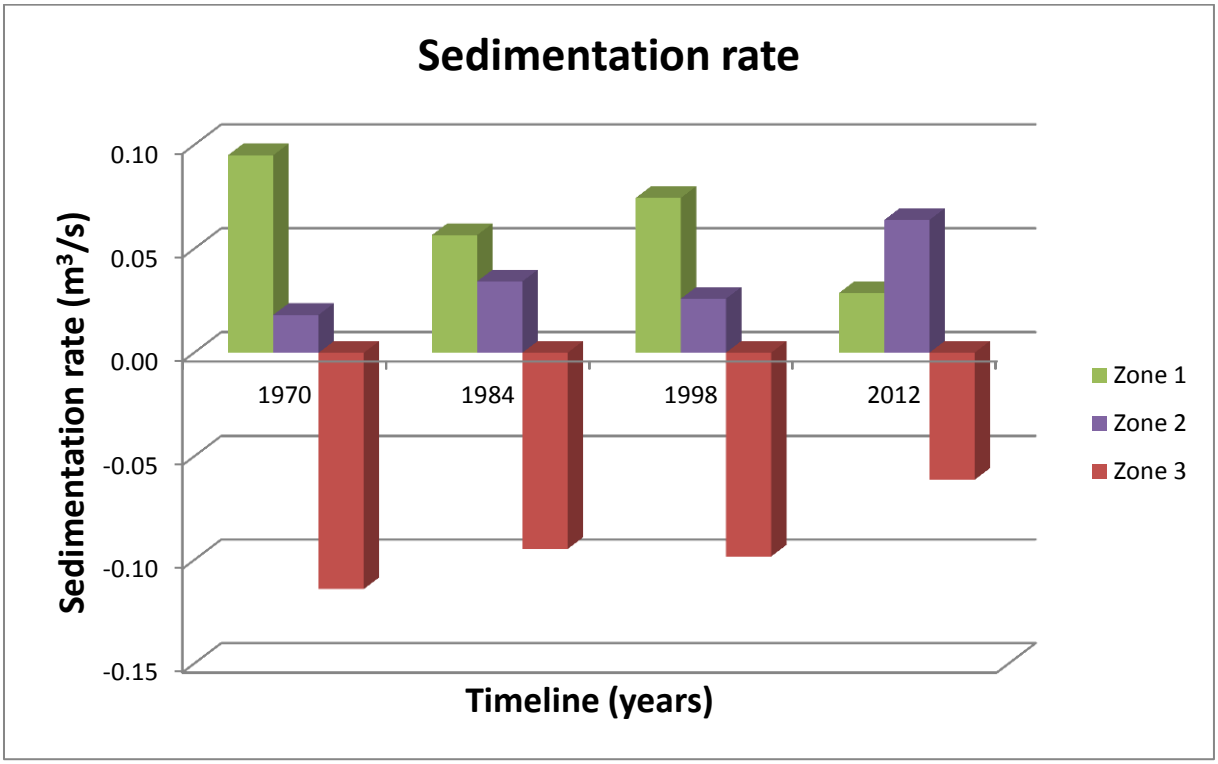

Figure 43. Sedimentation rates according to the Delft3D-modelling. Positive numbers represent import of sediment whereas negative numbers indicate a loss of sediment.

The wave influence and tidal influence on the sediment transport were researched. According to Tönis et al. (2002) the influence of waves on the Haringvliet tidal basin increased since closure. However this was not found in the present study. There was no change found in the influence of waves or tides over the years 1970 to 2012. It was found that tides had most influence on the outer area, whereas waves were dominant in the sediment transport into the inner area. There was no increasing trend found in wave influence since 1970.

4.5.3 Comparison GIS with Delft3D

The sediment transport values of both GIS and Delft3D-computer modelling were compared. In Figure 44 the sedimentation rate over the total area per fourteen year period is shown. The periods 1970-1984, 1984 – 1998, 1998 – 2012 and 2012 - 2026 are distinguished. For the last period no comparison with GIS could be made since the bathymetry of 2026 was not available yet. The total sedimentation per period calculated with GIS and the correction for dredging and dumping of sediment are given in Appendix E – Sediment volume changes GIS, table 11, 12 and 13. It is assumed that the bathymetries in GIS were correctly displaying height. Therefore, sedimentation differences between different bathymetries could be calculated accurately.

The GIS sedimentation rates incorporate the dredging and dumping in the area. They showed a declining trend of sedimentation from 1970 onwards and even a bit of erosion over the period 1998 to 2012. The sedimentation rates over the total area resulting from computer modelling did not show these trends. They showed almost no sediment transport up to 2012. However there seems to be an

increase in sedimentation in the total area from 2012 onwards, which is caused by a decrease in erosion in zone 3.

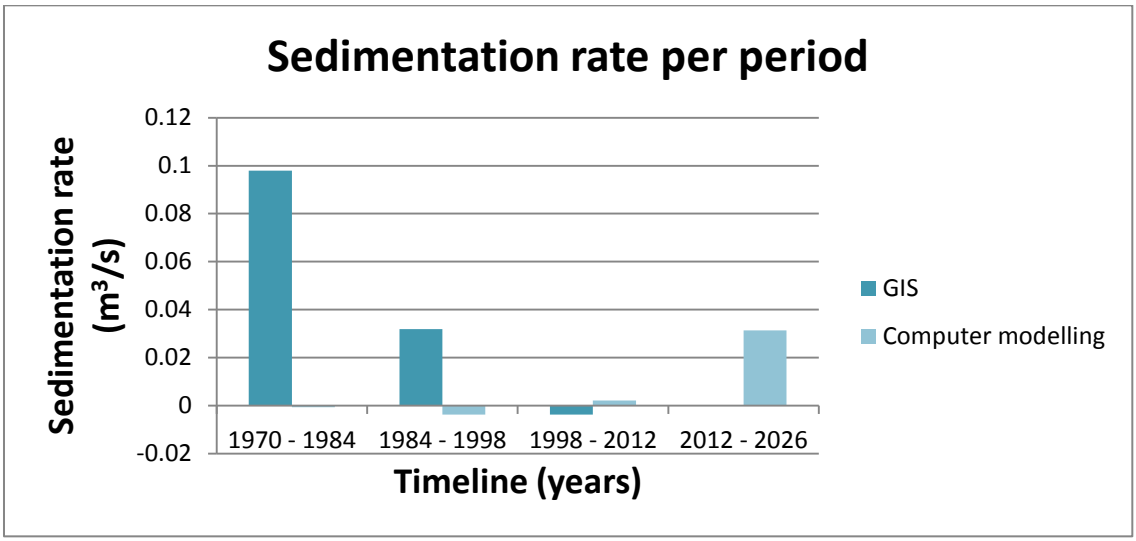

Figure 44. Comparison of the total area sedimentation rate of the GIS results with the Delft3D modelling results.

Sedimentation took place over all periods in the inner area (Figure 45). The GIS-results showed that there was an overall declining trend in sedimentation values from 1970 to 2012. Probably due to the approaching of a new equilibrium after closure in 1970. This was less clear for the computer modelling. Figure 43 showed that sedimentation in zone 1 decreased over time according to the computer model. However, the sedimentation in zone 2 increased. Therefore, the sedimentation in the inner area did not show a decline over time. The sedimentation rates in the inner area were in the same order of magnitude as the GIS results.

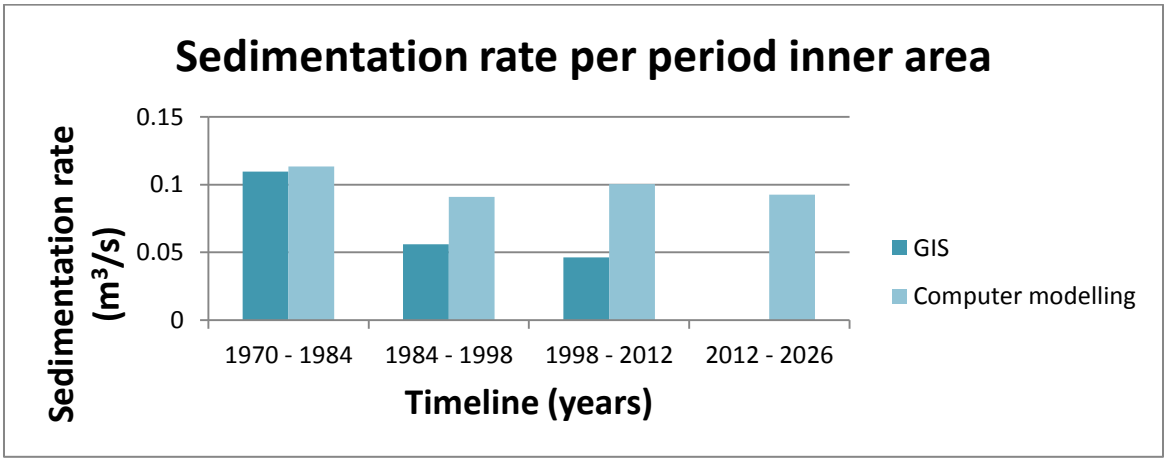

Figure 45. Comparison of the inner area sedimentation rate of the GIS results with the Delft3D modelling results.

The erosion in the outer area (Zone 3) increased over the period 1970 to 2012 according to GIS-results (Figure 46). The computer models showed larger erosion rates in the outer area than GIS and more of a decreasing than an increasing trend.

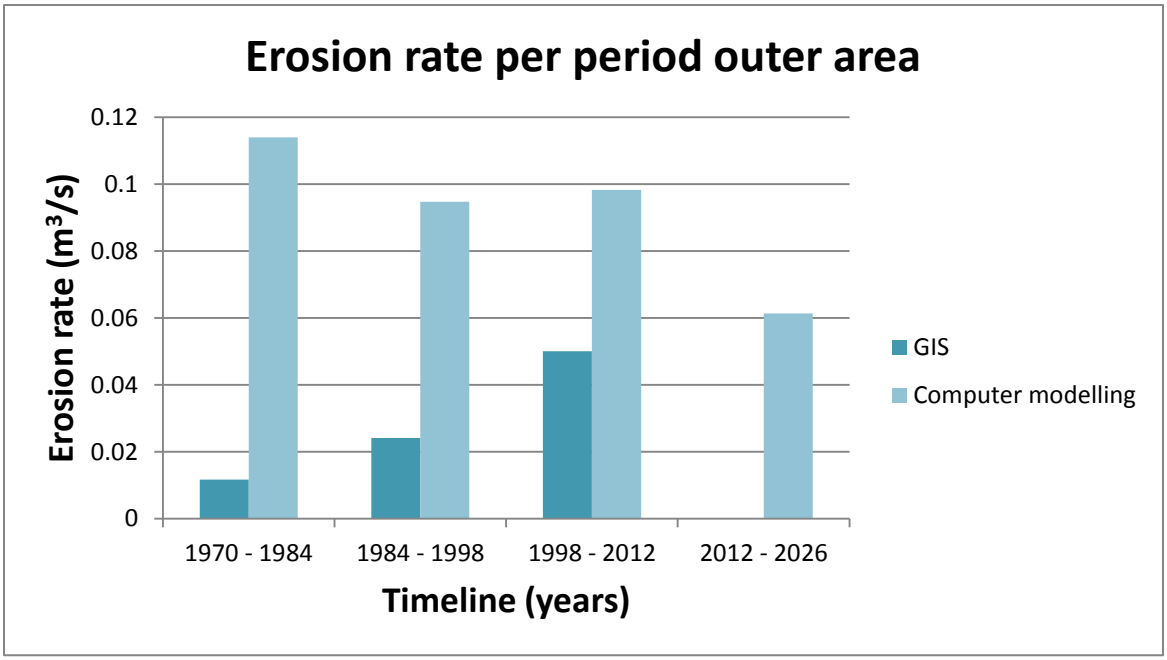

Figure 46. Comparison of the outer area erosion rate of the GIS results with the Delft3D modelling results.

Therefore, it can be concluded that the computer models correctly displayed the trend of erosion in the outer area and sedimentation in the inner area. However, the erosion in the outer area was a lot larger than was found with GIS. There can be several reasons for this overestimation of erosion by the computer models. First of all, there are large differences in sedimentation between consecutive years. Probably because fresh water release from the sluices differ. Furthermore, with the computer model only four tidal cycles were modelled and no bed level updating was incorporated. Therefore, natural bed level changes which inevitably took place over the 14 year period in between two consecutive bathymetries were not taken into account.

Moreover, the difference could have been caused by changes on the southwestern side of the Haringvliet tidal basin. Namely, the Grevelingen inlet was closed off in 1965, resulting in the decrease of its delta volume. Furthermore, the Eastern Scheldt was protected with a storm surge barrier which decreased the size of its delta as well. This sediment coming from the southwest probably ended up partly in the outer area of the Haringvliet tidal basin. The increase in erosion rates calculated with GIS could be understood by this. After the updrift deltas reached a new equilibrium, there was no extra sediment transported into the outer area. Resulting in a higher erosion rate. The inner area received most of its sediment cross-shore which is why it showed very similar behaviour with the GIS results. The outer area probably received a lot of sediment from eroding deltas in the southwest, which was not modelled by the computer model and resulted in higher erosion rates than encountered in reality. The rest of the magnitude difference should be subscribed to processes not taken into account by the computer model. Such as the effects flow has on waves via set-up, current refraction and enhanced bottom friction.

5. Discussion

5.1 Similar abandoned deltas

5.1.1 Frisian inlet

The Frisian inlet is situated in the north-eastern part of the Netherlands. It was closed off from its inner area in 1969. This closing reduced its tidal prism by approximately 30%, from 305 million m^3 to 200 million m^3 (Van de Kreeke, 2004). This decrease in tidal prism caused a decrease in volume of the

ebb-tidal delta of 20.66 million m^3. In the period 1970 to 1989, the back-barrier basin in the Frisian inlet experienced a total sedimentation of 30.82 million m^3. In the Haringvliet tidal basin 59 million m^3 was deposited between 1970 and 1987 (Louters et al., 1991). The cross-sectional area of all channels in the back- barrier basin of the Frisian inlet decreased (Biegel, 1991). Van de Kreeke (2004) argued that when there is little freshwater inflow, the tidal prism determines the opening or closing of the inlet channel. The Frisian inlet does not have any fresh water inflow, which makes it different from the Haringvliet tidal basin. Furthermore, the main channel for the Frisian inlet is a lot larger than the Slijkgat for the Haringvliet. The channel width is 1000 m whereas for the Slijkgat it is only 100-200 m. The depth of the main channel in the Frisian inlet has an average depth of 10 meter below MSL whereas for the Slijkgat it requires a lot of dredging to maintain it at 5.5 meter depth (Van de Kreeke, 2004).

The littoral drift in the Frisian inlet causes sediment to pass by the ebb-tidal delta to the downdrift coast. The sand is transported from the updrift coast towards the so called attachment bar. This bar is situated parallel to the coast and attached to the downdrift coast (van de Kreeke, 2006). The Hinderplaat shoal in the Haringvliet could be considered an attachment shoal as well. The small channel Hindergat becomes smaller over time due to this similar sediment bypassing system.

The mean tidal range close to the Frisian inlet is around 2.2 meter, which is almost equal to the mean tidal range of 2.4 meter on the seaward side of the Haringvliet. Furthermore, the ebb-tidal delta of the Frisian inlet has a cross-shore diameter of 5 kilometer. This is in the same order of magnitude as the Voordelta that extends approximately 10 kilometer into the sea (Biegel, 1991). Therefore, the Frisian inlet and Haringvliet are quite similar when considering their ebb-tidal deltas, they do differ in presence of river input.

5.1.2 Grevelingen

The Grevelingen is the tidal inlet directly south of the Haringvliet tidal basin. For the part of the Voordelta situated on the seaward side of the Grevelingen the behaviour was researched by looking at the change in position of the -5 meter MSL contourline (Louters et al., 1991). They found that the delta front of the Grevelingen ebb-tidal delta has been eroding from 1970 onwards. It moved landward by 3 km and the slope of the delta front is decreasing. Louters et al. (1991) relate this to the lengthening of the longshore shoals and the silting up of the former tidal channels in the area. This study showed that the delta front of the Haringvliet has been eroding since 1970 as well. Furthermore, the -5 meter MSL contourline of the Haringvliet delta front moved a maximum of 2 kilometer inland.

The Grevelingen and Haringvliet share several similar features such as disconnection of the back-barrier basins as well as the interconnected ebb-tidal delta. However, there is one big difference, Grevelingen never released significant amounts of fresh water to the sea. Via the Volkerak it was connected to the Hollands Diep, but it was a side channel for river discharge. The Haringvliet was one of the main transporting systems.

5.1.3 Eastern Scheldt

The Eastern Scheldt is situated in the southwestern part of the Netherlands. Its tidal hydrodynamics and sediment transport were changed by the implementation of a storm surge barrier and two back barrier dams. Similar to the Haringvliet dam, for the Eastern Scheldt the erection of the storm surge dam and back-barrier dams caused a strong decrease in tidal prism and tidal current velocities. The dams maintained the general erosive trend of the area and increased its magnitude.

The closure of the Eastern Scheldt caused its ebb-tidal delta to decrease in size (Eelkema et al., 2013). This might have influenced the Haringvliet sediment balance. According to Stive and Wang (2003) tidal basins can highly influence the sediment budgets of the adjacent coastline. Therefore, the sediment the ebb-tidal delta of the Eastern Scheldt lost might have ended up in the Haringvliet delta due to the littoral drift. Furthermore, sedimentation of channels and increase in wave driven features was found

for both the Eastern Scheldt and the Haringvliet. However, in the Eastern Scheldt the shoals were eroding, which did not happen in the Haringvliet delta. Moreover, the Haringvliet throat has a width of approximately 3.5 kilometer, whereas the smallest part of the Eastern Scheldt inlet is approximately 10 kilometer wide (Eelkema et al., 2013).

Therefore, the combination of factors contributing to the changes in the Haringvliet tidal basin after closure in 1970 are quite unique. However, there are tidal inlet systems and deltas which do have certain similar features.

5.2 Sediment balance

The sediment volume increase of the total area over the period 1970 to 2012 is 55.7 million m^3 (Appendix E – Sediment volume changes GIS). The increase in sediment volume of the total area over the period 1970 to 2012 is close to the 59 million m^3 as argued by Louters et al. (1991) for the period 1970 to 1987. Although the period over which this sediment volume was calculated differs, they are similar due to only a small loss of sediment volume in the period 1991 to 2012 (Figure 44). The increase in sediment volume of the inner area is 93.6 million m^3 over the period 1970 to 2012, which is close to the total sedimentation of 100 million m^3 mentioned by Dam et al. (2006). Therefore, it is probable that Dam et al. (2006) only researched the inner area, ignoring the delta front.

5.3 Modelling credibility

5.3.1 Cohesive sediment

The present study did not take different sediment grain sizes into account. In the Haringvliet tidal basin coarser sediments are found in the channels and finer sediment on the shoals. This distinction has not been implemented in the model simulations (Eelkema et al., 2013). Furthermore, the present study did not differentiate between cohesive and non-cohesive sediment. The critical bed shear stress for similar particle sizes differs greatly between cohesive grains and non-cohesive grains (Figure 47). The critical bed shear stress indicates when sediment particles will face enough stress to be entrained and to be available for sediment transport. Dredgers of the Port of Rotterdam know that there is very cohesive sediment in the area (de Winter, 2008). Especially the northern part of the area contains cohesive sediment According to Bliek cohesive sediment has a large influence on the study area (Bliek, personal communication, May 7th, 2015). Moreover, factors such as flocculation and the mud and sand interaction were ignored in the present study.

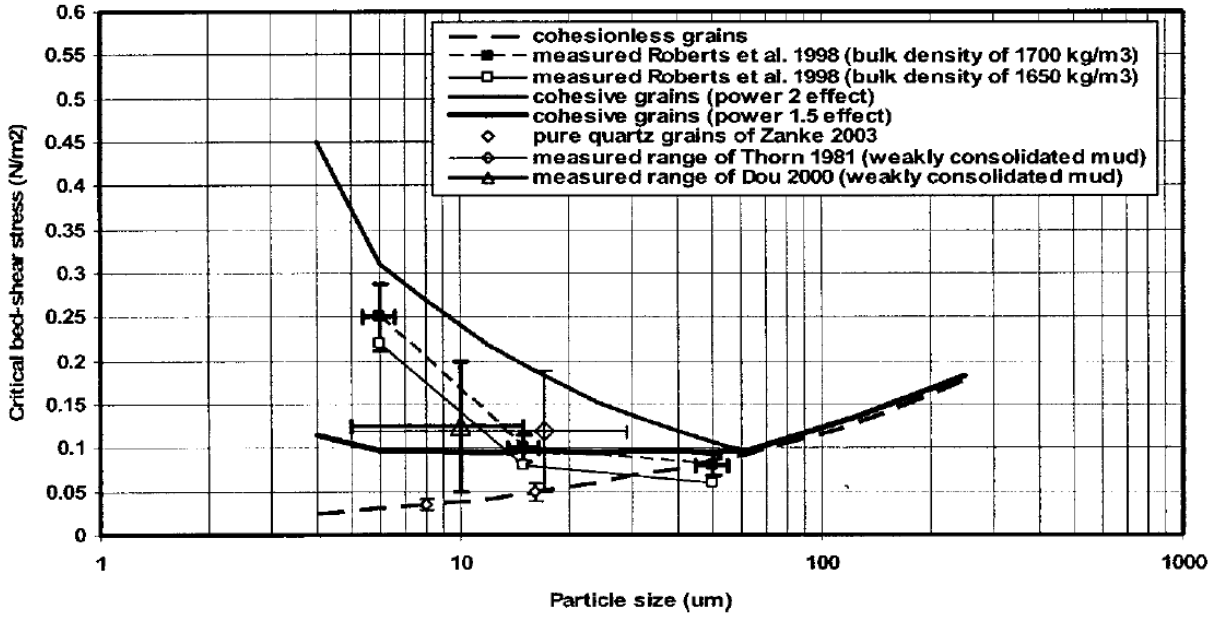

Figure 47. Particle size related to critical bed shear stress (van Maren, 2014).

However, as mentioned before this modelling study was not conducted to mimic reality as closely as possible. The Haringvliet tidal basin was used as a case study to research the behaviour of ebb-tidal deltas after human measures. Therefore, directions of transport and relative responses were considered more important than the correct representation of transport values. Furthermore,, the outer area consists mostly of non-cohesive sand (Koomans et al., 2001). Most sediment transported originated from the outer area. Therefore, cohesive sediment was not considered important for the present study.

5.3.2 Wind

Another parameter not taken into account in the present study is the wind-induced flow. Although waves were taken into account, they were not allowed to grow due to wind impact. In the morphodynamic evolution of the ebb-tidal delta of Grevelingen, wind-induced flow played a major role (Jongste et al., 2013). This implies that wind-induced flow could be important for the Haringvliet delta as well.

5.3.3 River

Every year approximately 30 trillion m^3 of fresh water is released through the sluices into the Haringvliet tidal basin (Steenbergen, 2004). However, in the present study river influence was not modelled due to computational expenses, large differences in river outflow per year and unnecessary complication of the results. Another study which did model river outflow in the Haringvliet tidal basin came to the conclusion that a higher river discharge resulted in less sedimentation in the inner area. River discharge transports the sediment out of the estuary. The differences with and without modelling fresh water discharge in the Haringvliet tidal basin are in the order of a few million m^3 (Dam et al., 2006). Therefore, the current influence of fresh water in the Haringvliet tidal basin was considered small. However, when a study focuses on the behavioural change of the system due to the implementation of the sluices, river influence would have been necessary to model this correctly. Because the period after 1970 was of interest of the present study, river influence did not need to be modelled.

5.3.4 Storms

The present study simulated storms simplistic way. Especially, the storm surge simulation by lowering the bottom topography has its downsides. Namely, storm surge is not just the heightening of the water level. It relies on non-linear interactions between tides and surges, the wind wave field and landscape change (Spencer et al., 2015). Furthermore, wind was not directly taken into account in the simulations, whereas wind plays an important role in a storm and the maintenance of the waves over the grid. Moreover, a proper storm surge model requires a larger model domain. Because a coastal surge is generated by wind drag effects and atmospheric pressure gradients which need to develop over large distances to develop properly (Herrling and Winter, 2014).

For a mixed-energy tidal inlet in dynamic equilibrium, the general opinion is that a storm event will counteract the trends during fair weather conditions. For a typical mixed-energy inlet this means that during fair-weather and tide conditions the ebb-tidal delta gains sediment. During storm conditions it loses sediment due to wave impact (FitzGerald et al., 2012; Herrling & de Winter, 2014). However, the Haringvliet ebb-tidal delta is not a typical mixed-energy tidal inlet anymore. It is a mixed-energy tidal inlet greatly affected by human measures. Therefore, it could be that similar but exaggerated behaviour as during normal conditions was found.

5.3.5 Spectrum of situations

The present study only considered typical situations. Namely, the modelling of waves with wave direction 220 and 310 degrees combined with normal tidal conditions and one storm. However, these conditions only appear slightly over 50% of the time. No spring- or neap tide conditions were modelled. Furthermore, only one storm was modelled and its sediment transport indicates a large influence of storms. However, the impact of different types and directions of storms were not taken

into account. Therefore, only a small spectrum of conditions was modelled in the present study. It is not clear if they were responsible for the largest changes in the area.

5.4 Haringvliet delta behaviour

The present study did not model the morphodynamic developments of the Haringvliet tidal basin directly, but only the transport vectors to indicate morphodynamic development. However, the present research did consider waves and tidal currents. Waves and tidal currents induce sediment stirring and transport. Those are the main drivers of morphodynamic development in mixed-energy tidal inlet systems (FitzGerald et al., 2012).

The Haringvliet delta front has moved inland over the period 1970 to 2012. This was expected due to a decrease in fresh water influence and therefore a decrease in equilibrium volume of the river delta. The decrease in fresh water discharge was caused by the sluices implemented in 1970. Furthermore, there was a transition from a long tidal basin to a short tidal basin in 1970. For a short tidal basin, ebb-tidal deltas are generally small due to net sediment transport being in landward direction (Ridderinkhof et al., 2014). This landward directed net sediment transport was found in all simulations in the present study due to the modelling of only short tidal basins.

Wave influence increased after closure of the dam (Tönis et al., 2002). However, the results of the present study showed no change in influence of either waves or tides. This was probably caused by the modelling technique of the present study. Namely, even the 1970 simulation was modelled as a short tidal basin. If the 1970 case was modelled as a long tidal basin, tides would have had a larger impact because they could penetrate up to 50 kilometer into the Haringvliet. The bathymetry change from 1970 to 2012 was the result of the implementation of the sluices. Therefore indirectly the implementation of the sluices was modelled. After 1970 only the land extension Maasvlakte 2 seems to have a large impact on the hydrodynamics of the Haringvliet.

Comparing the bathymetry of 2012 with the 1970 bathymetry of the Haringvliet, it appears that the dominant ebb-channel is directed more updrift. There is no agreement on the processes directing the main channel of an ebb-tidal delta. The main channel direction depends on the phase difference between tidal currents offshore to tidal currents inside the basin or the interaction of waves with tidal currents or to tidal prism (de Swart and Zimmerman, 2009; Sha and van den Berg, 1993; Tönis et al., 2002). The updrift behaviour could not have been forced by a large tidal prism, as was considered the main reason for updrift behaviour by Sha and Van den Bergh (1993). Namely, the tidal prism decreased over the period 1970 to 2012. It is most probable that the change in phase between the offshore tidal currents and the currents inside the basin induced the up drift behaviour (Tönis et al., 2002). Furthermore, waves increased in importance since closure in 1970. This will result in an asymmetric delta as well (de Swart and Zimmerman, 2009). A specific theory for the Haringvliet is that after closure the Slijkgat became the main transporting channel. This change in dominance was caused by the sluice opening being closer to the Slijkgat than to the Rak van Scheelhoek and dredging. The Slijkgat is situated updrift of the Rak van Scheelhoek, which might have caused the migration of the ebb-tidal delta of the Haringvliet updrift.

The sedimentation rates showed that Tönis et al. (2002) might have been right that the Haringvliet tidal basin had reached an (dynamic) equilibrium. However, in 2012 Maasvlakte 2 was constructed. This extension 8 kilometer into the sea caused hydrodynamic changes of which the consequences are not clear yet. According to the simulations especially the tidal alongshore current is heavily disrupted by the extension, which causes tidal asymmetry, mean velocity directions and sediment transport to change. In 2012 over the total area sedimentation took place, according to the computer models analysed in this study. Especially zone 2 received more sediment than in previous years. Contrary to the expectation, storms from the northwest induced more net sediment transport in 2012 than in the other bathymetries. In zone 1 there was less sedimentation because of shelter from Maasvlakte 2. During storms, sedimentation in zone 2 and erosion in zone 3 increased. It is therefore expected that

from 2012 onwards zone 2 is increasing in bed level height, whereas zone 1 and zone 3 became less dynamic.

Since the closure in 1970, the Haringvliet delta is the delta of an estuary. There are no examples of stable estuaries where the net sediment inflow is counteracted by the same net sediment outflow. There is always external forcing that makes the estuary unstable (Dronkers, 1986). It is expected that the trend of sedimentation in the inner area and erosion in the outer area will continue in the future.

5.5 Implication other deltas

The present study showed that disruption of the natural system by human measures can have a large impact on the hydrodynamics and morphodynamics of a tidal inlet system. By disconnection of a tidal inlet from its back-barrier basin, the relative importance of waves and tides changes. Therefore, waves should be taken into account to predict changes. When a tidal basin decreases in size the tidal influence will decrease. This causes the ebb-tidal delta to decrease in size. When there is a significant land extension, a distortion in tidal wave propagation or wave influence can be expected. This can lead to completely different current and transport patterns than before this land extension. It would therefore be wise to model the impact of such implementations beforehand, considering both tides and waves to be able to predict to some extent the hydrodynamic changes.

6. Conclusions

The present study showed that the redistribution of sediment of the Haringvliet delta was directed mostly cross-shore in a landward direction. Waves mainly influence the shallower areas of the Haringvliet tidal basin. More specifically, on the Hinderplaat shoal waves break, force a set-up and induce a landward directed wave induced current. Tidal influence is concentrated on the outer area of the Haringvliet delta and in the channels. The seaward side of a delta is also the place were tides have the largest influence on sediment transport because of the relatively high mean velocity rates, caused by tidal asymmetry.

The delta front of the Haringvliet migrated inland over the period 1970 to 2012. Furthermore, in the period 1970 to 2012 the delta front turned up drift. The Hinderplaat shoal has turned landward and moved inland over the period 1970 to 2012 as well. This reorientation of the Hinderplaat caused wave influence and tidal currents to change as well. There was a fairly diffusive energy distribution in 1970. In 1984 wave influence was very pronounced on a distinct longshore bar. The pattern was more fragmentised in 1998 and 2012.

The transportation rates calculated using both GIS and computer models are in the same order of magnitude. Delft3D modelling showed that the sediment of the Haringvliet delta was transported mostly cross-shore into the inner area and partly longshore to the northeast. The inner area of the Haringvliet experienced sedimentation over the period 1970 to 2012. There was continuous erosion in the outer area over the period 1970 to 2012. The land extension Maasvlakte 2 implemented in 2012 distorted the longshore tidal current. The consequences of this distortion are not clear yet.

7. Further research

The present study was conducted to model the hydrodynamics and sediment transport patterns of an ebb-tidal delta after the implementation of several human measures over the period 1970 to 2012. The land extension Maasvlakte 2 distorts the longshore tidal current and might shelter zone 1 from wave influence. The consequences of this distortion are not completely clear yet. Therefore, further research should focus on the behavioural change of the system at the moment. Furthermore, the research of the impact of storms in the area should be extended in the future. Due to the Haringvliet tidal basin being an area which is highly monitored and researched, it could be an example for other mixed-energy tidal inlet systems in the world where human measures are considered. Finally, it became clear that on the shoal Hinderplaat a grid cell size of 40 meter x 40 meter was too large to model wave transformation correctly. A future study should use a finer grid on these areas, to research the differences in velocity and transport.

8. References

Arends, A. A. (1997) *Toepassing van evenwichtsrelaties op de Haringvlietmond*. Rijksinstituut voor Kust en Zee. Rapport RIKZ-97.021.

Biegel, E. J. (1991) *Equilibrium relations in the ebb tidal delta, inlet and backbarrier area of the frisian inlet system*. Rijksuniversiteit Utrecht, Vakgroep Fysische Geografie.

Bliek, B. and De Gelder, A. (2014) *Expert beoordeling aanzanding Slijkgat t.b.v. Passende Beoordeling onderhoudsbaggerwerk*. Svasek Hydraulics and Rijkswaterstaat, WNZ-NeMo-AG-2014-002.

Booij, N., Ris, R. C., and Holthuijsen, L. H. (1999) A third-generation wave model for coastal regions: 1. Model description and validation. *Journal of Geophysical Research: Oceans (1978–2012)*, 104(C4), 7649-7666.

Dam, G., Bliek, A. J. and Bruens, A. W. (2006) *Band width analysis morphological predictions Haringvliet estuary*, River, Coastal and Estuarine Morphodynamics; RCEM 2005 – Parker and Garcia (eds). Taylor and Francis Group, London.

de Jongste, L., Dusseljee, D., Smit, M. and Jansen, M. (2013) Morphological impact on ebb-tidal deltas of reintroducing tide in a former estuary, *Coastal Dynamics*, 465 – 476.

de Kort, J. G. (2015) *An Assesment on Hydro- and Morphodynamic Processes at the Sand Motor During the Decemberstorm of 2013*. Masterthesis TU Delft.

Deltares (2014) *Delft3D-FLOW User manual and Delft3D-WAVE User manual*; online available from: www.deltares.nl (last access: December 2015).

de Swart, H. E., and Zimmerman, J. T. F. (2009) Morphodynamics of tidal inlet systems, *Annual Review of Fluid Mechanics*, *41*, 203-229.

de Winter, R. (2008) *Exploratory research into the maintenance of the Slijkgat, an analysis of the morphology of the Haringvliet*. Masterthesis TU Delft. In cooperation with the Port of Rotterdam and Deltares.

Dronkers, J. (1986) Tidal asymmetry and estuarine morphology, *Netherlands Journal of Sea Research*, *20*(2), 117-131.

Eelkema, M., Wang, Z. B. and Stive, J. F. (2012) Impact of Back-Barrier Dams on the Development of the Ebb-Tidal Delta of the Eastern Scheldt, *Journal of Coastal Research*, 28 (6), 1591-1605.

Eelkema, M., Wang, Z. B., Hibma, A., and Stive, M. J. (2013) Morphological effects of the Eastern Scheldt storm surge barrier on the ebb-tidal delta, *Coastal Engineering Journal*, 55(03), 1350010.

EMOD, European Marine Observation and Data Network (2015) Bathymetry data. Online available from: http://www.emodnet-hydrography.eu/ (last access: November 2015).

FitzGerald, D. M. (1982) Sediment bypassing at mixed energy tidal inlets, *Coastal Engineering Proceedings*, *1*(18).

FitzGerald, D. M. (1988) *Shoreline erosional-depositional processes associated with tidal inlets*. In: Hydrodynamics and sediment dynamics of tidal inlets, Springer New York, 186-225.

Fitzgerald, D. M., Kulp, M., Penland, S., Flocks, J., and Kindinger, J. (2004). Morphologic and stratigraphic evolution of muddy ebb-tidal deltas along a subsiding coast: Barataria Bay, Mississippi River delta. *Sedimentology*, *51*(6), 1157-1178.

FitzGerald, D. M., Buynevich, I., and Hein, C. (2012) *Morphodynamics and Facies Architecture of Tidal Inlets and Tidal Deltas*. In: Principles of Tidal Sedimentology SE 12, Davis Jr., R. A. and Dalrymple, R. W. (eds.), Springer Netherlands, 301–333.

Galloway, W. E. (1975) *Process framework for describing the morphologic and stratigraphic evolution of deltaic depositional systems*. In: Models for Exploration, Houston Geological Society, 87-98.

Gautier, C., Camarena, A. and van Nieuwkoop, J. (2014) *SWAN hindcasts Wadden Sea, December 2013*. Deltares report 1209433-007-HYE-0005.

Google Earth (2013) *Image of the Haringvliet tidal basin of 2013*.

Hayes, M. O. (1980) General morphology and sediment patterns in tidal inlets. *Sedimentary geology*, *26*(1), 139-156.

Herrling, G., and Winter, C. (2014) Morphological and sedimentological response of a mixed-energy barrier island tidal inlet to storm and fair-weather conditions. *Earth Surface Dynamics*, 2(1), 363-382.

Holthuijsen, L. H. (2007). *Waves in oceanic and coastal waters*. Cambridge University Press.

Koomans, R. L., De Meijer, B. A. and Nicolaas, J. F. (2001) *Multi-Element Detector system for Underwater (Medusa) Explorations: Bodemsamenstelling in de monding van het Haringvliet*: data report. Rijkswaterstaat.

Kraus, N. C. (1999) *Analytical model of spit evolution at inlets*. Army Engineer Waterways Experiment Station Vicksburg MS Coastal and Hydraulics lab.

Lesser, G. R., Roelvink, J. A., van Kester, J. A. T. M., and Stelling, G. S. (2004) Development and validation of a three-dimensional morphological model. *Coastal Engineering*, 51(8), 883-915.

Louters, T., Mulder, J. P. M., Postma, R. and Hallie, F. P. (1991) Changes in Coastal Morphological Processes due to the Closure of Tidal Inlets in the SW Netherlands. *Journal of Coastal Research*, 7(3), 635-652.

Louters, T. and Gerritsen, F. (1998) *The riddle of the sands. A tidal system's answer to a rising sea level*. RIKZ –workdocument 94.040.

Masselink, G. and Hughes, M. G. (2003*) Introduction to Coastal Processes and Geomorphology.* Hoddereducation, London.

Mulder, J. P. M., Louters, T., Hallie, F. P., Postma, R., Craeymeersch, J. A. and Hamerlynck, O. (1990) Integrated coastal research in the SW Netherlands. *Coastal Engineering,* 22, 2984 – 2997.

NAM (2010) *Memo vaklodingen*. Waterdienst.

Nienhuis, J. H., Ashton, A. D., Roos, P. C. and Hulscher, J. M. H. (2013) Wave reworking of abandoned deltas. *Geophysical Research Letters,* 40, 5899-5903.

Oertel, G. F. (1972). Sediment transport of estuary entrance shoals and the formation of swash platforms. *Journal of Sedimentary Research*, 42(4).

Pugh, D. T. (1987) *Tides, Surges and Mean Sea-Level.* John Wiley and Sons, Chichester.

Ridderinkhof, W., de Swart, H. E., van der Vegt, M. and Hoekstra, P. (2014) Influence of the back-barrier basin length on the geometry of ebb-tidal deltas. *Ocean dynamics*, 64(9), 1333-1348.

Rijkswaterstaat (2015) Vaklodingen, bathymetry files of the coastal zone. online available from: http://kml.deltares.nl/kml (last acces: November 2015).

Robinson, A. H. W. (1960) Ebb-flood channel systems in sandy bays and estuaries. *Geography*, 183-199.

Roelvink, J. A. and Walstra, D. J. (2004) Keeping it simple by using complex models. *Advances in Hydro-science and Engineering*, 6, 1-11.

Seybold, H., Andrade, J. S., and Herrmann, H. J. (2007) Modeling river delta formation. *Proceedings of the National Academy of Sciences*, *104*(43), 16804-16809.

Sha, L. P. and van den Berg, J. H. (1993) Variation in ebb-tidal delta geometry along the coast of the Netherlands and the German Bight. *Journal of Coastal Research,* 9 (3), 730-746.

Simeoni, U., Fontolan, G., Tessari, U. and Corbau, C. (2007) Domains of spit evolution in the Goro area, Po Delta, Italy. *Geomorphology*, 86(3), 332-348.

Snijders, G. H. (1998) *Morfologische ontwikkeling Voordelta 1980 – 1997*. Rijksinstituut voor Kust en Zee. Rapport RIKZ-98.019.

Spencer, T., Brooks, S. M., Evans, B. R., Tempest, J. A. and Möller, I. (2015) Southern North Sea storm surge event of 5 December 2013: Water levels, waves and coastal impacts. *Earth-Science Reviews*, 146, 120-145.

Steenbergen, J. (2004) *Het effect van sterk wisselende zoutgehalten op het benthos in de Westerschelde en de Haringvlietmonding* (No. C075/04, p. 39). RIVO Centrum voor Schelpdierenonderzoek.

Steetzel, H. J. (1990) Cross-shore transport during storm surges. *Coastal Engineering Proceedings*, 1(22).

Stive, M. J. F. and Wang, Z. B. (2003) Morphodynamic modelling of tidal basins and coastal inlets. In: Advances in Coastal Modelling, C. Lakhan (eds), Elsevier, Amsterdam, 367-392.

Tönis, I. E., Stam, J. M. T. and van de Graaf, J. (2002) Morphological changes of the Haringvliet estuary after closure in 1970. *Coastal Engineering*, 44(3), 191-203.

van de Kreeke, J. (2004) Equilibrium and cross-sectional stability of tidal inlets: application to the Frisian Inlet before and after basin reduction. *Coastal Engineering,* 51, 337-350.

van de Kreeke, J. (2006) An aggregate model for the adaptation of the morphology and sand bypassing after basin reduction of the Frisian Inlet. *Coastal engineering*, *53*(2), 255-263.

van Maren, D. S. (2014) Powerpoint presentation: *An introduction to cohesive sediment transport modelling*. Deltares.

van Rijn, L. C. and Walstra, D.J.R. (2003) *Modelling of Sand Transport in Delft3D*. Rijkswaterstaat, RIKZ.

van Rijn, L. C.,Walstra, D. J. R. and Van Ormondt, M. (2004) *Description of TRANSPOR2004 and implementation in Delft3D-ONLINE*. Interim Rep. Prep. DG Rijkswaterstaat, Rijksinst voor Kust en Zee, Delft Hydraul. Institute, Delft, the Netherlands.

van Rijn, L. C. (2011) *Principles of fluid flow and surface waves in rivers, estuaries, seas and oceans* (11). Amsterdam, The Netherlands: Aqua Publications.

van der Vegt, M., Schuttelaars, H. M. and de Swart, H. E. (2006) Modelling of equilibrium tide-dominated ebb-tidal deltas. *Journal of Geophysical Research,* 111 (F2).

van der Vegt, M., Schuttelaars, H. M., and De Swart, H. E. (2009) The influence of tidal currents on the asymmetry of tide-dominated ebb–tidal deltas. *Continental Shelf Research*, *29*(1), 159-174.

van Veen J. 2005 (1950) Ebb and flood channel systems in the Netherlands tidal waters. *Journal of Coastal Research,* 21, 1007–120.

van Wijngaarden, M. (1998) *Sediment transport tijdens de proef met open Haringvlietsluizen op 11 maart en 14 maart 1997*. RIZA-workdocument 98.020X.

van Wijngaarden, M., Backx, J. J. G. M., van den Berg, G. A., Geilen, E. F. M., de Hoog, J. E. W., Houwing, E. J., van Oirschot, M. and Ohm, M. (2002) *Heavily modified waters in Europe, Case Study on the Haringvliet estuary*, RIZA -workdocument 2003.166X.

Walton, T. L. and Adams, W. D. (1976) Capacity of inlet outer bars to store sand. *Proceedings 15th Conference on Coastal Engineering (New Yor*k), 919-1937.

Waterberichtgeving Rijkswaterstaat (2015) online available from: http://waterberichtgeving.rws.nl/nl/water-en-weer_dataleveringen_ophalen-opgetreden-data.htm (last access: October 2015).

Appendices

Appendix A – Dredging and dumping

Table 8. Overview of the dredging and dumping values from 1983 to 2013 (Bliek and de Gelder, 2014).

Year	Necessary dimensions Slijkgat compared w.r.t. MSL (m)	Sand mining (m^3)	Nourishment (m^3)	Other use (m^3)	Nourishment at the dump location (m^3)	Total sediment taken from Slijkgat (m^3)
1983	-4.5	380,000				380,000
1984	-4.5	50,000				50,000
1985	-4.5	50,000	450,000			500,000
1986	-4.5	20,000				20,000
1987	-4.5	145,000				145,000
1988	-4.5	108,324			357,585	465,909
1989	-4.5	155,743				155,743
1990	-4.5	251,719				251,719
1991	-4.5	170,818				170,818
1992	-4.5	331,078			73,527	404,605
1993	-4.5	69,330			29,495	98,825
1994	-4.5	55,459	505,678	200,000	97,806	858,943
1995	-4.5	160,000			234,109	394,109
1996	-4.5	130,000				130,000
1997	-4.5	130,000				130,000
1998	-4.5	30,000	780,000	190,000	90,000	1,090,000
1999	-4.5	210,000				210,000
2000	-4.5	242,104				242,104
2001	-4.5	210,000				210,000
2002	-4.5	200,000			170,000	370,000
2003	-4.5	270,000				270,000
2004	-4.5				200,000	200,000
2005	-5,0m*100m				150,000	150,000
2006	-5,0m*100m				84,000	84,000
2007	-5,0m*100m				103,000	103,000
2008	-5,0m*100m				221,000	221,000
2009	-5,5m*100m				569,500	569,500
2010	-5,5m*100m				182,000	182,000
2011	-5,5m*100m				942,000	942,000
2012	-5,5m*100m				429,000	429,000
2013	-5,5m*100m				513,924	513,924

Appendix B – Grid and Depth

Overview of the bathymetries of 1970, 1984, 1998 and 2012 used in the Delft3D modelling. For the GIS calculations and sediment transport calculations all bathymetries were resized to only incorporate zone 1 + zone 2 + zone 3.

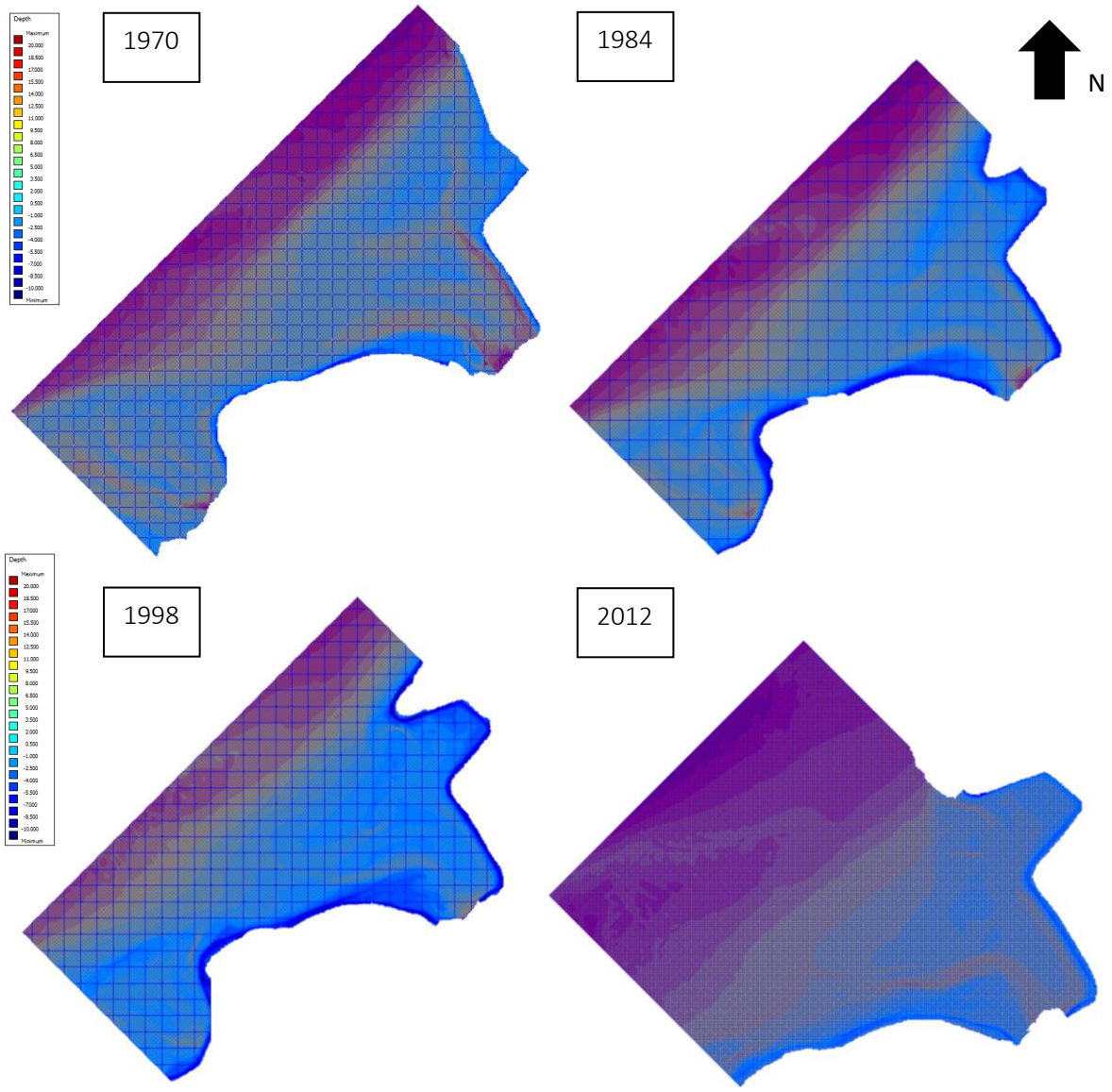

Figure 48. Overview of the bathymetries of 1970, 1984, 1998 and 2012 used in the Delft3D modelling.

Appendix C – Parameters

Parameters used in Delft3D modelling and the explanation why it was chosen. Both for the hydrodynamic simulations and wave simulations.

Table 9. Parameters hydrodynamic simulations.

Parameter	Why	Value/condition
Timeframe		
Timestep	Courant number	0.015625 min
Processes	Sediment Secondary flow (Waves)	On
Boundaries		
Flow conditions	Water level on seaward boundary Neumann on cross-shore boundaries	
Transport conditions	Only for seaward boundary initial transport from medium grid For cross-shore boundaries no initial transport values	
Physical parameters		
Gravity	Netherlands	9.81 m/s^2
Water density	Salt water	1025 kg/m^3
Beta_c	Default value	0.5
Equilibrium state	off	
Numerical parameters		
Rougness formula	Chezy Uniform Standard Value	50, 50
Slip condition	Default condition	Free
Horizontal eddy viscosity	Recommendation of supervisor, less instability	10 m^2/s
Horizontal eddy diffusivity	Uniform Default value	10 m^2/s
Morphology update bathymetry		Off
Drying and flooding check at	Default condition	Grid cell centres and faces
Depth at grid cell faces	Default condition	Mor
Threshold depth	Default value	0.012 m
Marginal depth	Default value	-999 m
Smoothing time	Default value	60 min
Advection scheme for momentum	Default condition	Cyclic
Advection scheme for transport	Default condition	Cyclic
Forester filter	Default condition	On
Additional parameters		
Cstbnd		#YES#
Trtrou		#Y#
Trtdef		#vrijn2004.trt#
TrtDt		100.
SgrThr		99.0

Gammax	0.5

Table 10. Parameters wave simulations.

Parameter	Why	Value/condition
Spectral resolution		
Sector (counter clockwise)	Direction from which waves can move into the area	180 – 40 degrees
Number of directions	Every 2 degrees	66
Frequency	Wind sea waves (typical according Holthuijsen, 2007)	0.04 – 1 Hz
Conditions along boundary		*Uniform*
Specification of spectra		*Parametric*
Shape JONSWAP	Default condition and value	Peak enh. Fact. 3.3
Period	Data is from peak period	Peak
Directional spreading	Used to working with stdev	Degrees (standard deviation)
Physical parameters		
Gravity	Typical gravity Netherlands	9.81 m/s^2
North w.r.t. x-axis	Default value	90 degrees
Minimum depth	Default value	0.05 m
Convention	Clockwise direction (incident) waves	nautical
Forces		Wave energy dissipation rate 3d
Wind	Not taken into account	0 m/s and 0 deg
Generation mode for physics	Most recent	3-rd generation
Depth induced breaking (BandJ model)	Default values	Alpha 1, Gamma 0.73
Non-linear triad interactions	For simplicity	Off
Bottom friction	Default condition and value	JONSWAP 0.067 m^2/s^3
Diffraction	For simplicity, does not always work properly	Off
Wind growth	No wind modelled	Off
White capping	Default condition	Komen et al.
Refraction	Default	On
Frequenty shift	Default	On
First order (SWAN 40.01)/Second-order (SWAN 40.11)	Third-order not available yet	On
Directional space	Default value	0.5
Frequency space	Default value	0.5
Hs-Tm01	Default value	0.02
Percentage of wet grid points		98%
Relative change w.r.t. mean value	Default value	Hs 0.02, Tm01 0.02
Maximum number of iterations	Default value	15
Level of test output	<50 can be interpreted by yourself	30
Computational mode	Default condition	Stationary

Appendix D - Mean velocity

For all simulations the Hinderplaat shoal and the inner area is depicted to show the largest currents and recirculation cells. To be able to see the patterns of the velocity vectors clearly, the vectors were not all scaled the same.

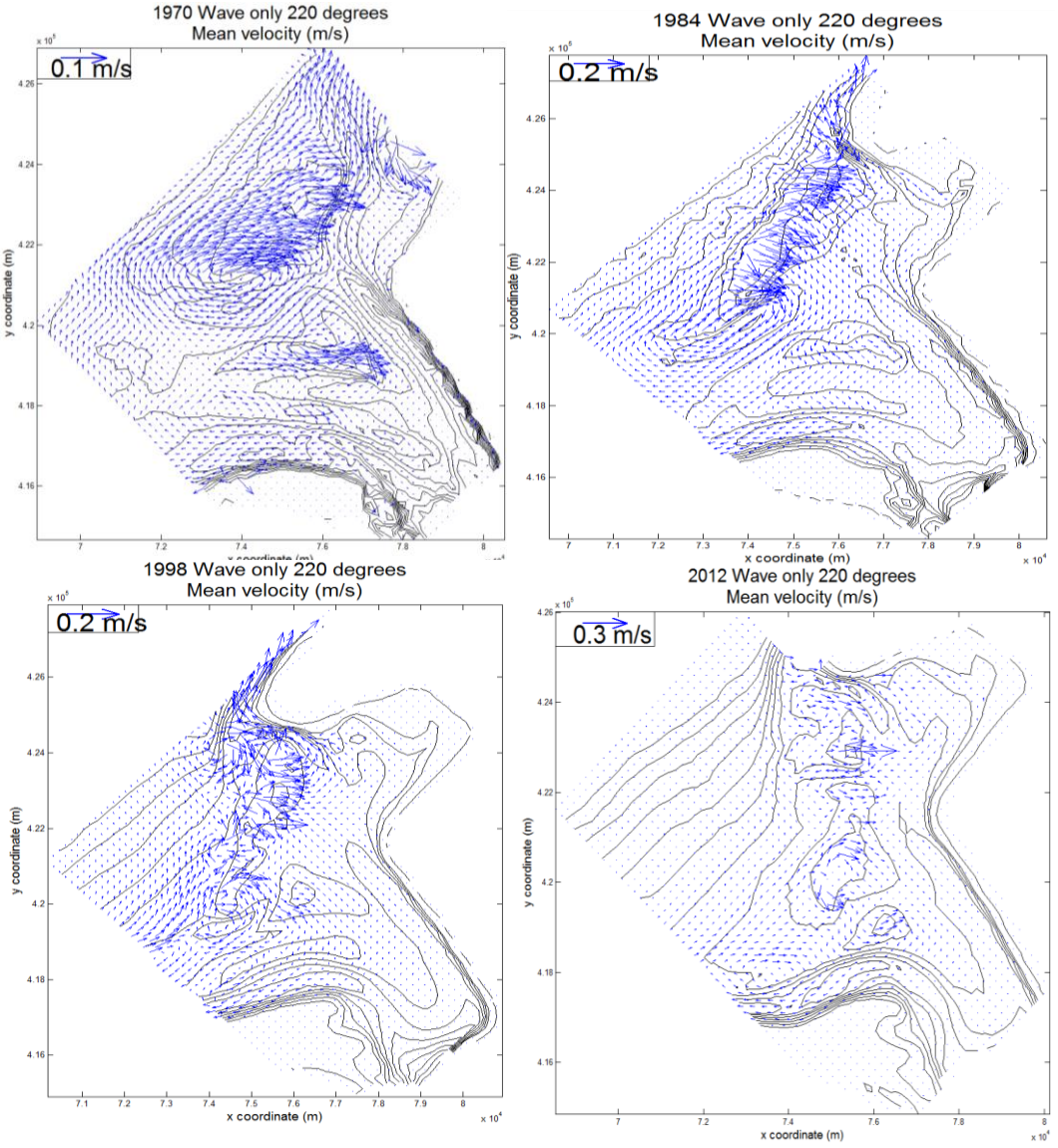

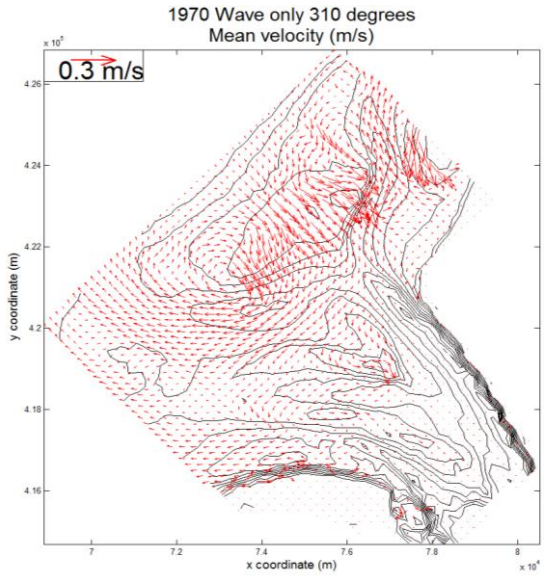
1970 Wave only 310 degrees
Mean velocity (m/s)
0.3 m/s
y coordinate (m)
x coordinate (m)

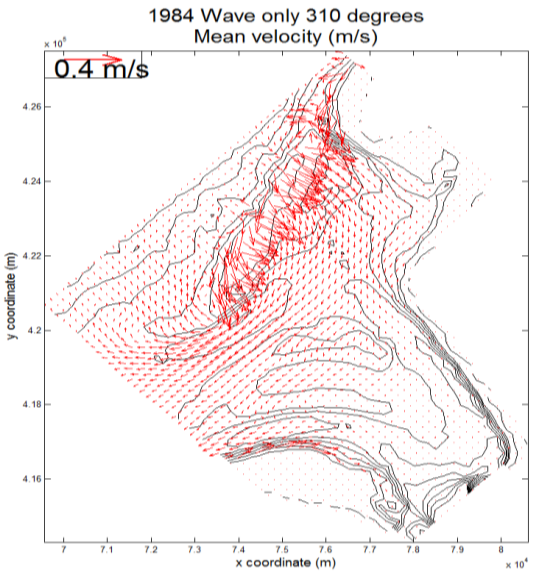
1984 Wave only 310 degrees
Mean velocity (m/s)
0.4 m/s
y coordinate (m)
x coordinate (m)

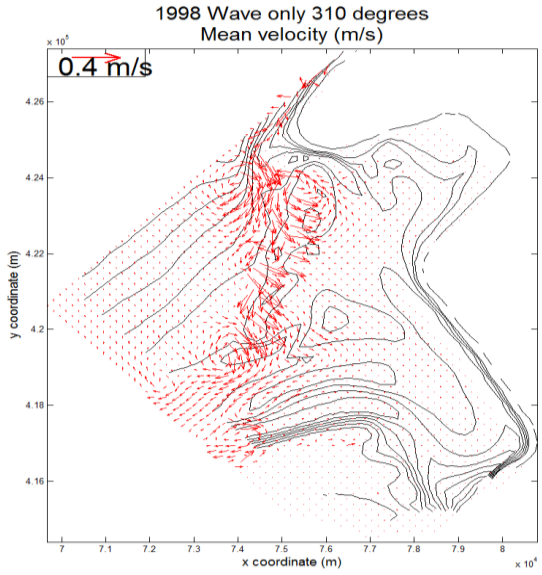
1998 Wave only 310 degrees
Mean velocity (m/s)
0.4 m/s
y coordinate (m)
x coordinate (m)

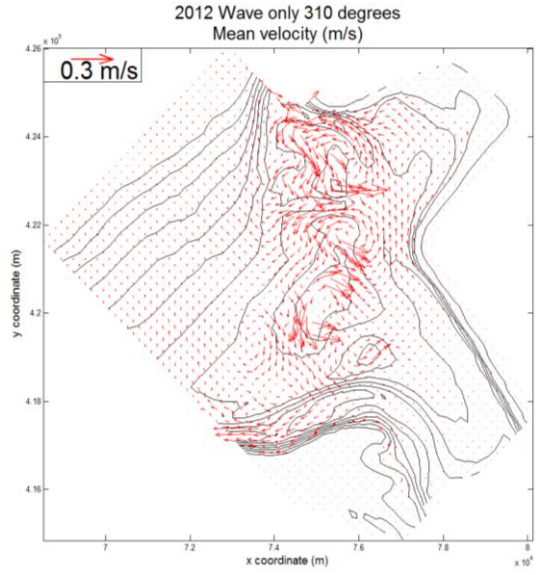
2012 Wave only 310 degrees
Mean velocity (m/s)
0.3 m/s
y coordinate (m)
x coordinate (m)

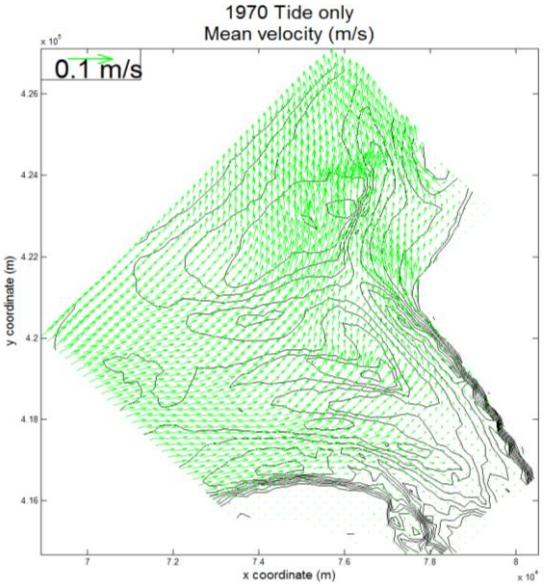
1970 Tide only
Mean velocity (m/s)
0.1 m/s
y coordinate (m)
x coordinate (m)

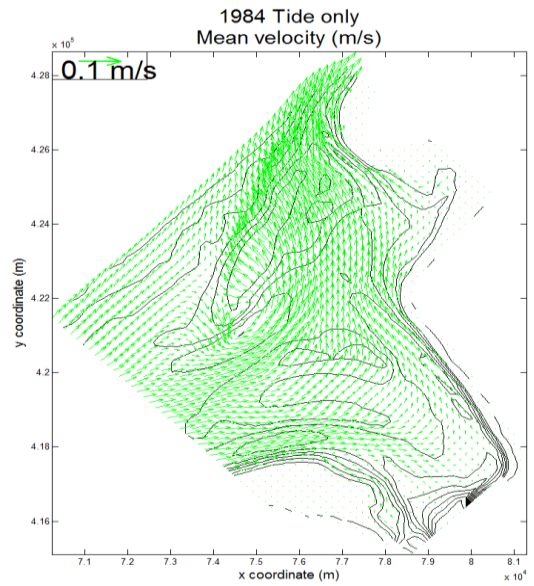
1984 Tide only
Mean velocity (m/s)
0.1 m/s
y coordinate (m)
x coordinate (m)

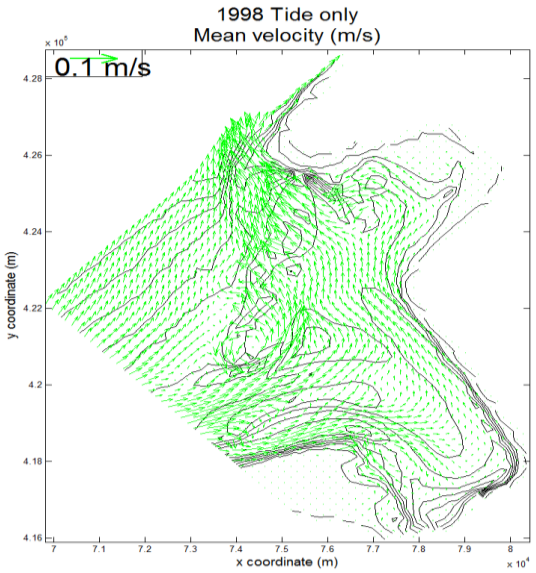
1998 Tide only
Mean velocity (m/s)
0.1 m/s
y coordinate (m)
x coordinate (m)

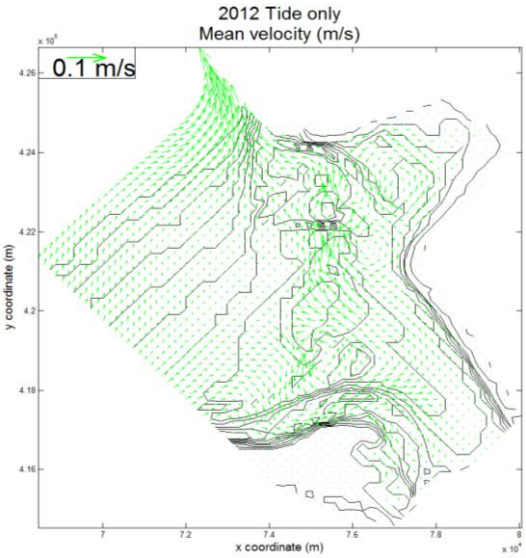
2012 Tide only
Mean velocity (m/s)
0.1 m/s
y coordinate (m)
x coordinate (m)

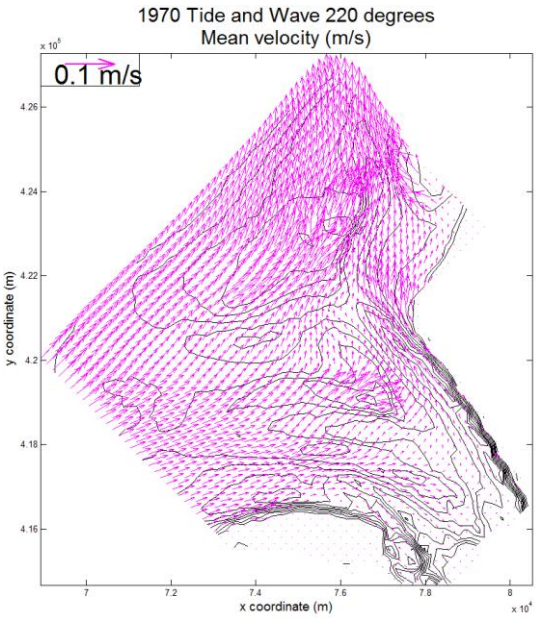
1970 Tide and Wave 220 degrees
Mean velocity (m/s)
0.1 m/s
y coordinate (m)
x coordinate (m)

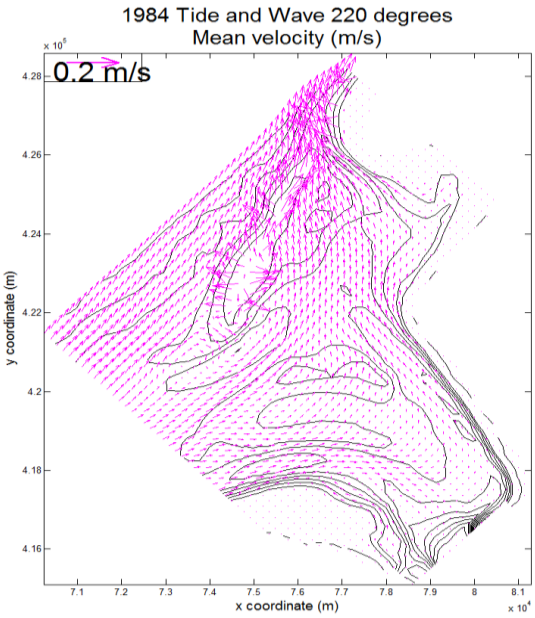
1984 Tide and Wave 220 degrees
Mean velocity (m/s)
0.2 m/s
y coordinate (m)
x coordinate (m)

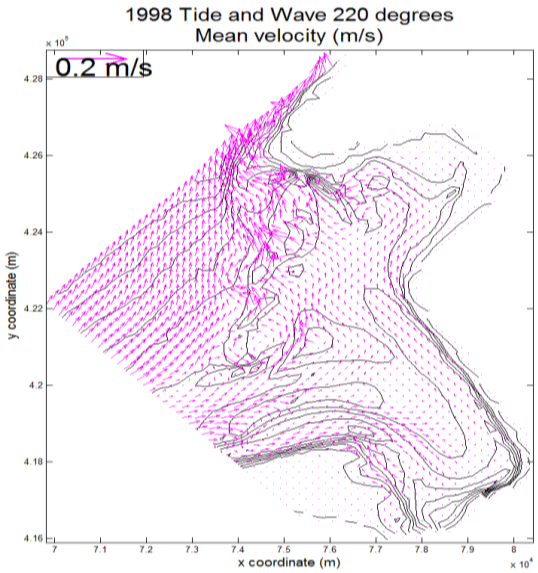
1998 Tide and Wave 220 degrees
Mean velocity (m/s)
0.2 m/s
y coordinate (m)
x coordinate (m)

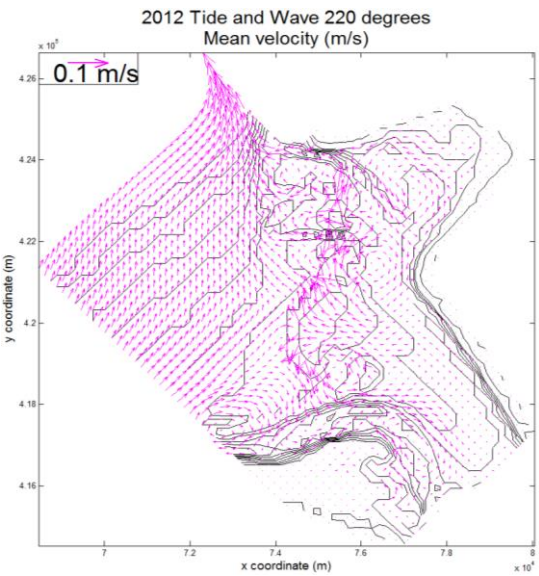
2012 Tide and Wave 220 degrees
Mean velocity (m/s)
0.1 m/s
y coordinate (m)
x coordinate (m)

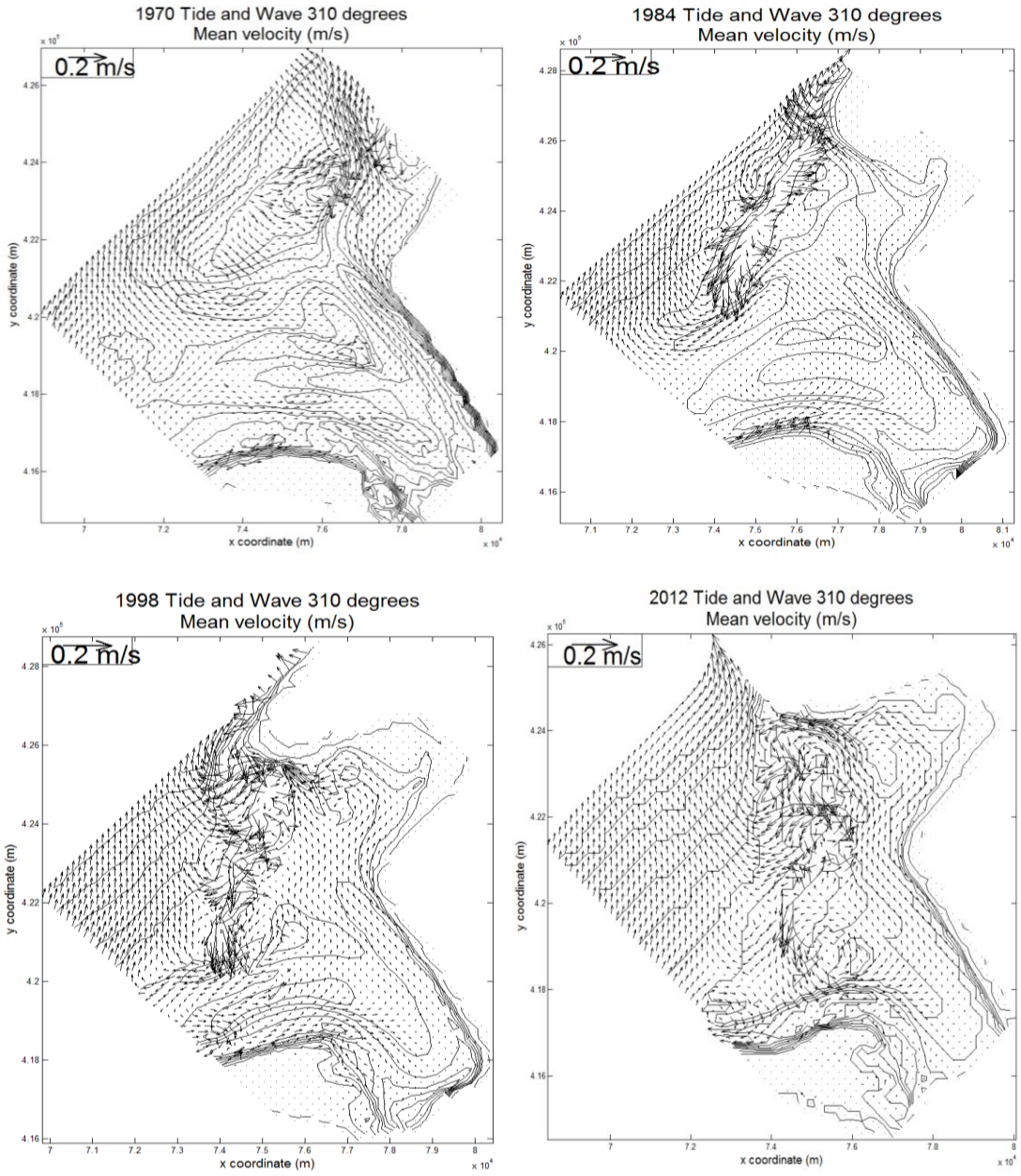

Figure 49. Mean depth averaged velocity plots of every 5th gridcell.

Appendix E – Sediment volume changes GIS

Negative values indicate erosion.

Table 11. Sediment gained or lost per period for the total area (GIS results).

Period	Sediment gain total area (m^3)	Dredging + sedimentation – dumping total area (m^3)
1970 - 1984	42.847.999	43.228.000
1984 - 1998	11.114.999	14.098.149
1998 - 2012	-4.000.000	-1.667.896
Total sedimentation	49.962.999	55.658.252

Table 12. Sediment gained per period for the inner area (GIS results).

Period	Sediment gain inner area (m^3)	Sediment gain inner area with dredging into account (m^3)
1970 - 1984	48.000.000	48.380.000
1984 - 1998	20.989.600	24.765.270
1998 - 2012	15.566.400	20.410.003
Total sedimentation	84.556.000	93.555.275

Table 13. Erosion per period for the inner area (GIS results).

Period	Erosion outer area (m^3)
1970 - 1984	5.152.000
1984 - 1998	10.667.122
1998 - 2012	22.077.900
Total erosion	37.897.022

Table 14. Sediment gained or lost calculated for all the bathymetries available (GIS results).

Period	Total sediment gain (m^3)	Dredging + sedimentation – dumping per period (m^3)	Dredging + sedimentation – dumping per year (m^3)
1970 - 1972	-2480000	-2480000	-1.311.424
1972 - 1976	9544000	9544000	2.517.397
1976 - 1979	14080000	14080000	4.705.642
1979 - 1980	11312000	11312000	11.292.317
1980 - 1984	-9776000	-9396000	-2.478.709
1984 - 1986	-6480000	-5930000	-3.802.265
1986 - 1989	7120000	7393324	2.489.676
1989 - 1992	5536000	6114280	2.061.091
1992 - 1998	-1,1E+07	-9394455	-1.588.925
1998 - 2003	-1,4E+07	-1,2E+07	-1.950.104
2003 - 2012	16128000	16398000	1.498.333
Total sedimentation	20120000	25615253	
Period	Total sediment gain inner area (m^3)	Dredging + sedimentation per period inner area (m^3)	Dredging + sedimentation per year (m^3)
1970 - 1972	2848000	2848000	1424000
1972 - 1976	12872000	12872000	3218000
1976 - 1979	12940800	12940800	4313600
1979 - 1980	5396000	5396000	5396000
1980 - 1984	5669600	6049600	1512400
1984 - 1986	-3368000	-2818000	-1409000
1986 - 1989	6768000	7398909	2466303
1989 - 1992	6775200	7353480	2451160

1992 - 1998	3738240	5754722	959120
1998 - 2003	-380800	1741304	348261
2003 - 2012	16094400	18815900	2090656
Total sedimentation	69353440	78352715	

Appendix F – Sedimentation rates Delft3D

Sedimentation rates (m^3/s) per zone calculated with Delft3D. The wave and tides combined simulations are incorporated in these figures as well as the storm. Negative values indicate erosion.

Table 15. Sedimentation rates (m^3/s) per zone calculated with Delft3D.

	Total area	Inner area	Outer area	Zone 1	Zone 2
1970	-6.4756E-04	0.113322	-1.14E-01	9.51E-02	1.82E-02
1984	-3.7505E-03	0.090934	-9.47E-02	5.66E-02	3.43E-02
1998	2.1364E-03	0.100429	-9.83E-02	7.45E-02	2.60E-02
2012	3.1307E-02	0.092613	-6.13E-02	2.87E-02	6.39E-02